ADAPTIVE POSITION AND FORCE CONTROL OF HYDRAULIC ROBOTS: THEORY, SIMULATION AND EXPERIMENTS

BY

GANG WU

A Thesis
Submitted to the Faculty of Graduate Studies
in Partial Fulfillment of the Requirements
for the Degree of

MASTER OF SCIENCE

Department of Mechanical and Industrial Engineering
University of Manitoba
Winnipeg, Manitoba

0-612-23554-8

THE UNIVERSITY OF MANITOBA

FACULTY OF GRADUATE STUDIES
*****
COPYRIGHT PERMISSION PAGE

ADAPTIVE POSITION AND FORCE CONTROL OF HYDRAULIC ROBOTS: THEORY, SIMULATION AND EXPERIMENTS

BY

GANG WU

A Thesis/Practicum submitted to the Faculty of Graduate Studies of The University of Manitoba in partial fulfillment of the requirements of the degree

of

MASTER OF SCIENCE

To my parents, my sister and her family.

ABSTRACT

The thesis investigates the adaptive control of hydraulically-actuated manipulators using a Generalized Predictive Control (GPC) algorithm. Poor dynamics and high nonlinearities form part of the difficulties in the control of these systems, and make the application of adaptive controls an attractive solution. The feasibility of applying GPC to a two-link hydraulic manipulator is first studied through computer simulation, and its control performance is compared with that of the well known adaptive Minimum Variance Control (MVC) algorithm. Issues relevant to position and force controls are addressed. Experimental study on a single hydraulic actuator is then carried out on both position and force control. Special care is taken to the application of on-line parameter estimation using the method of Recursive Least Squares (RLS) to guarantee numerical accuracy and stability. The work consists of the following main parts:

1. A linear mathematical plant model is established suitable for the control equation formulated in single-input single-output (SISO) GPC algorithm. Comprehensive study is conducted to find the effect of design parameters and to test the adaptability of the algorithm through computer simulation. Computer simulation results of minimum variance control are also compared with those belonging to GPC to identify their respective characteristics with the emphasis on adaptability.

2. SISO-GPC algorithm is extended to multiple-input multiple-output (MIMO) GPC algorithm, paying attention to the interaction between links in order to improve the response. Consequently, the control is performed in the Cartesian space instead of the joint space.

3. The adaptive control strategy using SISO-GPC algorithm is then applied to the force control of the manipulator after the establishment of the system model theoretically. Results are also compared with those belonging to MVC algorithm. Finally, MIMO-GPC algorithm is adopted towards position/force of the manipulator.

4. The efficiency of adaptive control using SISO-GPC algorithm is verified by experimentation, performed on a hydraulic actuator. The results are also compared with those belonging to MVC algorithm.

The significance of this thesis is firstly, a comprehensive study on the position and force control of hydraulic manipulators using adaptive SISO- and MIMO- GPC scheme is conducted. Literature survey suggests that no previous research has been reported on the introduction of SISO- and MIMO- GPC to force control of hydraulic manipulators. Secondly, comparisons between SISO-GPC, SISO-MVC and MIMO-GPC applications to hydraulic manipulators are made for the first time through computer simulation and/or experimentation. Finally, the work in this thesis demonstrates the state-of-the-art performance of GPC algorithm on the control of hydraulic manipulators, offering relevant industries the option of applying advanced control solution.

ACKNOWLEDGMENTS

During the author's two-year study at the Department of Mechanical and Industrial Engineering, he has enjoyed the pleasure to work with his advisor, Dr. N. Sepehri. The thesis would not have been possible without the support and guidance from him.

The author would like to express his deepest thanks to Amir A. Khayyat, a Ph. D. candidate, and Kamyar Ziaei, a M. Sc. student, for their precious ideas, suggestions, and efforts to complete the thesis. Amir A. Khayyat helped to derive the transfer functions in Chapter 2. He also verified the *z*-transformations derived in chapters 4, 5 and 6. The test station on which all the experiments in Chapter 6 were performed was set up and calibrated by Kamyar Ziaei who also wrote the I/O interface software. The author also wishes to thank Mr. Allan Lohse, the Department's technician, who helped in maintaining the experimental test rig.

Finally, the author acknowledges the support of the National Science and Engineering Research Council (NSERC) of Canada, the Institute of Robotics and Intelligent Systems (IRIS) and Preccam Associates Incorporation.

TABLE OF CONTENTS

LIST OF FIGURES

LIST OF TABLES

NOMENCLATURE

A_I, A_O	piston effective areas
C_1, C_2	hydraulic compliance coefficients
K	metering coefficient
K_p	flow-pressure coefficient
K_u	flow-gain coefficient
N_1	minimum output horizon
N_2	maximum output horizon
N_u	control horizon
P_I	supply line pressure
P_O	return line pressure
P_l	load pressure
P_r	return tank pressure
P_s	supply pump pressure
T	torque generated by actuator
d	viscous damping coefficient
d_{ex}	environment damping coefficient along x axis
d_{ey}	environment damping coefficient along y axis
f_x	contact force along x axis
f_y	contact force along y axis
f_{ai}	actuating force of cylinder I
f_{ci}	Coulomb friction of cylinder I
f_{ei}	effective force of cylinder I
i	index representing the actuator number
k_{ex}	environment stiffness along x axis
k_{ey}	environment stiffness along y axis
l	length of manipulator link

m	mass of manipulator link
m_{ex}	environment mass along x axis
m_{ey}	environment mass along y axis
q^{-1}	backward shift operator
u	servovalve input voltage
w	spool area gradient
x	shaft displacement
x_v	spool displacement
λ_c	control weighting factor
λ_f	forgetting factor
λ_r	control relaxing factor
θ	joint displacement

CHAPTER ONE

INTRODUCTION

1.1 BACKGROUND

As one of the most challenging multi-disciplinary areas of research and development, robotics has been experiencing a rapid growth over years. Amongst the three types of actuators to power a robotic arm, *i.e.*, electric, pneumatic and hydraulic, the utilization of hydraulic ones is very attractive, even becoming inevitable in certain scenarios, for their standard, safe and easy-to-maintain components as well as their reliable performance and ability to generate high forces for a sustained period of time. For instance, in large resource based industries or in hazardous, explosive atmospheres where electric devices are either incapable to produce forces large enough, or would not survive at all, the utilization of hydraulic actuators is obviously the best choice.

On the other hand, hydraulically-actuated manipulators do have disadvantages. Specially from the control view point, hydraulic systems are complex, nonlinear and difficult to analyze. A close investigation has suggested that the problems are mostly related to the nature of hydraulic functions [1].

First of all, in a hydraulic drive unit, flexible connecting hoses, large volume of fluid under compression and trapped air in the hydraulic fluid lead to high compliance. The high inertia and high compliance reduce the natural frequency and the damping effect of the joint mechanism. In addition, the interaction effect between links is intensified by the hydraulic compliance which may deteriorate control performance. Further, hydraulic compliance can not remain constant. During operations, as fluid temperature rises, air starts to dissolve in the system, resulting in a substantial change in the compliance [1]. Secondly, as in other types of robotic manipulators, dynamic characteristics of linkages vary as a function of the joint positions and velocities, the payload being manipulated, the stiffness of the environment being interacted, *etc*. Besides, the performance of hydraulic valves is highly sensitive to payload and/or environmental interaction.

Furthermore, as robotic manipulators extend their capabilities, their significant interaction with environment is necessary to be brought into account when the manipulators are performing certain tasks. Examples include pushing/pulling, scraping, grinding, twisting, deburring, drilling, *etc*. Thus the problem of force control need to be addressed. Over years, force control has enjoyed great popularity among all kinds of research topics in robotics. Whitney [2] provided an excellent review. Usually, the force control is not a stand-alone problem. Many tasks require the end-effector to follow trajectories in both position and force regards. A common scenario is that the end-effector is commanded to travel the contour of environment while exerting a constant force on the environment surface along the orthogonal direction. One common solution to this problem is hybrid position/force control structure [3]. The basic idea behind the hybrid control is that the physical constraints of the task should dictate those axes along which force is controlled and those axes along which position is controlled.

The aforementioned dynamic uncertainties and requirements constitute the uniqueness and difficulties of the control of hydraulic manipulators, which also make the circumstance suitable for adaptive control approaches.

Much attention and substantial research has recently been devoted to the study of adaptive robot control, reflecting its current importance in robotics [4, 5]. An adaptive system measures a performance index which is a function of the inputs, states, or outputs of the system. Using the performance index, an adaptation mechanism modifies the parameters of the controller. Two philosophically different approaches exist for the solution of adaptive control [6]. In the first approach, referred to as *indirect adaptive control*, control action is updated based on the on-line estimation of system's parameters. Conversely, the method that bypasses the system parameter estimation and directly adjusts the control action is termed *direct adaptive control*. The first approach, *i.e.*, *indirect adaptive control*, is adopted in this thesis.

Several published work has examined various *indirect adaptive control* algorithms such as Minimum Variance Control [7], single-variable Generalized Predictive Control [8], and Pole Placement Method [9] on position control of hydraulic manipulators. The focus in the present work is on the adaptive position and force control of hydraulic manipulators utilizing Generalized Predictive Control algorithm. GPC algorithm has gained intensive attention since it was first documented by Clarke, *et al* [10, 11] in late 1980s. The algorithm predicts the plant's future outputs for a sequence of future desired set-points. A cost function defined based on the future output errors and control inputs is minimized to produce a set of optimized future control signals. The algorithm has an inherent integral control action, and claims to be capable of stable control of processes having variable parameters, of variable dead time, with nonminimum-phase plants, and with badly damped poles [10].

To the best of our knowledge, there is no published work on position control of hydraulic manipulators using multiple-variable GPC algorithm, nor on force control using either single-variable or multiple-variable GPC algorithm.

1.2 OBJECTIVES

The purposes of the present thesis are twofold: (i) to explore the feasibility of the application of a generalized predictive control strategy to adaptive position and force control of hydraulic manipulators, aiming at acquiring true and accurate information on how and to what extend the strategy can be applied; (ii) to document the comparison between GPC and the well known method of Minimum Variance Control (MVC), in order to facilitate the decision-making for future research and/or application about which strategy should be further pursued. The comparison is based on the criterion that the characteristics of the chosen one could be exploited to the maximum extend on both advantageous and disadvantageous ends. The specific objectives of the research are as follows:

1. To derive appropriate mathematical models representing the controlled plant, depending on which variable is to be controlled, position, force or both, and, on which control algorithm is to be used, single-variable GPC, multiple-variable GPC or single-variable MVC.

2. To evaluate and compare the control performances of both GPC and MVC algorithms via computer simulation and to investigate the adaptability of both algorithms under various scenarios. Also, to study the effects that the design parameters might have on the controlled system.

3. To experimentally verify the above findings by conducting experiments on a single hydraulically-actuated test rig, on both position and force control. During the experimentation, careful attention is paid to the on-line parameter estimation using the method of RLS in order to achieve numerical accuracy and stability.

1.3 OUTLINE OF THE THESIS

This thesis consists of seven chapters. In Chapter Two, the nonlinear system dynamics of a two-link hydraulic manipulator is described in time domain. The Laplace transfer functions are developed in Chapter Two for both single-link and multi-link hydraulic manipulators to enable applications of adaptive control algorithms. A review of single-variable GPC, multiple-variable GPC and single-variable MVC algorithms is presented in Chapter Three. Chapter Three also presents the application issues of an on-line estimation algorithm, the Recursive Least Squares (RLS) method. Chapter Four is dedicated to the position control studies. The application of single-variable GPC algorithm is first studied, and the control performance is compared with that of single-variable MVC algorithm through computer simulations. The study is then extended to multiple-variable GPC case, in an attempt to achieve more accurate tracking. Force control issues are addressed in Chapter Five with an outline similar to that of Chapter Four. Experimental results on the control of a single hydraulic actuator are presented in Chapter Six. First, the validity of the experimentation, as an approach to test control schemes originally intended for hydraulic manipulators, is justified. Then GPC and MVC strategies are implemented, on both position and force control. Chapter Seven summarizes the research, presenting several conclusions and recommendations for future work.

CHAPTER TWO

HYDRAULIC MANIPULATOR'S DYNAMICS AND TRANSFER FUNCTIONS

The understanding of the dynamics of a system forms the very basis of any control problem. The control of hydraulic manipulators distinguishes itself from others by taking into account the high nonlinearity and uncertainty in the dynamics, especially those pertaining to hydraulic functions. This chapter serves to describe the hydraulic manipulator, and provides derivations of s-domain transfer functions. The dynamics of the robotic links and the hydraulic driving units are first presented in time domain. Next, the system dynamics are analyzed in frequency domain, resulting in establishment of Laplace transfer functions from system inputs to various system outputs depending on different cases.

2.1 SYSTEM DYNAMICS

2.1.1 Robotic Links

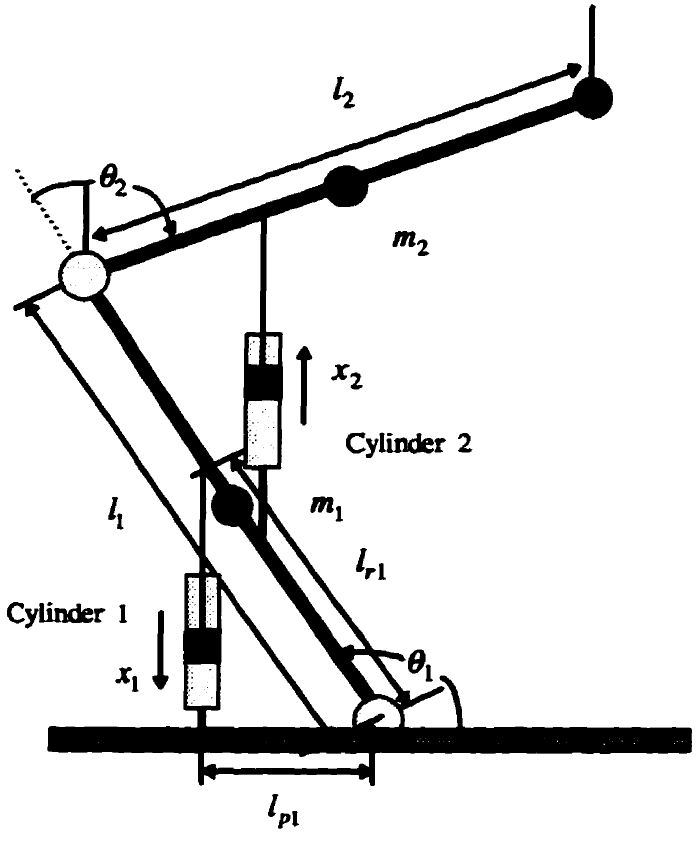

Fig. 2-1 Two-link hydraulic manipulator.

The mechanism of a two-link hydraulic manipulator to be studied in the thesis is illustrated in Fig. 2-1. l_1, l_2, m_1, and m_2 represent the lengths and masses of links 1 and 2, respectively. As shown in the figure, it has been assumed that the center of gravity of each link is located at the middle of the link. θ_1 and θ_2 are joint displacements. x_1 and x_2 are piston displacement of cylinders 1 and 2, respectively.

Derived through the Lagrange approach [12], the equation of motion of link i is :

$$T_i = \sum_{j=1}^{n} M_{ij}(\theta_1,\cdots,\theta_n)\ddot{\theta}_j + \sum_{j=1}^{n}\sum_{k=1}^{n} C_{ijk}\dot{\theta}_j\dot{\theta}_k + G_i \qquad i=1,\cdots,n \tag{2-1}$$

for an n-link manipulator, where T_i is the torque generated by the actuator, θ_i is the joint displacement of link i, $\dot{\theta}_i$ and $\ddot{\theta}_i$ are the corresponding joint velocity and acceleration, and coefficients M_{ij}, C_{ijk} and G_i are functions of $\theta_1,\cdots,\theta_n$.

For the case of a two-link manipulator,

$$T_1 = [k_1 + 2k_3\cos\theta_2]\ddot{\theta}_1 + [k_2 + k_3\cos\theta_2]\ddot{\theta}_2 - k(2\dot{\theta}_1 + \dot{\theta}_2)\dot{\theta}_2\sin\theta_2$$
$$+ k_4\cos\theta_1 + k_5\cos\theta_1 + k_6\cos(\theta_1 + \theta_2) \tag{2-2a}$$

$$T_2 = [k_2 + k_3\cos\theta_2]\ddot{\theta}_1 + k_2\ddot{\theta}_2 + k_3\dot{\theta}_1^2\sin\theta_2 + k_6\cos(\theta_1 + \theta_2) \tag{2-2b}$$

where $k_{i(i=1,\cdots,6)}$ are evaluated as:

$$k_1 = \frac{m_1 l_1^2}{3} + \frac{m_2 l_2^2}{3} + m_2 l_1^2$$

$$k_2 = \frac{m_2 l_2^2}{3}$$

$$k_3 = \frac{m_2 l_1 l_2}{2}$$

$$k_4 = \frac{m_1 g l_1}{2}$$

$$k_5 = m_2 g l_1$$

$$k_6 = \frac{m_2 g l_2}{2}$$

Equations (2-2) are nonlinear. For further analysis it can be linearized about reference point $(\hat{\theta}_1, \hat{\dot{\theta}}_1, \hat{\ddot{\theta}}_1, \hat{\theta}_2, \hat{\dot{\theta}}_2, \hat{\ddot{\theta}}_2)$. For small variation about the reference point and neglecting small terms, the final linearized model becomes [1]:

$$\begin{bmatrix} \Delta T_1 \\ \Delta T_2 \end{bmatrix} = \begin{bmatrix} H_{11} & H_{12} \\ H_{21} & H_{22} \end{bmatrix} \begin{bmatrix} \Delta\ddot{\theta}_1 \\ \Delta\ddot{\theta}_2 \end{bmatrix} \tag{2-3}$$

where $\Delta\ddot{\theta}_1$ and $\Delta\ddot{\theta}_2$ represent small changes near the corresponding reference points $\ddot{\theta}_1$ and $\ddot{\theta}_2$. Further,

$$H_{11} = k_1 + 2k_3 \cos\hat{\theta}_2$$

$$H_{12} = k_2 + k_3 \cos\hat{\theta}_2$$

$$H_{21} = k_2 + k_3 \cos\hat{\theta}_2$$

$$H_{22} = k_2.$$

2.1.2 Hydraulic Actuator

Each link is driven by one hydraulic actuator. The main components of hydraulic actuator are directional valves, connecting hoses, and cylinders. Fig. 2-2 shows the schematic of the hydraulic driving unit for link 1 using a closed-center four-way valve operating from a constant pressure pump system.

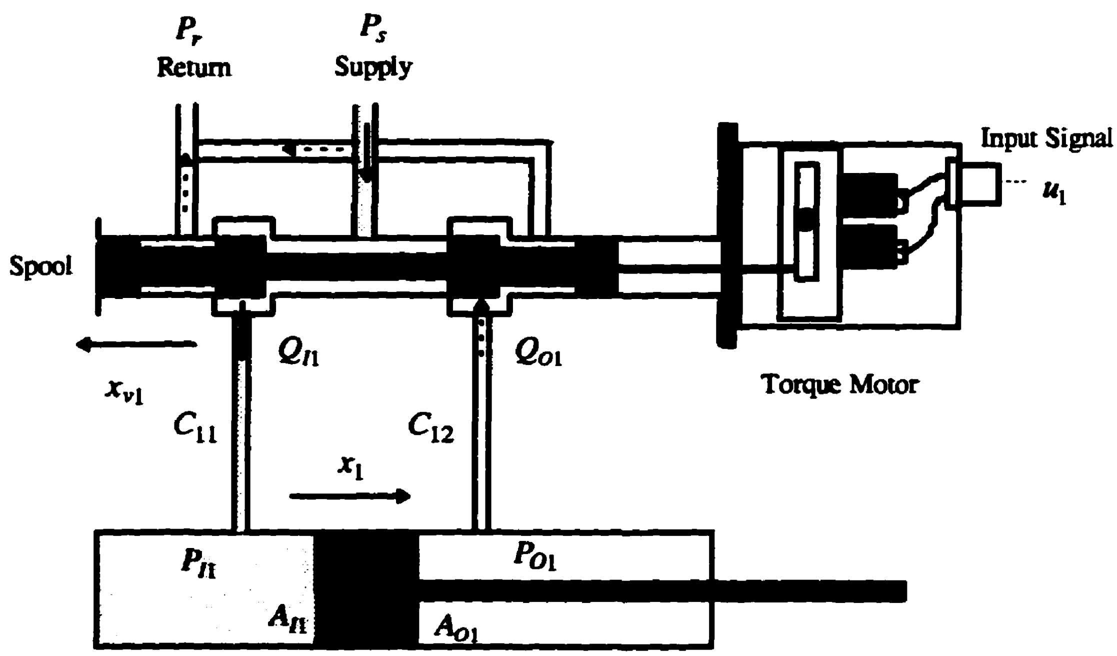

Fig. 2-2 Typical hydraulic actuator.

2.1.2.1 Valve Dynamics

For the *i*th actuator, the valve variables are the spool displacement x_{vi}, the supply pump pressure P_s, the return pressure P_r. Q_{Ii} and Q_{Oi} are the flow rates, and P_{Ii} and P_{Oi} are the pressures of supply line and return line, respectively. The nonlinear relationship between pressures and flows is described as:

$x_{vi}>0$,

$$Q_{Ii} = K_i w_i x_{vi}\sqrt{P_s - P_{Ii}} \tag{2-4a}$$

$$Q_{Oi} = K_i w_i x_{vi}\sqrt{P_{Oi} - P_r} \tag{2-4b}$$

$x_{vi}<0$,

$$Q_{Ii} = K_i w_i x_{vi}\sqrt{P_{Ii} - P_r} \tag{2-4c}$$

$$Q_{Oi} = K_i w_i x_{vi}\sqrt{P_s - P_{Oi}} \tag{2-4d}$$

where the spool displacement, x_{vi}, is proportional to the servovalve voltage input u_i. $K_i = c_d\sqrt{\frac{2}{\rho}}$ is the metering coefficient, and w_i is the spool area gradient.

2.1.2.2 Pipe Dynamics

The *i*th servovalve output ports dynamics are described as following:

$$C_{i1}\dot{P}_{Ii} = Q_{Ii} - A_{Ii}\dot{x}_i \tag{2-5a}$$

$$C_{i2}\dot{P}_{Oi} = A_{Oi}\dot{x}_i - Q_{Oi} \tag{2-5b}$$

where A_{Ii} and A_{Oi} are piston's effective areas, $\dot{x}_i$ is the piston velocity. C_{i1} and C_{i2} are the hydraulic compliance of supply line and return line, respectively. It is assumed that $C_{i1} = C_{i2} = C_i$.

The joint displacement, θ_i, and the piston displacement, x_i, are related by geometrical configuration. Within the vicinity of certain angle $\hat{\theta}_i$, the following relation holds [1]:

$$dx_i = J_i(\hat{\theta}_i)d\theta_i \tag{2-6}$$

where $J_i(\hat{\theta}_i) = \dfrac{-l_{pi}l_{ri}\sin\hat{\theta}_i}{\sqrt{l_{pi}^2 + l_{ri}^2 + 2l_{pi}l_{ri}\cos\hat{\theta}_i}}$. Refer to Fig. 2-2 for the definition of l_{pi} and l_{ri}.

2.1.2.3 Effective Actuating Force and Joint Torque

The actuating force, f_{ai}, the effective actuating force, f_{ei}, and the joint torque, T_i, are given as the following [1]:

$$f_{ai} = P_{Ii}A_{Ii} - P_{Oi}A_{Oi} \tag{2-7a}$$

$$f_{ei} = f_{ai} - d_i\dot{x}_i - f_{ci} \tag{2-7b}$$

$$T_i = f_{ei}J_i(\hat{\theta}_i) \tag{2-7c}$$

where d_i represents viscous damping coefficient of *i*th cylinder and f_{ci} is the equivalent Coulomb friction reflected on the actuator.

2.2 SINGLE-LINK ANALYSIS IN LAPLACE DOMAIN

2.2.1 Joint Position Analysis

Neglecting the dynamic coupling between the links, each link of the two-link planar hydraulic manipulator shown in Fig. 2-1 can be viewed individually as a single-input single-output system.

The Laplace transfer function from the servovalve input, u_i, to the joint angle, θ_i, and the transfer function from the servovalve input, u_i, to the joint velocity, $\dot{\theta}_i$, are to be obtained in this section. In the remaining text, all variables such as θ_i and T_i are used to represent a small change near the corresponding reference point without the gradient, Δ. In addition, $\hat{J}_i$ is used instead of $J_i(\hat{\theta}_i)$ for the sake of simplicity.

By combining equations (2-3), (2-6) and (2-7), the following relationship is obtained:

$$\begin{bmatrix} \hat{J}_1 F_{a1}(s) \\ \hat{J}_2 F_{a2}(s) \end{bmatrix} = \begin{bmatrix} H_{11}s^2 + \hat{J}_1^2 d_1 s & H_{12}s^2 \\ H_{21}s^2 & H_{22}s^2 + \hat{J}_2^2 d_2 s \end{bmatrix} \begin{bmatrix} \Theta_1(s) \\ \Theta_2(s) \end{bmatrix} \tag{2-8}$$

Equation (2-8) can be represented as follows:

$$\begin{bmatrix} \hat{J}_1 F_{a1}(s) \\ \hat{J}_2 F_{a2}(s) \end{bmatrix} = \mathbf{H}(s) \begin{bmatrix} \Theta_1(s) \\ \Theta_2(s) \end{bmatrix} \tag{2-9}$$

where $\mathbf{H}(s)=\begin{bmatrix} H_{11}s^2+\hat{J}_1^2 d_1 s & H_{12}s^2 \\ H_{21}s^2 & H_{22}s^2+\hat{J}_2^2 d_2 s \end{bmatrix}$.

On the other hand, the actuating force vector can be derived from the characteristics of the hydraulic driving system. Linearizing the valve dynamics equations (2-4) and writing the result in s-domain give [1]:

$$Q_{Ii}=K_{ui}U_i-K_{pi}P_{Ii} \tag{2-10a}$$

$$Q_{Oi}=K_{ui}U_i+K_{pi}P_{Oi} \tag{2-10b}$$

where

$$K_{ui}=K_i w_i\sqrt{\frac{P_s-P_{li}}{2}},\ K_{pi}=\frac{K_i w_i x_i}{\sqrt{2(P_s-P_{li})}},\ P_{li}=P_{Ii}-P_{Oi} \tag{2-10c}$$

Here the servovalve input voltage, U_i, instead of the spool displacement, X_{Vi}, is considered as the system input.

Transforming the pipe dynamics equations (2-5) into s-domain gives:

$$Q_{Ii}=C_i P_{Ii}s+A_{Ii}X_i s \tag{2-11a}$$

$$Q_{Oi}=-C_i P_{Oi}s+A_{Oi}X_i s \tag{2-11b}$$

Equating equations (2-10) and (2-11) to remove Q_{Ii} and Q_{Oi} arrives at:

$$P_{Ii}=\frac{K_{ui}U_i-A_{Ii}X_i s}{K_{pi}+C_i s}=\frac{K_{ui}U_i-A_{Ii}s\hat{J}_i\Theta_i}{K_{pi}+C_i s} \tag{2-12a}$$

$$P_{Oi} = \frac{-K_{ui}U_i + A_{Oi}X_i s}{K_{pi} + C_i s} = \frac{-K_{ui}U_i + A_{Oi}s\hat{J}_i\Theta_i}{K_{pi} + C_i s} \tag{2-12b}$$

Substituting P_{Ii} and P_{Oi} into equations (2-7) and then multiplying both sides by $\hat{J}_i$ yield:

$$\begin{bmatrix} \hat{J}_1 F_{a1}(s) \\ \hat{J}_2 F_{a2}(s) \end{bmatrix} = \mathbf{A}(s)\begin{bmatrix} U_1(s) \\ U_2(s) \end{bmatrix} - \mathbf{B}(s)\begin{bmatrix} \Theta_1(s) \\ \Theta_2(s) \end{bmatrix} \tag{2-13}$$

where $\mathbf{A}(s) = \begin{bmatrix} \dfrac{K_{u1}(A_{I1} + A_{O1})\hat{J}_1}{C_1 s + K_{p1}} & 0 \\ 0 & \dfrac{K_{u2}(A_{I2} + A_{O2})\hat{J}_2}{C_2 s + K_{p2}} \end{bmatrix}$ and

$$\mathbf{B}(s) = \begin{bmatrix} \dfrac{(A_{I1}^2 + A_{O1}^2)\hat{J}_1^{\,2} s}{C_1 s + K_{p1}} & 0 \\ 0 & \dfrac{(A_{I2}^2 + A_{O2}^2)\hat{J}_2^{\,2} s}{C_2 s + K_{p2}} \end{bmatrix}.$$

Comparing equations (2-9) and (2-13) gives

$$\mathbf{H}(s)\begin{bmatrix} \Theta_1(s) \\ \Theta_2(s) \end{bmatrix} = \mathbf{A}(s)\begin{bmatrix} U_1(s) \\ U_2(s) \end{bmatrix} - \mathbf{B}(s)\begin{bmatrix} \Theta_1(s) \\ \Theta_2(s) \end{bmatrix} \tag{2-14}$$

or,

$$\begin{bmatrix} \Theta_1(s) \\ \Theta_2(s) \end{bmatrix} = [\mathbf{H}(s) + \mathbf{B}(s)]^{-1}\mathbf{A}(s)\begin{bmatrix} U_1(s) \\ U_2(s) \end{bmatrix} \tag{2-15}$$

The transfer function from the servovalve input, u_i, to the joint angle, θ_i, of a single link mechanism is given by the diagonal components of equation (2-15) as follows:

$$\frac{\Theta_i(s)}{U_i(s)} = \frac{K_{ui}(A_{Ii} + A_{Oi})\hat{J}_i}{H_{ii}C_i s^3 + (\hat{J}_i^2 d_i C_i + K_{pi}H_{ii})s^2 + \hat{J}_i^2(d_i K_{pi} + A_{Ii}^2 + A_{Oi}^2)s} \tag{2-16}$$

From equation (2-16) it is easy to find the transfer function representing the relationship between the servovalve input, u_i, and the joint velocity, $\dot{\theta}_i$, of a single link:

$$\frac{s\Theta_i(s)}{U_i(s)} = \frac{K_{ui}(A_{Ii} + A_{Oi})\hat{J}_i}{H_{ii}C_i s^2 + (\hat{J}_i^2 d_i C_i + K_{pi}H_{ii})s + \hat{J}_i^2(d_i K_{pi} + A_{Ii}^2 + A_{Oi}^2)} \tag{2-17}$$

2.2.2 Force Analysis

Figure 2-3 shows the two-link manipulator in contact with the environment. f_x is the force on the end-effector imposed by the environment along the Cartesian x direction. The environment is modeled as a second order mass-damper-spring system. The contact force f_x is governed by the following s-domain equation:

$$F_x = (m_{ex}s^2 + d_{ex}s + k_{ex})X \tag{2-18}$$

Assuming that link 1 is fixed at a certain angle of $\hat{\theta}_1$, the s-domain transfer function from the servovalve input voltage of link 2, u_2, to the contact force, f_x, is to be formed in the following.

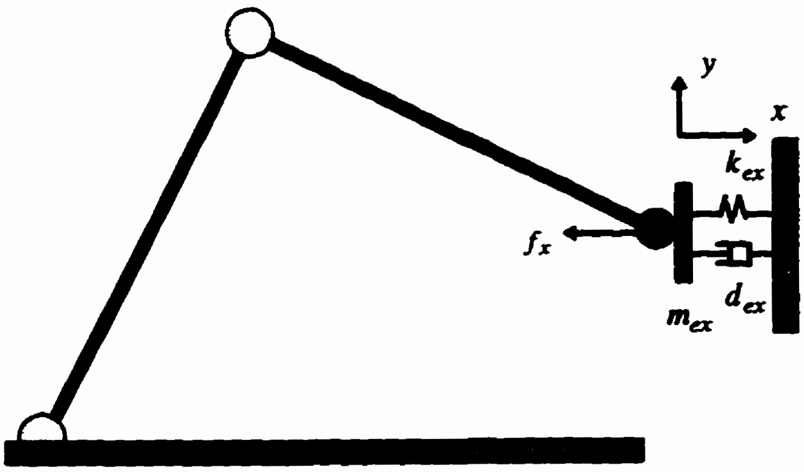

Fig. 2-3 Two-link hydraulic manipulator in contact with environment.

According to equations (2-12), for link 2, P_{I2} and P_{O2} are:

$$P_{I2} = \frac{K_{u2}U_2 - A_{I2}X_2 s}{K_{p2} + C_2 s} \tag{2-19a}$$

$$P_{O2} = \frac{-K_{u2}U_2 + A_{O2}X_2 s}{K_{p2} + C_2 s} \tag{2-19b}$$

Neglecting the Coulomb friction term f_{c2} in equation (2-7b) and transforming (2-7b) into s-domain gives the effective actuating force as follows:

$$F_{e2} = F_{a2} - d_2 X_2 s = P_{I2}A_{I2} - P_{O2}A_{O2} - d_2 X_2 s \tag{2-20}$$

Substituting (2-19) into (2-20) yields:

$$F_{e2} = \frac{(K_{u2}U_2 - A_{I2}X_2 s)A_{I2}}{K_{p2} + C_2 s} - \frac{(-K_{u2}U_2 + A_{O2}X_2 s)A_{O2}}{K_{p2} + C_2 s} - d_2 X_2 s \tag{2-21}$$

or

$$F_{e2} = \frac{(A_{I2} + A_{O2})K_{u2}U_2 - (A_{I2}^2 + A_{O2}^2)X_2 s}{K_{p2} + C_2 s} - d_2 X_2 s \tag{2-22}$$

The actuating torque T_2 is given in (2-7c) and is rewritten here as (2-23)

$$T_2 = F_{e2} J_2(\hat{\theta}_2) \tag{2-23}$$

On the other hand, neglecting the nonlinear and coupling terms in (2-2b), the joint displacement θ_2 is related to T_2, in s-domain, by the following equations:

$$T_2 = k_2 \theta_2 s^2 \tag{2-24a}$$

$$k_2 = \frac{m_2 l_2^2}{3} \tag{2-24b}$$

Equations (2-24a) and (2-24b) describe the free motion of link 2. In the case of contacting with the environment, the contact force $F_x(s)$ has impact on the link dynamics. Therefore, (2-24a) should be revised as

$$T_2 - T_{2e} = k_2 \theta_2 s^2 \tag{2-25}$$

where T_{2e} is the external torque generated by F_x. It is well known that [5]:

$$\begin{bmatrix} T_{1e} \\ T_{2e} \end{bmatrix} = \begin{bmatrix} P_{11} & P_{12} \\ P_{21} & P_{22} \end{bmatrix}^T \begin{bmatrix} F_x \\ F_y \end{bmatrix} \tag{2-26}$$

where $\mathbf{J} = \begin{bmatrix} P_{11} & P_{12} \\ P_{21} & P_{22} \end{bmatrix} = \begin{bmatrix} -l_1 \sin\hat{\theta}_1 - l_2 \sin(\hat{\theta}_1 + \hat{\theta}_2) & -l_2 \sin(\hat{\theta}_1 + \hat{\theta}_2) \\ l_1 \cos\hat{\theta}_1 + l_2 \cos(\hat{\theta}_1 + \hat{\theta}_2) & l_2 \cos(\hat{\theta}_1 + \hat{\theta}_2) \end{bmatrix} \begin{bmatrix} P_{11} & P_{12} \\ P_{21} & P_{22} \end{bmatrix}$ is called the Jacobian matrix. In the case presented here, since $F_y = 0$, therefore,

$$T_{2e} = P_{12} F_x \tag{2-27}$$

Considering small Cartesian displacement $[\Delta x, \ \Delta y]^T$ around the operating point $[\hat{\theta}_1, \ \hat{\theta}_2]^T$, it is known that

$$\begin{bmatrix} \Delta x \\ \Delta y \end{bmatrix} = \begin{bmatrix} P_{11} & P_{12} \\ P_{21} & P_{22} \end{bmatrix} \begin{bmatrix} \Delta\theta_1 \\ \Delta\theta_2 \end{bmatrix} \tag{2-28}$$

In the case that link 1 is fixed, $\Delta\theta_1$ is equal to zero. Hence,

$$\Delta x = P_{12}\Delta\theta_2 \tag{2-29}$$

By considering small changes at certain angle $\hat{\theta}_2$, the following relation holds [1]:

$$\Delta x_2 = \hat{J}_2\Delta\theta_2 \tag{2-30}$$

In the remaining text, x_2 and θ_2 are used to represent small changes near the corresponding reference point without the gradient, Δ. Then, equations (2-29) and (2-30) can be re-presented as following:

$$x = P_{12}\theta_2 \tag{2-31}$$

$$x_2 = J_2(\hat{\theta}_2)\theta_2 \tag{2-32}$$

Now, all the equations to establish an s-domain transfer function between F_x and U_2 are found. The block diagram is first drawn in the following, then the transfer function is derived from it. Using equations (2-18), (2-22) through (2-25), (2-27), (2-31) and (2-32), the block diagram can be drawn in Fig. 2-4.

From Fig. 2-4, it is not difficult to get the transfer function as following:

$$\frac{F_x}{U_2}=\frac{J_2P_{12}K_{u2}(A_{I2}+A_{O2})(m_{ex}s^2+d_{ex}s+k_{ex})}{(K_{p2}+C_2s)[k_2s^2+J_2^2d_2s+P_{12}^2(m_{ex}s^2+d_{ex}s+k_{ex})]+J_2^2(A_{I2}^2+A_{O2}^2)s} \tag{2-33}$$

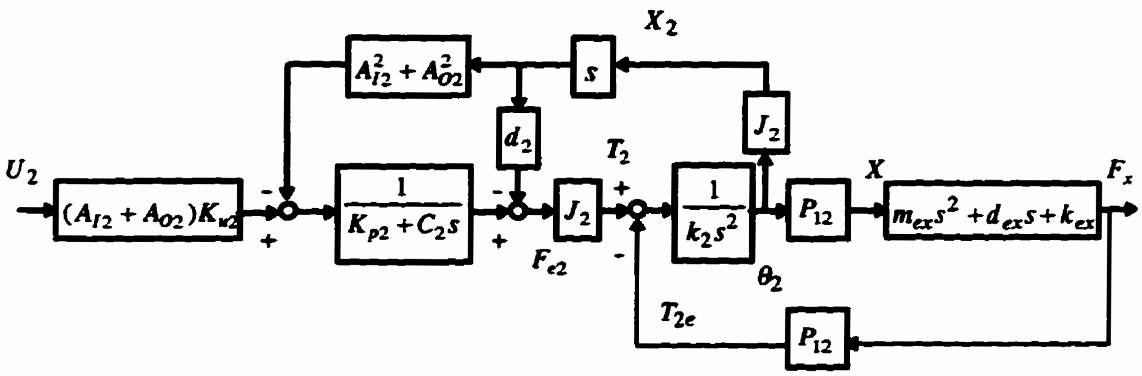

Fig. 2-4 Open loop block diagram of link 2 interacting with environment.

The successful establishment of the transfer function of (2-33) enables the application of linear adaptive controllers using GPC and MVC algorithms.

2.3 MULTI-LINK ANALYSIS IN LAPLACE DOMAIN

In this section, a general equation describing the two-link manipulator in contact with the environment is derived.

2.3.1 Formulation in Cartesian Coordinates

The dynamic equations of the two-link manipulator in free motion shown by is rewritten again:

$$\begin{bmatrix} \hat{j}_1 F_{a1}(s) \\ \hat{j}_2 F_{a2}(s) \end{bmatrix} = \mathbf{H}(s) \begin{bmatrix} \Theta_1(s) \\ \Theta_2(s) \end{bmatrix} \tag{2-34}$$

Considering the contact force f_x and f_y applied to the end-effector by the environment along x and y directions, respectively (see Fig. 2-5), (2-34) should be modified as [5]

$$\begin{bmatrix} \hat{j}_1 F_{a1}(s) \\ \hat{j}_2 F_{a2}(s) \end{bmatrix} = \mathbf{H}(s) \begin{bmatrix} \Theta_1(s) \\ \Theta_2(s) \end{bmatrix} + \mathbf{J}^T \begin{bmatrix} F_x \\ F_y \end{bmatrix} \tag{2-35}$$

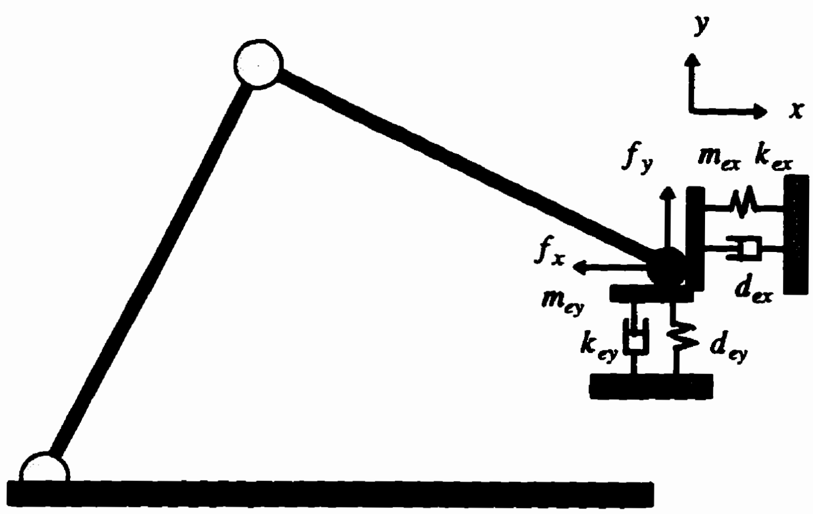

Fig. 2-5 Manipulator in contact with environment in both x and y directions.

The relationship between the joint displacement and the Cartesian displacement is [5]:

$$\begin{bmatrix} \Theta_1 \\ \Theta_2 \end{bmatrix} = \mathbf{J}^{-1} \begin{bmatrix} X \\ Y \end{bmatrix} \tag{2-36}$$

where $\mathbf{J}^{-1} = \begin{bmatrix} O_{11} & O_{12} \\ O_{21} & O_{22} \end{bmatrix}$ is the inverse of the Jacobian matrix $\mathbf{J}$. Here, $[\Theta_1, \Theta_2]^T$ and $[X, Y]^T$ are used to represent small changes near the corresponding reference point without the gradient, Δ.

Substituting equation (2-36) into (2-35) yields:

$$\begin{bmatrix} \hat{J}_1 F_{a1}(s) \\ \hat{J}_2 F_{a2}(s) \end{bmatrix} = \mathbf{H}(s)\mathbf{J}^{-1} \begin{bmatrix} X \\ Y \end{bmatrix} + \mathbf{J}^T \begin{bmatrix} F_x \\ F_y \end{bmatrix} \tag{2-37}$$

On the other hand, according to equation (2-13) the following equation holds:

$$\begin{bmatrix} \hat{J}_1 F_{a1}(s) \\ \hat{J}_2 F_{a2}(s) \end{bmatrix} = \mathbf{A}(s) \begin{bmatrix} U_1(s) \\ U_2(s) \end{bmatrix} - \mathbf{B}(s) \begin{bmatrix} \Theta_1(s) \\ \Theta_2(s) \end{bmatrix} \tag{2-38}$$

Recalling equation (2-36), equation (2-38) can be re-written as

$$\begin{bmatrix} \hat{J}_1 F_{a1}(s) \\ \hat{J}_2 F_{a2}(s) \end{bmatrix} = \mathbf{A}(s) \begin{bmatrix} U_1 \\ U_2 \end{bmatrix} - \mathbf{B}(s)\mathbf{J}^{-1} \begin{bmatrix} X \\ Y \end{bmatrix} \tag{2-39}$$

Comparing (2-37) with (2-39) yields the following:

$$\mathbf{H}(s)\mathbf{J}^{-1} \begin{bmatrix} X \\ Y \end{bmatrix} + \mathbf{J}^T \begin{bmatrix} F_x \\ F_y \end{bmatrix} = \mathbf{A}(s) \begin{bmatrix} U_1 \\ U_2 \end{bmatrix} - \mathbf{B}(s)\mathbf{J}^{-1} \begin{bmatrix} X \\ Y \end{bmatrix} \tag{2-40}$$

or

$$\mathbf{J}^T\begin{bmatrix}F_x\\F_y\end{bmatrix}+[\mathbf{H}(s)+\mathbf{B}(s)]\mathbf{J}^{-1}\begin{bmatrix}X\\Y\end{bmatrix}=\mathbf{A}(s)\begin{bmatrix}U_1\\U_2\end{bmatrix} \tag{2-41}$$

Equation (2-41) is a general form equation governing the dynamics of the two-link manipulator with an external force vector $\left[F_x,\ F_y\right]^T$ exerted on its end-effector.

2.3.2 Cartesian Position Analysis

The s-domain transfer function of the manipulator in free motion in the Cartesian space can be easily obtained by setting the external force vector $\left[F_x,\ F_y\right]^T$ in equation (2-41) to zero:

$$\begin{bmatrix}X(s)\\Y(s)\end{bmatrix}=\mathbf{J}[\mathbf{H}(s)+\mathbf{B}(s)]^{-1}\mathbf{A}(s)\begin{bmatrix}U_1(s)\\U_2(s)\end{bmatrix} \tag{2-42}$$

Matrices **J**, **H**(s), **B**(s) and **A**(s) were previously defined in equations (2-26), (2-9) and (2-13), respectively. Substituting them into equation (2-42),

$$\begin{bmatrix}X(s)\\Y(s)\end{bmatrix}=\begin{bmatrix}D_{11} & D_{12}\\D_{21} & D_{22}\end{bmatrix}\begin{bmatrix}U_1\\U_2\end{bmatrix} \tag{2-43}$$

where $D_{11}=\dfrac{1}{D}\{[(H_{22}s+\hat{J}_2^2d_2)(C_2s+K_{p2})+(A_{I2}^2+A_{O2}^2)\hat{J}_2^2]K_{u1}(A_{I1}+A_{O1})\hat{J}_1P_{11}$

$$-s(C_2s+K_{p2})K_{u1}H_{21}\hat{J}_1(A_{I1}+A_{O1})P_{12}\}$$

$$D_{12} = \frac{1}{D}\{[(H_{11}s + \hat{J}_1^2 d_1)(C_1 s + K_{p1}) + (A_{I1}^2 + A_{O1}^2)\hat{J}_1^2]K_{u2}(A_{I2} + A_{O2})\hat{J}_2 P_{12}$$

$$- s(C_1 s + K_{p1})K_{u2}H_{12}\hat{J}_2(A_{I2} + A_{O2})P_{11}\}$$

$$D_{21} = \frac{1}{D}\{[(H_{22}s + \hat{J}_2^2 d_2)(C_2 s + K_{p2}) + (A_{I2}^2 + A_{O2}^2)\hat{J}_2^2]K_{u1}(A_{I1} + A_{O1})\hat{J}_1 P_{21}$$

$$- s(C_2 s + K_{p2})K_{u1}H_{21}\hat{J}_1(A_{I1} + A_{O1})P_{22}\}$$

$$D_{22} = \frac{1}{D}\{[(H_{11}s + \hat{J}_1^2 d_1)(C_1 s + K_{p1}) + (A_{I1}^2 + A_{O1}^2)\hat{J}_1^2]K_{u2}(A_{I2} + A_{O2})\hat{J}_2 P_{22}$$

$$- s(C_1 s + K_{p1})K_{u2}H_{12}\hat{J}_2(A_{I2} + A_{O2})P_{21}\}$$

$$D = s[(H_{11}s + \hat{J}_1^2 d_1)(C_1 s + K_{p1}) + (A_{I1}^2 + A_{O1}^2)\hat{J}_1^2][(H_{22}s + \hat{J}_2^2 d_2)(C_2 s + K_{p2})$$

$$+ (A_{I2}^2 + A_{O2}^2)\hat{J}_2^2] - s^3(C_1 s + K_{p1})(C_2 s + K_{p2})H_{12}H_{21}$$

Clearly, (2-43) is a 5th order system.

Equation (2-43) indicates that the above multivariable system is in the so-called P-canonical form [13] which means that each process output is only affected by the various inputs.

2.3.3 Cartesian Force Analysis

In the case that external forces are presented in both x and y directions, the transfer function can be derived from equation (2-41). The following equation can be obtained through the basic physics

$$\begin{bmatrix} X \\ Y \end{bmatrix} = \mathbf{E}(s) \begin{bmatrix} F_x \\ F_y \end{bmatrix} \tag{2-44}$$

where $\mathbf{E}(s) = \begin{bmatrix} \dfrac{1}{m_{ex}s^2 + d_{ex}s + k_{ex}} & 0 \\ 0 & \dfrac{1}{m_{ey}s^2 + d_{ey}s + k_{ey}} \end{bmatrix}$, equation (2-41) can be further written as

$$\begin{bmatrix} F_x \\ F_y \end{bmatrix} = \{[\mathbf{H}(s) + \mathbf{B}(s)]\mathbf{J}^{-1}\mathbf{E}(s) + \mathbf{J}^T\}^{-1}\mathbf{A}(s) \begin{bmatrix} U_1 \\ U_2 \end{bmatrix} \tag{2-45}$$

Substituting **A**(s), **B**(s), **E**(s), **H**(s) and **J** into (2-45) arrives at

$$\begin{bmatrix} F_x \\ F_y \end{bmatrix} = \frac{1}{N_1N_4 - N_2N_3} \begin{bmatrix} T_1 & T_2 \\ T_3 & T_4 \end{bmatrix} \begin{bmatrix} U_1 \\ U_2 \end{bmatrix} \tag{2-46}$$

where

$$N_1 = [(H_{11}O_{11} + H_{12}O_{21} + m_{ex}P_{11})s^2 + (\hat{J}_1^2 d_1 O_{11} + d_{ex}P_{11})s + k_{ex}P_{11}](C_1 s + K_{p1}) + (A_{I1}^2 + A_{O1}^2)\hat{J}_1^2 O_{11}s$$

$$N_2 = [(H_{11}O_{12} + H_{12}O_{22} + m_{ey}P_{21})s^2 + (\hat{J}_1^2 d_1 O_{12} + d_{ey}P_{21})s + k_{ey}P_{21}](C_1 s + K_{p1}) + (A_{I1}^2 + A_{O1}^2)\hat{J}_1^2 O_{12}s$$

$$N_3 = [(H_{21}O_{11} + H_{22}O_{21} + m_{ex}P_{12})s^2 + (\hat{J}_2^2 d_2 O_{21} + d_{ex}P_{12})s + k_{ex}P_{12}](C_2 s + K_{p2}) + (A_{I2}^2 + A_{O2}^2)\hat{J}_2^2 O_{21}s$$

$$N_4 = [(H_{21}O_{12} + H_{22}O_{22} + m_{ey}P_{22})s^2 + (\hat{J}_2^2 d_2 O_{22} + d_{ey}P_{22})s + k_{ey}P_{22}](C_2 s + K_{p2}) + (A_{I2}^2 + A_{O2}^2)\hat{J}_2^2 O_{22}s$$

$$T_1 = N_4(m_{ex}s^2 + d_{ex}s + k_{ex})K_{u1}\hat{J}_1(A_{I1} + A_{O1})$$

$$T_2 = -N_2(m_{ex}s^2 + d_{ex}s + k_{ex})K_{u2}\hat{J}_2(A_{I2} + A_{O2})$$

$$T_3 = -N_3(m_{ey}s^2 + d_{ey}s + k_{ey})K_{u1}\hat{J}_1(A_{I1} + A_{O1})$$

$$T_4 = N_1(m_{ey}s^2 + d_{ey}s + k_{ey})K_{u2}\hat{J}_2(A_{I2} + A_{O2})$$

Clearly, (2-46) represents a 6th order system.

2.3.4 Cartesian Hybrid Position/Force Analysis

A common scenario that involves robotic force control is that force control is only performed along certain directions, while along other directions position control is required. Consider a two-link manipulator (see Fig. 2-6) which has two degree-of-freedom, the manipulator may be required to perform a task such that along one direction it is force controlled and along the other direction it is position controlled.

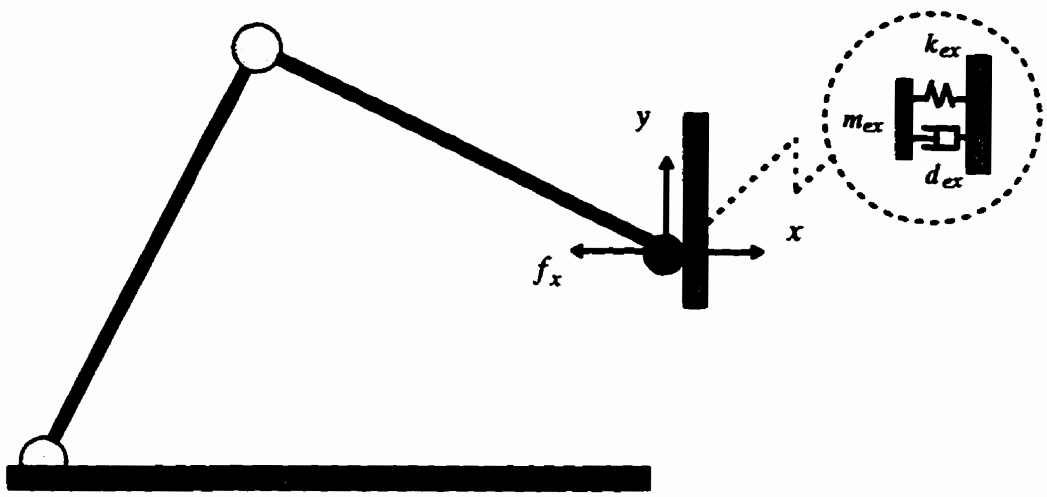

Fig. 2-6 Hybrid position/force control in two-link manipulator.

The end-effector applies a certain force along x-direction to the environment. At the same time, it follows a specified trajectory along the y-direction on the environment surface.

This section analyzes the system to find the s-domain transfer function relating the output vector $[F_x,\ Y]^T$ to the input vector $[U_1,\ U_2]^T$.

To eliminate F_y and X in (2-41), let $X = \dfrac{F_x}{m_{ex}s^2 + d_{ex}s + k_{ex}}$ and $F_y = 0$. Substituting them into (2-41) yields

$$\mathbf{J}^T \begin{bmatrix} F_x \\ 0 \end{bmatrix} + [\mathbf{H}(s) + \mathbf{B}(s)]\mathbf{J}^{-1} \begin{bmatrix} \dfrac{F_x}{m_{ex}s^2 + d_{ex}s + k_{ex}} \\ Y \end{bmatrix} = \mathbf{A}(s) \begin{bmatrix} U_1 \\ U_2 \end{bmatrix} \tag{2-47}$$

which is equivalent to

$$\mathbf{J}^T \begin{bmatrix} 1 & 0 \\ 0 & 0 \end{bmatrix} \begin{bmatrix} F_x \\ Y \end{bmatrix} + [\mathbf{H}(s) + \mathbf{B}(s)]\mathbf{J}^{-1} \begin{bmatrix} \dfrac{1}{m_{ex}s^2 + d_{ex}s + k_{ex}} & 0 \\ 0 & 1 \end{bmatrix} \begin{bmatrix} F_x \\ Y \end{bmatrix} = \mathbf{A}(s) \begin{bmatrix} U_1 \\ U_2 \end{bmatrix} \tag{2-48}$$

or

$$\{\mathbf{J}^T \begin{bmatrix} 1 & 0 \\ 0 & 0 \end{bmatrix} + [\mathbf{H}(s) + \mathbf{B}(s)]\mathbf{J}^{-1} \begin{bmatrix} \dfrac{1}{m_{ex}s^2 + d_{ex}s + k_{ex}} & 0 \\ 0 & 1 \end{bmatrix}\} \begin{bmatrix} F_x \\ Y \end{bmatrix} = \mathbf{A}(s) \begin{bmatrix} U_1 \\ U_2 \end{bmatrix} \tag{2-49}$$

Then it is easy to get

$$\begin{bmatrix} F_x \\ Y \end{bmatrix} = \{\mathbf{J}^T \begin{bmatrix} 1 & 0 \\ 0 & 0 \end{bmatrix} + [\mathbf{H}(s) + \mathbf{B}(s)]\mathbf{J}^{-1} \begin{bmatrix} \dfrac{1}{m_{ex}s^2 + d_{ex}s + k_{ex}} & 0 \\ 0 & 1 \end{bmatrix}\}^{-1} \mathbf{A}(s) \begin{bmatrix} U_1 \\ U_2 \end{bmatrix} \tag{2-50}$$

Simplifying equation (2-50) arrives at

$$\begin{bmatrix} F_x \\ y \end{bmatrix} = \frac{1}{W_1W_4 - W_2W_3} \begin{bmatrix} V_1 & V_2 \\ V_3 & V_4 \end{bmatrix} \begin{bmatrix} U_1 \\ U_2 \end{bmatrix} \tag{2-51}$$

where

$$W_1 = [(H_{11}O_{11} + H_{12}O_{21} + m_{ex}P_{11})s^2 + (\hat{J}_1^2 d_1 O_{11} + d_{ex}P_{11})s + k_{ex}P_{11}](C_1 s + K_{p1})$$
$$+ (A_{I1}^2 + A_{O1}^2)\hat{J}_1^2 O_{11} s$$

$$W_2 = [(H_{11}O_{12} + H_{12}O_{22})s^2 + \hat{J}_1^2 d_1 O_{12} s](C_1 s + K_{p1}) + (A_{I1}^2 + A_{O1}^2)\hat{J}_1^2 O_{12} s$$

$$W_3 = [(H_{21}O_{11} + H_{22}O_{21} + m_{ex}P_{12})s^2 + (\hat{J}_2^2 d_2 O_{21} + d_{ex}P_{12})s + k_{ex}P_{12}](C_2 s + K_{p2})$$
$$+ (A_{I2}^2 + A_{O2}^2)\hat{J}_2^2 O_{21} s$$

$$W_4 = [(H_{21}O_{12} + H_{22}O_{22})s^2 + \hat{J}_2^2 d_2 O_{22} s](C_2 s + K_{p2}) + (A_{I2}^2 + A_{O2}^2)\hat{J}_2^2 O_{22} s$$

$$V_1 = W_4(m_{ex}s^2 + d_{ex}s + k_{ex})K_{u1}\hat{J}_1(A_{I1} + A_{O1})$$

$$V_2 = -W_2(m_{ex}s^2 + d_{ex}s + k_{ex})K_{u2}\hat{J}_2(A_{I2} + A_{O2})$$

$$V_3 = -W_3 K_{u1}\hat{J}_1(A_{I1} + A_{O1})$$

$$V_4 = W_1 K_{u2}\hat{J}_2(A_{I2} + A_{O2})$$

Equation (2-51) suggests that the system is of 6th order.

2.4 SUMMARY

This chapter presented the dynamics of a two-link hydraulic manipulator in time domain. The system was then analyzed in *s*-domain with results of successful derivations of various transfer functions from system inputs to outputs. In a single link case, with the servovalve input voltage as the input, the system can be shown as a third order system when the angular displacement or the contact force is chosen to be system output. When both links are taken into account simultaneously, the process from the servovalve input voltage vector $[U_1, U_2]^T$ to the Cartesian coordinates of the end-effector $[X, Y]^T$ is a fifth order system. When the output is $[F_x, F_y]^T$ or $[F_x, Y]^T$, the system is of the order of six. These transfer functions found will be used in Chapters 4 and 5 to facilitate adaptive control of hydraulic manipulators using Generalized Predictive Control and Minimum Variance Control algorithms.

CHAPTER THREE

GENERALIZED PREDICTIVE AND MINIMUM VARIANCE ADAPTIVE CONTROLS

The last twenty years has witnessed a steady progress on the research of adaptive control. One can easily find a number of books describing various aspects of adaptive control [14, 15]. Together with the availability of more and more powerful microcomputers, the evolution of adaptive control techniques has led to a series of successful applications. In this chapter, a review is given on two control algorithms and one estimation algorithm. The two control algorithms are the Generalized Predictive Control (GPC) algorithm and the Minimum Variance Control (MVC) algorithm. The estimation algorithm described in this chapter is the popular Recursive Least Squares (RLS) technique.

3.1 GENERALIZED PREDICTIVE CONTROL ALGORITHM

Generalized Predictive Control (GPC) algorithm, developed by Clarke, *et al* [10, 11], predicts future outputs of a process for a sequence of future desired set points . A cost function that depends on the future output error and future process input is minimized to generate a set of optimized control increments. The method is known to be capable of stable control of processes with variable parameters and dead-time [10].

3.1.1 Single-Input Single-Output System

GPC strategy exploits one particular kind of linear plant model, *i.e.*, Controlled Auto-Regressive Integrated Moving Average (CARIMA) model:

$$A(q^{-1})y(t) = B(q^{-1})u(t-1) + \frac{\xi(t)}{\Delta} \tag{3-1}$$

where $A(q^{-1})$ and $B(q^{-1})$ are polynomials in the backward shift operator q^{-1}:

$$A(q^{-1}) = 1 + a_1 q^{-1} + \cdots + a_{n_a} q^{-n_a}$$

$$B(q^{-1}) = b_0 + b_1 q^{-1} + \cdots + b_{n_b} q^{-n_b}$$

$\xi(t)$ is an uncorrelated random sequence, and $\Delta = 1 - q^{-1}$ is the differencing operator. $u(t)$ and $y(t)$ are scalars representing the input and the output, respectively.

Solving the Diophantine identity, which is,

$$1 = E_j(q^{-1})A(q^{-1})\Delta + q^{-j}F_j(q^{-1}) \tag{3-2}$$

a *j*-step ahead prediction of $y(t+j)$ up to time t, i.e., $\hat{y}(t+j)$, is obtained

$$\hat{y}(t+j) = F_j(q^{-1})y(t) + E_j(q^{-1})B(q^{-1})\Delta u(t+j-1) + E_j\left(q^{-1}\right)\xi(t+j) \tag{3-3}$$

where $E_j(q^{-1}) = 1 + e_1q^{-1} + e_2q^{-2} + \cdots + e_{j-1}q^{-(j-1)}$ and $F_j(q^{-1}) = f_0 + f_1q^{-1} + f_2q^{-2} + \cdots + f_{n_a}q^{-n_a}$, which are both uniquely defined given $A(q^{-1})$ and the prediction interval *j*. Note that the values of $e_{i(i=1,\cdots,j-1)}$ and $f_{i(i=0,\cdots,n_a)}$ depend on the number of prediction steps, *j*.

Further, the coefficients in E_j and F_j are computed recursively as:

$$E_{j+1}(q^{-1}) = E_j(q^{-1}) + q^{-j}f_0 \tag{3-4a}$$

$$F_{j+1} = q[F_j(q^{-1}) - f_0A(q^{-1})\Delta] \tag{3-4b}$$

with initial condition:

$$E_1(q^{-1}) = 1 \tag{3-4c}$$

$$F_1(q^{-1}) = q[1 - A(q^{-1})\Delta] \tag{3-4d}$$

Since the disturbance consists only the unknown future values, the optimal predictor is:

$$\hat{y}(t+j) = F_j(q^{-1})y(t) + G_j(q^{-1})\Delta u(t+j-1) \tag{3-5a}$$

where

$$G_j(q^{-1}) = E_j(q^{-1})B(q^{-1}). \tag{3-5b}$$

Considering predictions at each of N steps into the future, the optimal predictor can also be written in the key vector form:

$$\hat{\mathbf{y}} = \mathbf{G}\mathbf{u} + \mathbf{f} \tag{3-6}$$

where vectors $\hat{\mathbf{y}} = [\hat{y}(t+1), \hat{y}(t+2), \cdots, \hat{y}(t+N)]^T$,

$\mathbf{u} = [\Delta u(t), \Delta u(t+1), \cdots, \Delta u(t+N-1)]^T$ and

$\mathbf{f} = [f(t+1), f(t+2), \cdots, f(t+N)]^T$.

Vector $\mathbf{f}$ is composed of signals which are known at time t. For example,

$$f(t+1) = [G_1(q^{-1}) - g_{10}]\Delta u(t) + F_1 y(t)$$

$$f(t+2) = q[G_2(q^{-1}) - q^{-1}g_{21} - g_{20}]\Delta u(t) + F_2 y(t)$$

$$\vdots$$

where $G_i(q^{-1}) = g_{i0} + g_{i1}q^{-1} + \cdots$, note $g_{i0} = g_{i1} = \cdots = g_{i(i-1)}$, or for short, $g_{ij} = g_j$, for $j = 0,1,2,\cdots,< i$, which is independent of the particular G polynomial. Therefore, G is a lower-triangular of dimension $N \times N$:

$$G = \begin{bmatrix} g_0 & 0 & \cdots & 0 \\ g_1 & g_0 & \cdots & 0 \\ \vdots & \vdots & \ddots & \vdots \\ g_{N-1} & g_{N-2} & \cdots & g_0 \end{bmatrix}$$

A cost function is chosen:

$$J(N1, N2, N_u) = E\{\sum_{j=N_1}^{N_2} [y(t+j) - w(t+j)]^2 + \sum_{j=1}^{N_u} \lambda(j)[\Delta u(t+j-1)]^2\} \tag{3-7}$$

where N_1 is the minimum output horizon, N_2 is the maximum output horizon, N_u is the control horizon, $\lambda(j)$ is a control weighting sequence which is usually set to a constant of λ, *y(t+j)* is the output *j*-step ahead and *w(t+j)* is the future set point.

Minimization of this equation yields the control increment vector:

$$\Delta\mathbf{u} = (\mathbf{G}^{\mathbf{T}}\mathbf{G} + \lambda\mathbf{I})^{-1}\mathbf{G}^{\mathbf{T}}(\mathbf{w} - \mathbf{f}) \tag{3-8}$$

The first element of vector $\Delta\mathbf{u}$ is $\Delta u(t)$, then the current control input is:

$$u(t) = u(t-1) + \Delta u(t) \tag{3-9}$$

GPC controller can be tuned by adjusting the values of parameters N_1, N_2, Nu and $\lambda(j)$.

N_1 is the ***minimum output horizon.*** If the system has a time delay of k sampling periods, then a control signal will not go into effect earlier. It is not necessary to bring the control signal into consideration in equation (3-7) before it has impact on the system. Thus, in order to save computation load, N_1 is normally set to k. If k is not known or is variable, then N_1 can be set to 1 with no loss of stability.

N_2 is the ***maximum output horizon.*** Both parameters N_1 and N_2 are used in equation (3-6) in which the number of prediction steps j vary from N_1 to N_2 and then used in calculating the control law (3-9). In other words, $(N_2 - N_1)$ is the number of the future response errors that are to be minimized in the cost function. Generally speaking, the system response is more stable if more future control increments are taken into minimization.

Nu is the *control horizon*. GPC technique assumes that after $Nu < N_2$ number of time steps, the control signal is held constant. Based on this assumption, the number of future control increments to be calculated is reduced from $(N_2 - N_1)$ to Nu in order to reduce the computational load when Nu is much smaller than $N_2 - N_1$. In equation (3-8), $\mathbf{G}$ is a $(N_2 - N_1) \times Nu$ matrix, $(\mathbf{G}^T\mathbf{G} + \lambda\mathbf{I})$ is a $Nu \times Nu$ matrix. The computation of inverting a $Nu \times Nu$ matrix involves solving $\Delta\mathbf{u}$. Usually, Nu is set to 1 for stable plants [10]. Plants can have delay or can be non-minimum phase ones. If $Nu = 1$, inverting a matrix is reduced to finding the inverse of a scalar. $\lambda(j)$ is the control weighting sequence which acts as a damping agent for the system.

3.1.2 Multiple-Input Multiple-Output System

The multiple-input multiple-output (MIMO) solution of a GPC algorithm [16] is basically the same as the SISO case except that the plant model (3-1) should be modified as:

$$\mathbf{A}(q^{-1})\mathbf{y}(t) = \mathbf{B}(q^{-1})\mathbf{u}(t-1) + \frac{\xi(t)}{\Delta} \qquad (3\text{-}10)$$

where $\mathbf{y}(t)$, $\mathbf{u}(t)$ and $\xi(t)$ are now p-dimensional vectors denoting a p-input p-output system. $\mathbf{A}(q^{-1})$ and $\mathbf{B}(q^{-1})$ are p-dimensional matrices of which each element is a polynomial in q^{-1}.

Considering predictions at each of N steps into the future, the j-step ahead predictor is

$$\hat{\mathbf{y}} = \mathbf{gu} + \mathbf{f} \tag{3-11}$$

where $\hat{\mathbf{y}} = [\hat{y}_1(t+1),\cdots,\hat{y}_p(t+1),\hat{y}_1(t+2),\cdots,\hat{y}_p(t+N)]^T{}_{1\times pN}$

$$\hat{\mathbf{u}} = [\Delta u_1(t),\cdots,\Delta u_p(t+1),\Delta u_1(t+1),\cdots,\Delta u_p(t+N-1)]^T{}_{1\times pN}$$

$$\mathbf{f} = [f_1(t+1),\cdots,f_p(t+1),f_1(t+2),\cdots,f_p(t+N)]^T{}_{1\times pN}$$

$$\mathbf{g} = \begin{bmatrix} G_1 & O & O & \cdots \\ G_2 & G_1 & O & \cdots \\ \vdots & \vdots & \ddots & \vdots \\ G_N & G_{N-1} & G_{N-2} & \cdots \end{bmatrix}$$

where G_j is the jth step response coefficient matrix of the transfer function matrix, O is a null matrix of dimension $p \times p$.

The cost function is

$$J = E\{\sum_{i=1}^{p}[\sum_{j=1}^{N}\mu_i(j)[y_i(t+j) - w_i(t+j)]^2 + \sum_{j=1}^{N_u}\lambda_i(j)[\Delta u_i(t+j-1)]^2]\} \tag{3-12}$$

where $\mu_i(j) = \begin{Bmatrix} 1, \ j \in [N_{1i}, N_{2i}] \\ 0, \ \text{otherwise} \end{Bmatrix}$, $N = \max\{N_{21}, N_{22},\cdots,N_{2p}\}$. The control weighting sequence $\lambda_i(j)$ is usually set to a constant, λ_i.

Minimizing the cost function gives the following control signal,

$$\Delta\mathbf{u}(t) = \begin{bmatrix}\mathbf{I} & \mathbf{O} & \cdots & \mathbf{O}\end{bmatrix}(\mathbf{g}^T\mathbf{g} + \Lambda)^{-1}\mathbf{g}^T(\mathbf{w} - \mathbf{f}) \tag{3-13}$$

where control weighting matrix $\Lambda = \text{diag}\{\lambda_1\cdots\lambda_p\cdots\lambda_1\cdots\lambda_p\}_{pN_u \times pN_u}$, and set point vector

$\mathbf{w} = [w_1(t+1),\cdots,w_p(t+1),w_1(t+2),\cdots,w_p(t+N)]^T{}_{1\times pN}$

3.2 MINIMUM VARIANCE CONTROL ALGORITHM

The well known Minimum Variance Control (MVC) algorithm has many existing applications. In the field of robotics, Koivo *et al* [17] introduced an approach into the motion control of manipulators. In 1990, Sepehri *et al* [7] applied MVC technique to the motion control of hydraulically-actuated manipulators. MVC algorithm in references [17] and [7] assumes an auto-regressive plant model of the form

$$A(q^{-1})y(t) = B(q^{-1})u(t-1) + h(t) + \xi(t) \tag{3-14}$$

where $A(q^{-1})$ and $B(q^{-1})$ are polynomials in the backward shift operator q^{-1}:

$$A(q^{-1}) = 1 + a_1 q^{-1} + \cdots + a_{n_a} q^{-n_a}$$

$$B(q^{-1}) = b_0 + b_1 q^{-1} + \cdots + b_{n_b} q^{-n_b}$$

and $\xi(t)$ is an uncorrelated random sequence, while *h(t)* here is a forcing term that includes the effects of the gravitational forces. Note in the above model a dealy of 1 sampling period has been assumed.

The above model can alternatively be rearranged to form the following relation

$$y(t) = \hat{\theta}^T(t)\phi(t-1) + \xi(t) \tag{3-15}$$

where $\hat{\theta}^T(t)$ is a parameter vector which is usually obtained by on-line estimation. Vector $\phi(t-1)$ contains the information of system input and output up to time *t*-1, *i.e.*, $\hat{\theta}^T(t) = [a_1, \cdots, a_{n_a}, b_0, \cdots, b_{n_b}, h(t)]$, $\phi(t-1) = [y(t-1), \cdots, y(t-n_a), u(t-1), \cdots, u(t-n_b), 1]$.

A cost function is then chosen as

$$J = E\{\| y(t+1) - y^d(t+1)\|_Q^2 + \|u(t)\|_R^2\} \tag{3-16}$$

where $\|\|_R$ indicates the norm with weight R, *i.e.*, $\|u\|_R^2 = u^T Ru$, and R is a positive semi-definite symmetric matrix; Q is a positive definite symmetric weighting matrix. $y(t+1)$ is the optimal prediction of the system output at time $t+1$, which is calculated as following based on the information up to time t-1,

$$\hat{y}(t+1) = \hat{\theta}^T(t-1)\phi(t-1) \tag{3-17}$$

The control which minimizes (3-16) is determined by

$$Ru(t) + b_0 Q[\hat{y}(t+1) - y^d(t+1)] = 0 \tag{3-18}$$

3.3 RECURSIVE LEAST SQUARES ALGORITHM

In this thesis, the applications of GPC and MVC algorithms to the control of hydraulic manipulators fall in the category called indirect adaptive control. This means the parameters of plant model are to be first estimated on-line, then a control signal is calculated based on the current plant model. Least squares method is a widely used method for such estimation. For on-line applications, the recursive algorithm of least squares (RLS) method has been developed as [18]

$$\hat{\theta}(t) = \hat{\theta}(t-1) + \mathrm{L}(t)[y(t) - \hat{\theta}^T(t-1)\Phi(t)] \tag{3-19a}$$

$$\mathbf{L}(t) = \frac{\mathbf{P}(t-1)\mathbf{\Phi}(t)}{\lambda(t) + \mathbf{\Phi}^{\mathbf{T}}(t)\mathbf{P}(t-1)\mathbf{\Phi}(t)} \tag{3-19b}$$

$$\mathbf{P}(t) = [\mathbf{P}(t-1) - \frac{\mathbf{P}(t-1)\mathbf{\Phi}(t)\mathbf{\Phi}^{\mathbf{T}}(t)\mathbf{P}(t-1)}{\lambda(t) + \mathbf{\Phi}^{\mathbf{T}}(t)\mathbf{P}(t-1)\mathbf{\Phi}(t)}] / \lambda(t) \tag{3-19c}$$

where $\hat{\theta}^T(t)$ is the parameter vector to be estimated, $\Phi(t)$ is the regression vector which is known, *y(t)* is the current scalar observation. The presentation of $\lambda(t)$ in equations (3-19) allows the method to track the variation of the time varying properties of the system if $\lambda(t)$ is chosen less than 1. This is handled in a natural way by assigning less weight to older measurements that are no longer representatives for this system. Since equations (3-19) are derived from the minimization of

$$J(\theta) = \sum_{t=1}^{N} \lambda^{N-t} [y(t) - \mathbf{\Phi}^{\mathbf{T}}(t)\theta]^2 \tag{3-20}$$

If the $\lambda(t)$ is chosen to a constant equal to $\lambda < 1$, the λ is called the *forgetting factor*.

In digital implementation the RLS method given in equations (3-19) may not guarantee positivity of the so called covariance matrix **P**(t) due to the unavoidable computer round-off errors. This is because some important information may be lost between each identification due to universal round-off errors specially for high sampling frequencies. There exist two algorithms to recover from this problem and to ensure the positivity of the covariance matrix:

a) Peterka's Square Root Algorithm

b) Bierman's U-D factorization method

Bierman's U-D factorization method [19] is used in this thesis to update the covariance matrix **P**(t) in such a way that **P**(t) can be uniquely factored as $\mathbf{P}=\mathbf{UDU}^{\mathbf{T}}$ in which 'U' is an upper triangular matrix and 'D' is a diagonal matrix. **P**(t) can then be updated by updating **U** and **D** to ensure a stable numerical calculation and speed up the computational process. Given a prior covariance $\tilde{\mathbf{P}}=\tilde{\mathbf{U}}\tilde{\mathbf{D}}\tilde{\mathbf{U}}^{\mathbf{T}}$, the scalar observation $z=\Phi^{\mathbf{T}}(k)\theta(k)+v(k)$ and the mathematics expectation $E[v(k)^2]=R$, the Kalman gain **K** and the updated covariance factors $\hat{\mathbf{U}}$ and $\hat{\mathbf{D}}$ can be obtained from the following algorithm:

$$\mathbf{f}=\tilde{\mathbf{U}}^{\mathbf{T}}\Phi, \mathbf{f}^{\mathbf{T}}=(f_1\cdots f_n) \tag{3-21a}$$

$$\mathbf{v}=\tilde{\mathbf{D}}\mathbf{f}, \qquad v_j=\tilde{d}_j f_j, \quad j=1 \ldots n \tag{3-21b}$$

$$\hat{d}_1=\tilde{d}_1 R/\alpha_1, \qquad \alpha_1=R+v_1 f_1 \tag{3-21c}$$

$$\mathbf{K}^{\mathbf{T}}{}_2=(v_1 0\cdots 0) \tag{3-21d}$$

for j=2,...,n recursively cycle through equations:

$$\alpha_j=\alpha_{j-1}+v_j f_j, \qquad \hat{d}_j=\tilde{d}_j\alpha_{j-1}/\alpha_j \tag{3-21e}$$

$$\hat{u}_j=\tilde{u}_j+\lambda_j k_j, \qquad \lambda_j=-f_j/\alpha_{j-1} \tag{3-21f}$$

$$K_{j+1}=k_j+v_j\tilde{u}_j \tag{3-21g}$$

where $\tilde{\mathbf{U}}=[\tilde{u}_1\cdots\tilde{u}_n]$, $\hat{\mathbf{U}}=[\hat{u}_1\cdots\hat{u}_n]$, $K=K_n/\alpha_n$.

It is well known that sufficient excitation is vitally important to a correct estimation. If the control signal ceases to be general enough, the elements of **P(t)** start to increase exponentially with the rate of $1/\lambda(t)$. A technique called ***Regularization*** [18] is then taken as a counter-measure. ***Regularization*** of U-D factorization method can be easily incorporated as [18]

$$d_i = \min(c_i, d_i) \tag{3-22}$$

where c_i is a positive number that bounds d_i, the element of **D**.

3.4 SUMMARY

- GPC algorithm is related to the linear quadratic control strategy in the sense that the objective is to find value for $u(t)$ which minimize a quadratic cost function. The robustness of a generalized predictive controller is gained through minimizing a multi-step cost function. The inherent integral action of GPC guarantees an off-set free performance. However, the relationship between the desired performance and the values of design parameters is not clear.

- Similar to a GPC algorithm, MVC also minimizes a quadratic cost function. There is no integral property inside the algorithm. The algorithm has been extensively studied and has been reported quite successful in many applications.

CHAPTER FOUR

POSITION CONTROL OF A TWO-LINK HYDRAULIC MANIPULATOR

The highly nonlinear and time varying properties in a hydraulically actuated manipulator requires special treatment to achieve good performance during a position control. This chapter which consists of two parts is dedicated to the position control of hydraulic manipulators. The first part studies a joint position control, where each link of a two-link planar rigid hydraulic manipulator is viewed to be independent from the other. Both GPC and MVC algorithms are examined. The second part is dedicated to multi-link position control. In the case of two-link hydraulic manipulator, it means to control both links simultaneously by taking into account the interaction between links and, therefore, seeing the manipulator as a whole single system, *i.e.*, a two-input two-output multivariable system. Only GPC algorithm is applied to this case.

4.1 MANIPULATOR SPECIFICATIONS

As shown in Fig. 2-1, the manipulator used in the simulation in the thesis is a two-link rigid planar robotic manipulator powered by two closed-center, constant-supply-pressure hydraulic actuators. Table 4-1 lists the link and the actuator specifications.

Table 4-1 Link and actuator specifications

Link 1 / Actuator 1	**Link 2 / Actuator 2**
$l_1 = 1.0$ m	$l_2 = 1.0$ m
$m_1 = 20$ kg	$m_2 = 20$ kg
Center of Gravity at 0.5 m	Center of Gravity at 0.5 m
$\theta_1 \in [\ 33.26°,\ 115.6°\ ]$	$\theta_2 \in [\ -125.0°,\ -35.00°\ ]$
$A_{I1} = 3.12\times10^{-3}\ \mathrm{m}^2$	$A_{I2} = 1.90\times10^{-3}\ \mathrm{m}^2$
$A_{O1} = 2.12\times10^{-3}\ \mathrm{m}^2$	$A_{O2} = 1.40\times10^{-3}\ \mathrm{m}^2$
$l_{p1} = 0.22$ m	$l_{p2} = 0.75$ m
$l_{r1} = 0.80$ m	$l_{r2} = 0.20$ m
$K_1 = 0.03\sqrt{\mathrm{m}^3/\mathrm{kg}}$	$K_2 = 0.03\sqrt{\mathrm{m}^3/\mathrm{kg}}$
$w_1 = 0.01$ m	$w_2 = 0.01$ m
$C_1 = 2.2\times10^{-12}\ \mathrm{m}^5/\mathrm{N}$	$C_2 = 2.2\times10^{-12}\ \mathrm{m}^5/\mathrm{N}$

$d_1 = 8000.0$ N·s/rad	$d_2 = 8000.0$ N·s/rad
$P_s = 6204.6$ kPa	$P_s = 6204.6$ kPa
$x_{v1} \in [-5\text{mm}, 5\text{mm}]$	$x_{v2} \in [-5\text{mm}, 5\text{mm}]$
$P_r = 0.0$ kPa	$P_r = 0.0$ kPa

A computer program in C code was written to simulate the control system. Non-linearities such as interaction between links, gravity term, saturation of on variables, the hydraulic system, *etc.*, were incorporated.

4.2 SINGLE-LINK POSITION CONTROL

Adaptive position control using GPC and MVC algorithms is studied in the following, and comparison is made between the two algorithms through computer simulations.

4.2.1 GPC Implementation

The control scheme of GPC implementation is shown in Fig. 4-1, which is in the category of indirect adaptive control.

Referring to Fig. 4-1, θ_i is the joint displacement of link i, u_i is the control voltage. To implement GPC strategy, it is required to model the hydraulic manipulator in the form of

$$A(q^{-1})\theta_i(t) = B(q^{-1})u_i(t) + e(t) \tag{4-1}$$

The degrees of $A(q^{-1})$ and $B(q^{-1})$ are to be found. The s-domain transfer function of Θ_i over U_i was previously found in equation (2-16) which is re-written here again as equation (4-2):

$$\frac{\Theta_i(s)}{U_i(s)} = \frac{K_{ui}(A_{Ii} + A_{Oi})\hat{J}_i}{H_{ii}C_i s^3 + (\hat{J}_i^2 d_i C_i + K_{pi}H_{ii})s^2 + \hat{J}_i^2(d_i K_{pi} + A_{Ii}^2 + A_{Oi}^2)s} \tag{4-2}$$

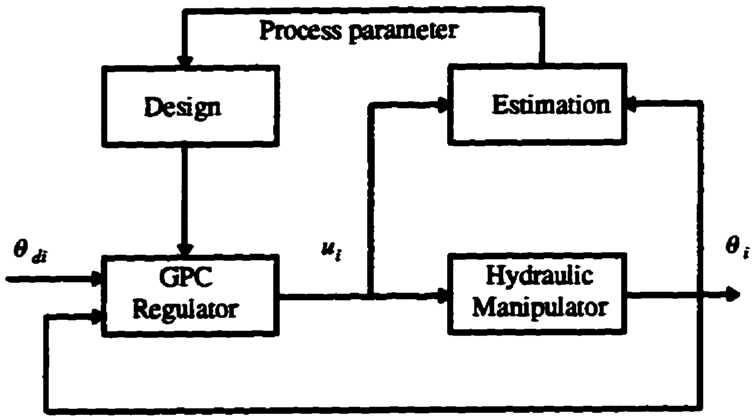

Fig. 4-1 Single link GPC system; position control.

The z-transform of equation (4-2) with zero order holder is of the form

$$\frac{\Theta_i(z)}{u_i(z)} = \frac{b_{i0}z^{-1} + b_{i1}z^{-2} + b_{i2}z^{-3}}{1 + a_{i1}z^{-1} + a_{i2}z^{-2} + a_{i3}z^{-3}} \tag{4-3}$$

In other words, it is a third order system and the output in discrete time form is

$$\begin{aligned}\theta_i(t) = &-a_{i1}\theta_i(t-1) - a_{i2}\theta_i(t-2) - a_{i3}\theta_i(t-3) \\ &+ b_{i0}u_i(t-1) + b_{i1}u_i(t-2) + b_{i2}u_i(t-3) + h_i(t)\end{aligned} \tag{4-4}$$

Here $h_i(t)$ is added as a forcing term to look after the nonlinear effects such as gravitational force.

To find the best values for the coefficients of $A(q^{-1})$ and $B(q^{-1})$, in the sense of minimum squared errors, the RLS algorithm is used to perform the on-line estimation based on the input-output data pairs, *i.e.*, $u_i - \theta_i$ pairs. From (4-4) it is clear that seven parameters are to be estimated.

The design block is to update polynomials of $E(q^{-1})$, $F(q^{-1})$ and $G(q^{-1})$ using equations (3-4) and (3-5b). The control increment to be applied to the actuator at time t is calculated according to equation (3-8) and (3-9).

The RLS algorithm was a translation from Astrom's PASCAL code [20]. In the computer simulation, the input signal was the spool displacement of the hydraulic actuator of link 2 instead of the servovalve input voltage u_2. Because the spool displacement was proportional to u_2, it did not change the order of the system but only added a constant coefficient to the system transfer function, equation (4-2). The spool displacement was within the range of [-5mm, 5mm]. The sampling time T was chosen to be 0.001s.

If all the coefficients in equation (4-2) are known, the values of the parameters could be obtained mathematically by taking a z-transformation of (4-2). As a matter of fact, in the computer simulation case the parameters can be found easily as following given the operating point. In the computer simulation, link 1 and 2 were initially set to 60 and -60 degrees, respectively. It was found that around the operating point ($\theta_1 = 60°$, $\theta_2 = -60°$) the spool displacement was 0mm, the supply line pressure was 2.2689×10^6Pa and the return line pressure was 2.3020×10^6Pa. Knowing these, all the parameters in equation (4-2)can be calculated as listed in Table 4-2.

Table 4-2 Parameter values in s-domain transfer function

Parameters	Values	Source
A_{I2}	1.90×10^{-3} m^2	Table 4-1
A_{O2}	1.40×10^{-3} m^2	Table 4-1
$\hat{J}_2$	0.19914 m/rad	Equation (2-6)
K_{u2}	0.54176 m^4/s	Equation (2-10c)
K_{p2}	0.0 m^5/N·s	Equation (2-10c)
H_{22}	6.6667 m·N·s^2 / rad	Equation (2-3)
C_2	2.2×10^{-12} m^5/N	Table 4-1
d_2	8000.0 N·s/rad	Table 4-1

Using the parameters in Table 4-2, for link 2, equation (4-2) is re-written as:

$$\frac{\Theta_2(s)}{U_2(s)} = \frac{2.6182\times10^{-4}}{1.2491\times10^{-7}s + 3.9468\times10^{-10}s^2 + 1.4667\times10^{-11}s^3} \tag{4-5}$$

Taking a z-transformation of the above equation with a zero order holder gives us:

$$\frac{\Theta_2(z)}{U_2(z)} = \frac{0.0030z^{-1} + 0.0117z^{-2} + 0.0029z^{-3}}{1 - 2.9651z^{-1} + 2.9385z^{-2} - 0.9734z^{-3}} \tag{4-6}$$

or

$$a_1 = -2.9651,\ a_2 = 2.9385,\ a_3 = -0.9734,\ b_0 = 0.0030,\ b_1 = 0.0117,\ b_2 = 0.0029 \tag{4-7}$$

Here, for simplicity a_{2i} and b_{2i} are denoted as a_i and b_i, respectively.

The parameter values in (4-7) could have been used as initial values for the on-line estimator. However, those values were only used later for the verification of the on-line estimation. Instead, the initial values of them were assigned as:

$$a_1 = 0,\ a_2 = 0,\ a_3 = 0,\ b_0 = 1,\ b_1 = 0,\ b_2 = 0,\ h = 0 \tag{4-8a}$$

There were two reasons that the initial values were set as in (4-8a): first, by doing so the controller was given no prior information about the plant, therefore, the adaptability could be well tested; secondly, in practice some parameter values listed in Table 4-1 may not be available and, hence, the initial values could not be obtained by this method.

The design parameters of GPC include N_1, N_2, N_u and λ_c which are called ***minimum output horizon, maximum output horizon, control horizon*** and ***control weighting factor***, respectively. Further, as will be demonstrated, in order to achieve good results, the control input value needs to be scaled by a factor called ***control relaxing factor***, λ_r. λ_r is defined as $\Delta u_i = \lambda_r \times \Delta u_i$. For the on-line estimator, the forgetting factor λ_f is also to be tuned.

The best step response was achieved, based on trial and error, using the following parameter setting for link 2:

$$N_1=1,\ N_2=40,\ N_u=1,\ \lambda_c=1000,\ \lambda_r=0.4,\ \lambda_f=0.99 \qquad (4\text{-}8b)$$

Figure 4-2 shows the joint displacement and the control input results. The response was fast, overshoot free and offset free despite the different scales of set-points. Fig. 4-3 shows the performance of the on-line estimator. The parameters converged after 1.8th second and roughly remained constant. It is clear that the estimation was consistent with the values obtained in (4-7). Before the model was correctly established at $t = 1.8$second, the response was oscillatory, which clearly showed how the on-line estimation helped the control performance.

Tests were also carried out to study the effects that the design parameters might have on the controller performance. Using (4-8) as the standard parameter setting, the tests were carried out in such a way that only one parameter's value was changed at a time. See Table 4-3 for a summarized description. In the study, we assumed to have no knowledge about the delay of the system, and, therefore, N_1 was simply set to 1.

To verify the robustness of the GPC controller, two more tests were done. The first one was with load changing suddenly from 0kg to 40kg at $t = 4$second and changing back to 0kg at $t = 8$second. The second one was with the hydraulic compliance of the actuator changing from 2.2×10^{-12} m^5 / N to 4.4×10^{-11} m^5 / N at $t = 4$second and changing

Table 4-3 Step responses with different system design parameter settings

Figure number	**Parameter setting**	**Remarks**
Fig. 4-2/4-3	Standard (4-8)	Fast response, no overshoot, no steady state error
Fig. 4-4	N_2 changed to 20 and then 80	Smaller N_2 resulted in a faster response with overshoot while larger N_2 produced a sluggish response
Fig. 4-5	N_u changed to 4	Faster response with overshoot
Fig. 4-6	λ_c changed to 100 and then 20000	Larger λ_c resulted in a response with overshoot and oscillation
Fig. 4-7	λ_r changed to 0.5 and then 0.1	Larger λ_r led to a stronger control action which may worse the response when the plant model was not completely identified; smaller λ_r resulted in a response with overshoot and oscillation
Fig. 4-8	λ_f changed to 0.95	Smaller λ_f made the parameter converge faster and the response became more sensitive to error

again at $t = 8$second to $1.1\times10^{-14}\ \mathrm{m}^5/\mathrm{N}$. Figure 4-9 shows the result when the load was changed. The controller rejected the load disturbance immediately, and it was interesting to see that the response with the 40kg load was as good as the response without load. Similar observation can be made when the hydraulic compliance was changed (see Fig. 4-10).

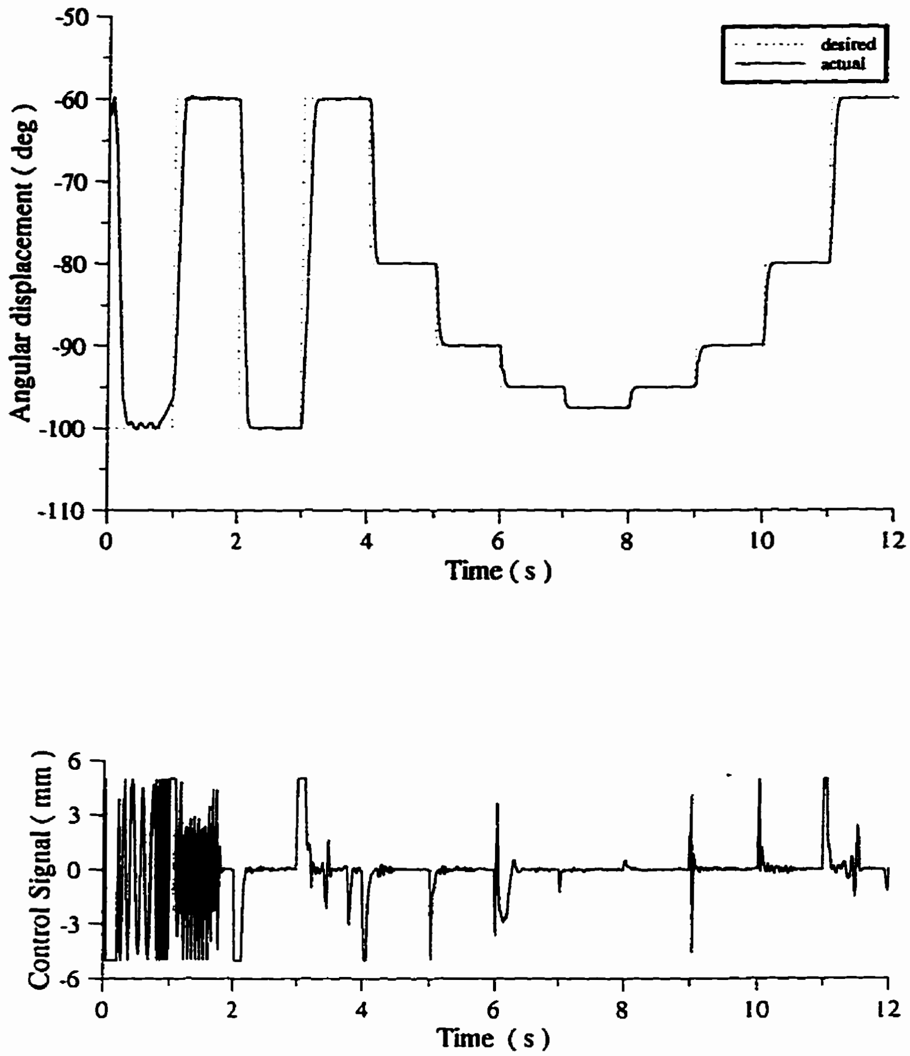

Fig. 4-2 Joint displacement and control input with $N_1=1$.

$N_2=40$, $N_u=1$, $\lambda_c=1000$, $\lambda_r=0.4$, $\lambda_f=0.99$.

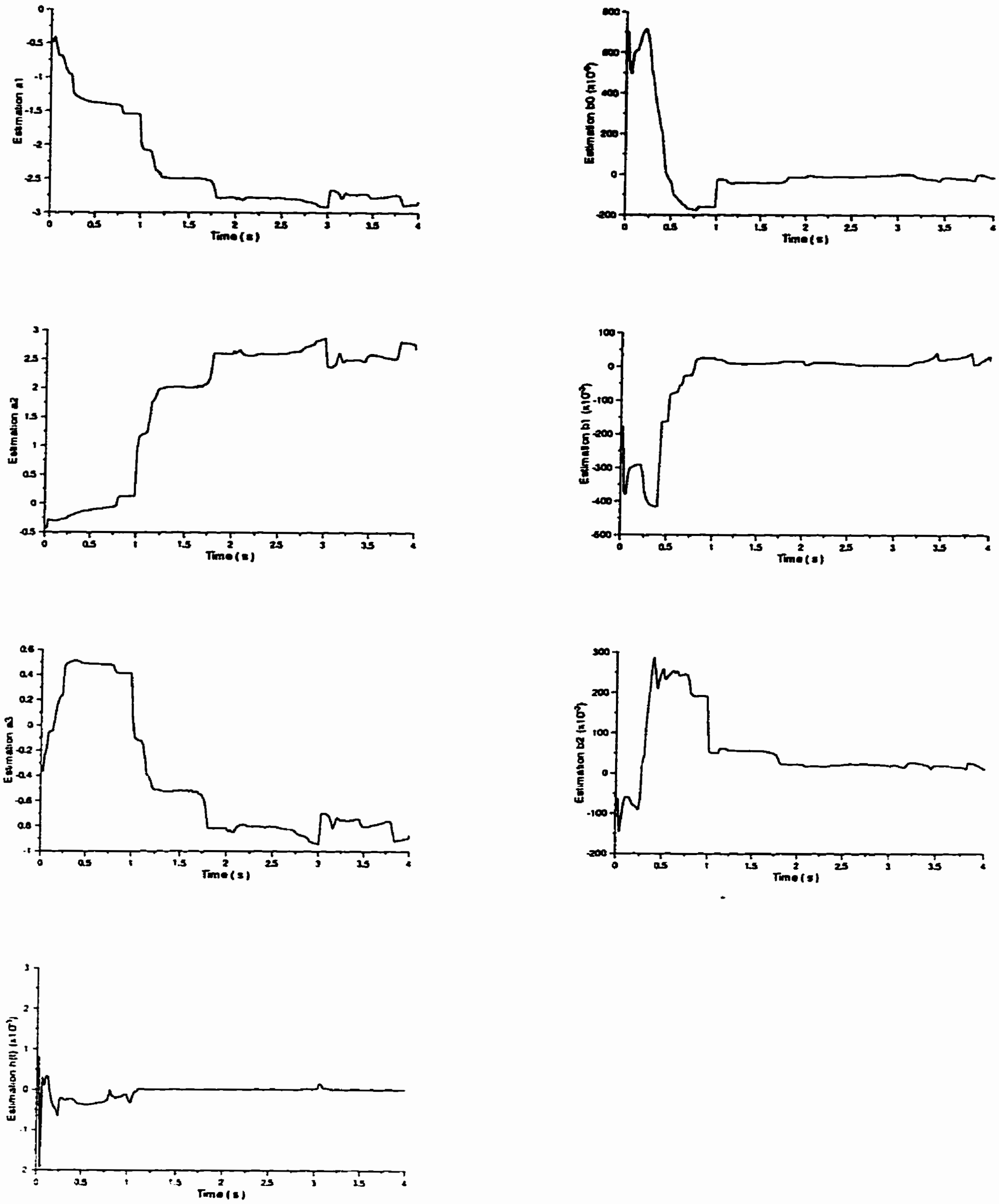

Fig. 4-3 Parameter estimation pertaining to Fig. 4-2.

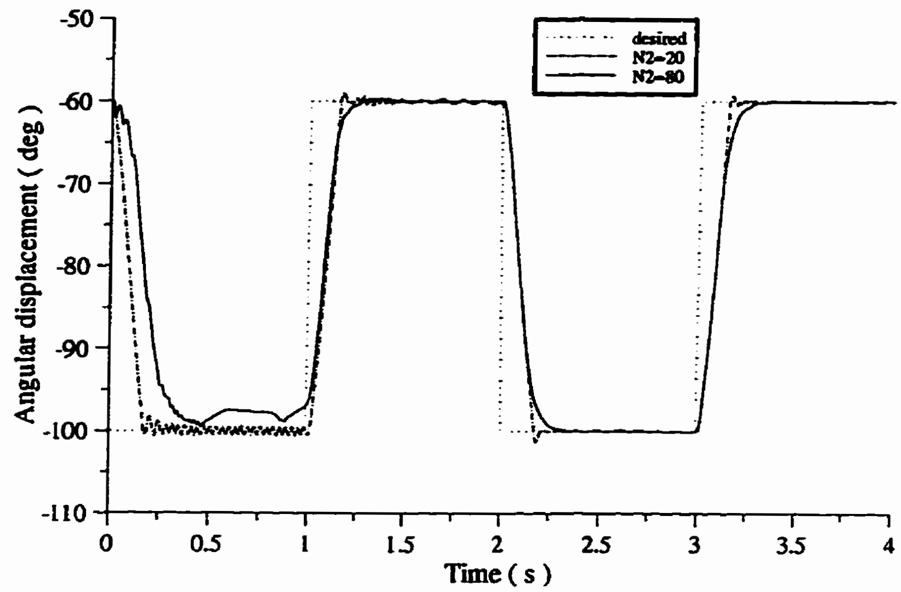

Fig. 4-4 Joint displacement responses with various N_2.

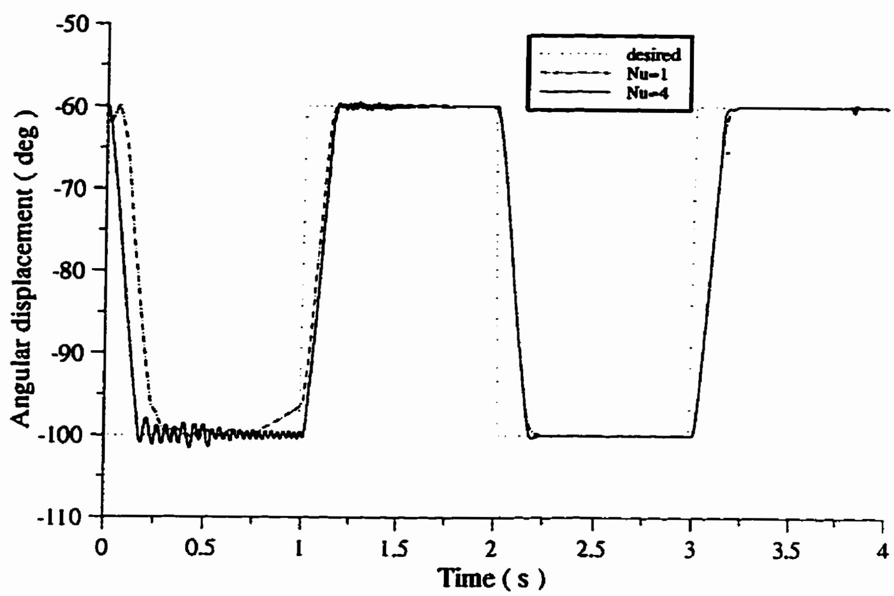

Fig. 4-5 Joint displacement response with $N_u = 4$.

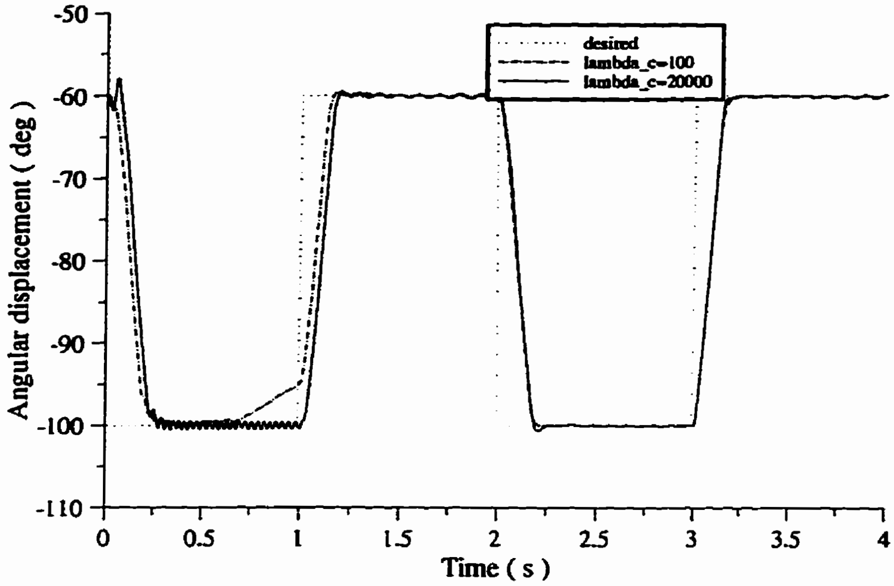

Fig. 4-6 Joint displacements response with various λ_c.

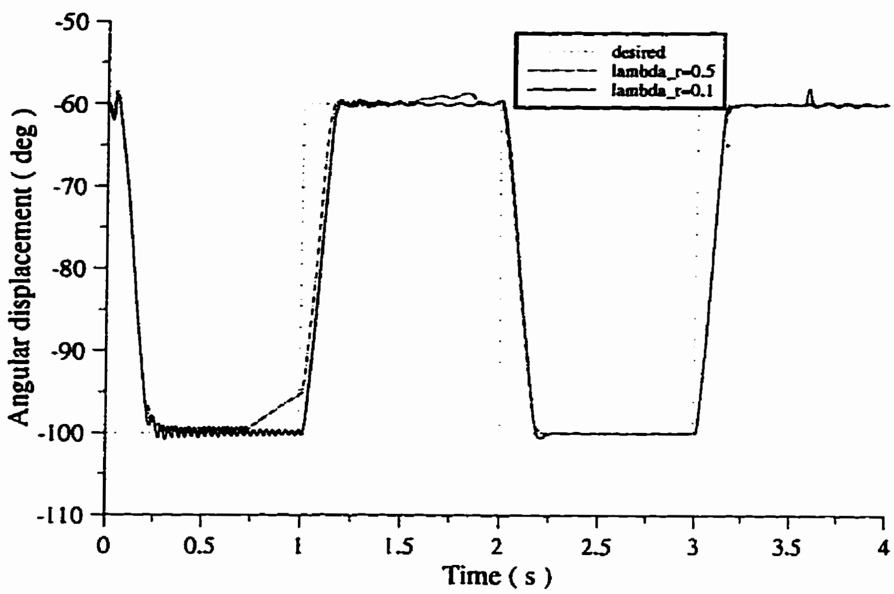

Fig. 4-7 Joint displacements response with various λ_r.

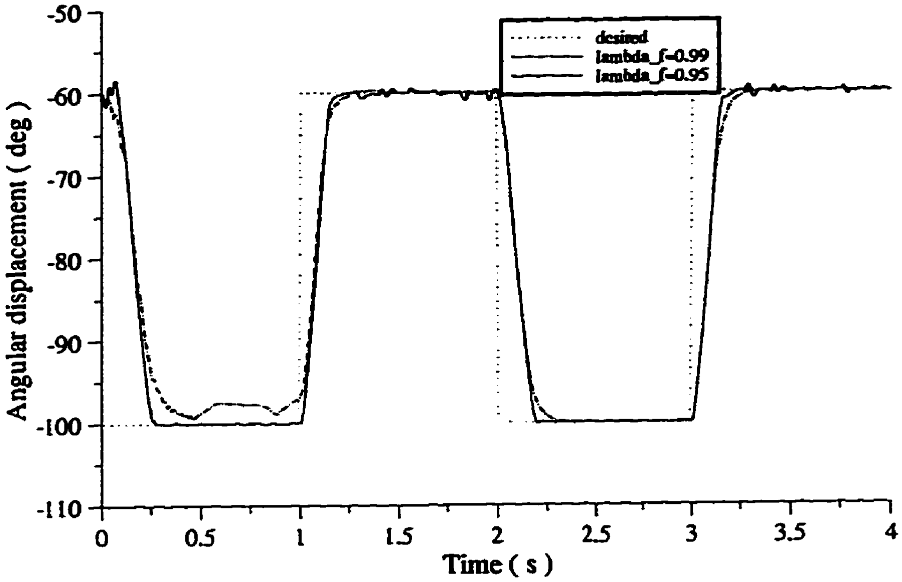

Fig. 4-8 Joint displacement response with $\lambda_f = 0.95$.

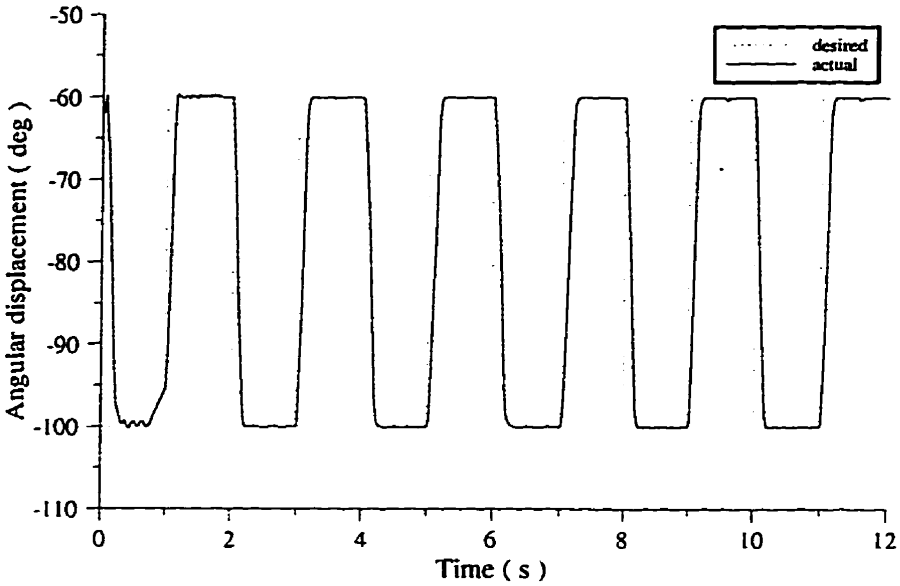

Fig. 4-9 Joint displacement responses with varying load.

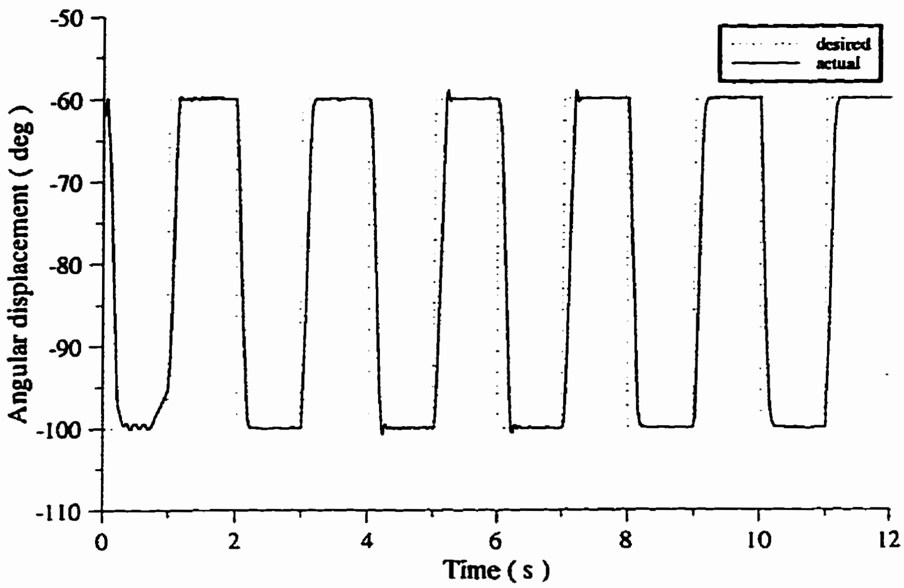

Fig. 4-10 Joint displacement responses with varying hydraulic compliance.

GPC also demonstrated good capability to track a specified the trajectory. Figures 4-12 and 4-13 show the tracking errors and control signals for the ramp and the cosine set-points shown in Fig. 4-11. respectively. Due to the inherent integral action of the controller, there was no steady state error for the ramp input response. The parameter settings were exactly the same as those in (4-8).

Tests were also carried out to see how well the GPC could perform when two links were controlled simultaneously. Figure 4-14 shows the joint displacements of both links. The design parameters and initial plant model parameters of link 2 were previously given in (4-8). For link 1. the initial values of the plant model were:

$$a_1 = 0,\ a_2 = 0,\ a_3 = 0,\ b_0 = 1,\ b_1 = 0,\ b_2 = 0,\ h = 0 \tag{4-9a}$$

Here, for clarity a_{1i}, b_{1i} and h_1 are denoted as a_i, b_i and h, respectively.

The design parameters of link 1 were:

$$N_1 = 1,\ N_2 = 60,\ N_u = 1,\ \lambda_c = 3000,\ \lambda_r = 0.4,\ \lambda_f = 0.99 \tag{4-9b}$$

Figure 4-15 indicates a good performance of the controllers for both links. The small fluctuations during the steady state implies that the interaction between links did have impact on the response.

Using the parameter setting given by (4-8) and (4-9), the manipulator was also commanded to follow a square trajectory in the Cartesian space. The length of each side of the square equaled to 0.5 meter. The initial position of the end point was 0.256m upper and 0.342m left to the upper-left corner of the square. At the very beginning a step set-point was given for each link so that the end point was controlled to reach the upper-left corner of the square and stay there during the first two seconds. From 3rd second the manipulator followed the trajectory and reached the lower-right corner at 12th second and picked up a load of 40kg. Then it took another 10 seconds to move back to the upper-left corner via the lower-left one.

With reference to Fig. 4-16, two points can be made regarding the end point response: firstly, the deviation from the desired trajectory might be caused by the dynamic coupling between the links; secondly, it is seen that the trajectory portion with 40kg load is better than the part without load. This phenomenon is caused by high supply pressure, which has been determined so that it could handle heavy loads [7]. Figure 4-17 shows the joint displacement of both links, and this concludes all the tests in this section.

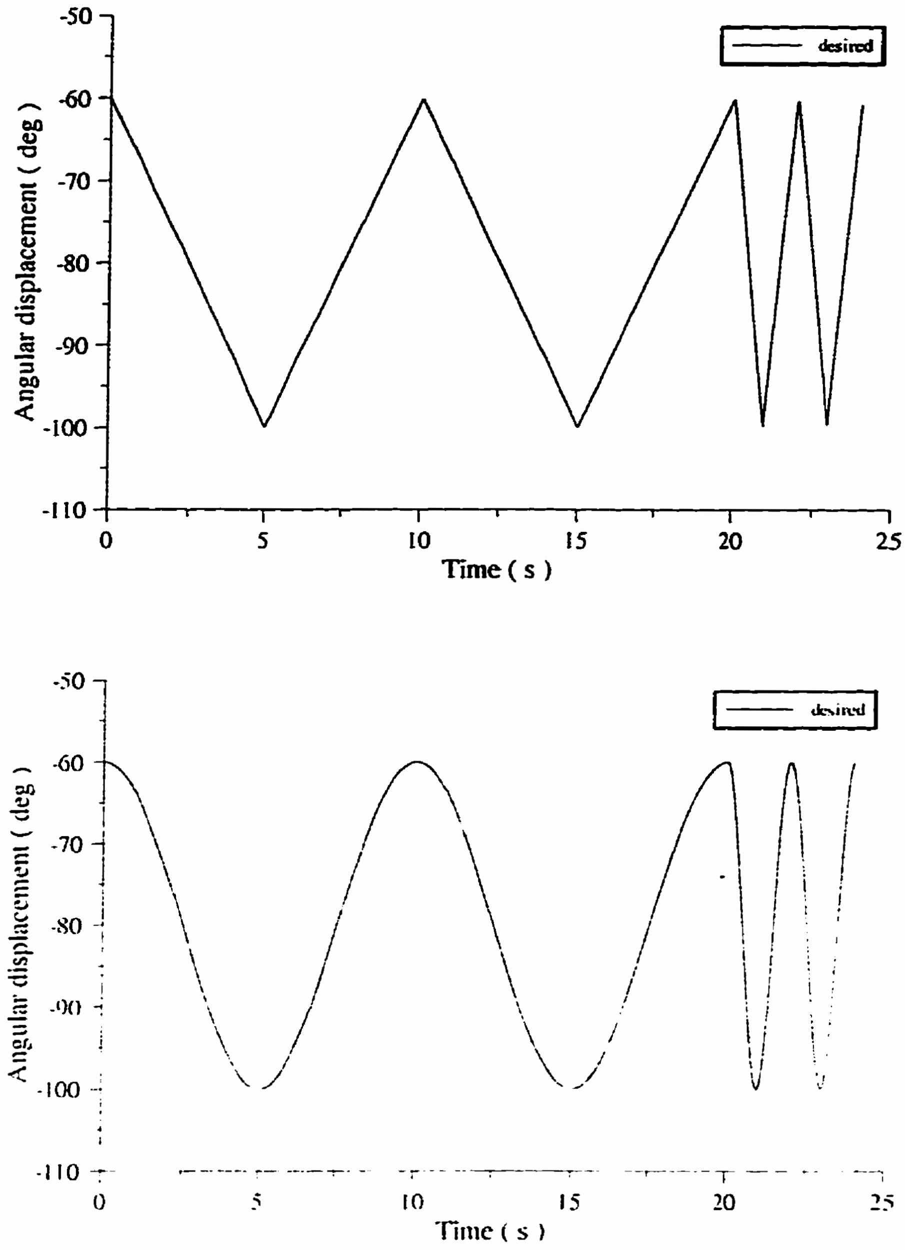

Fig. 4-11 Ramp and cosine tracking inputs.

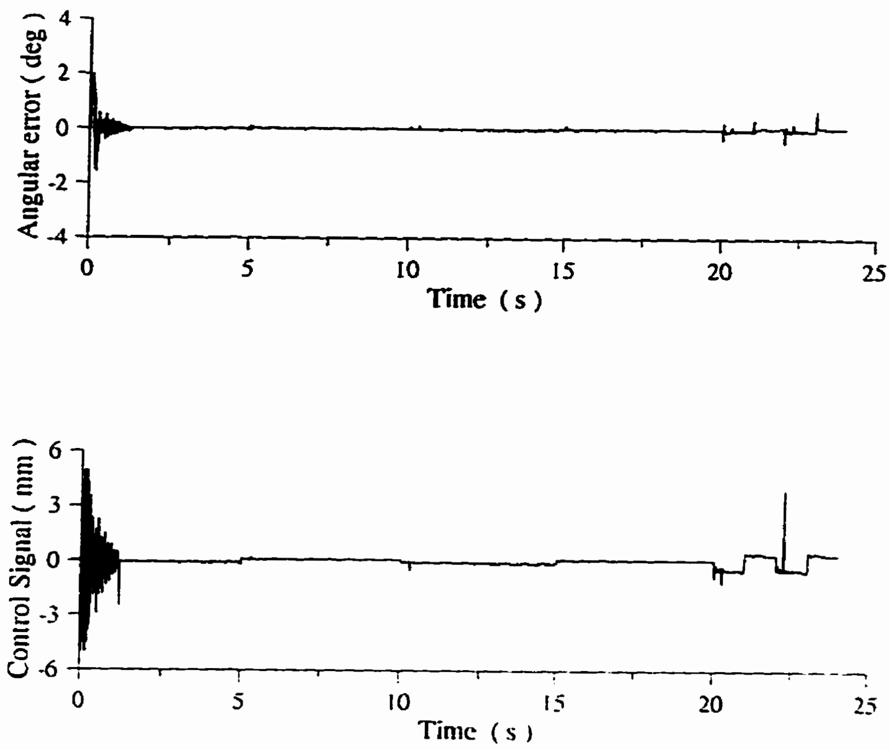

Fig. 4-12 Tracking error and control input for ramp input response.

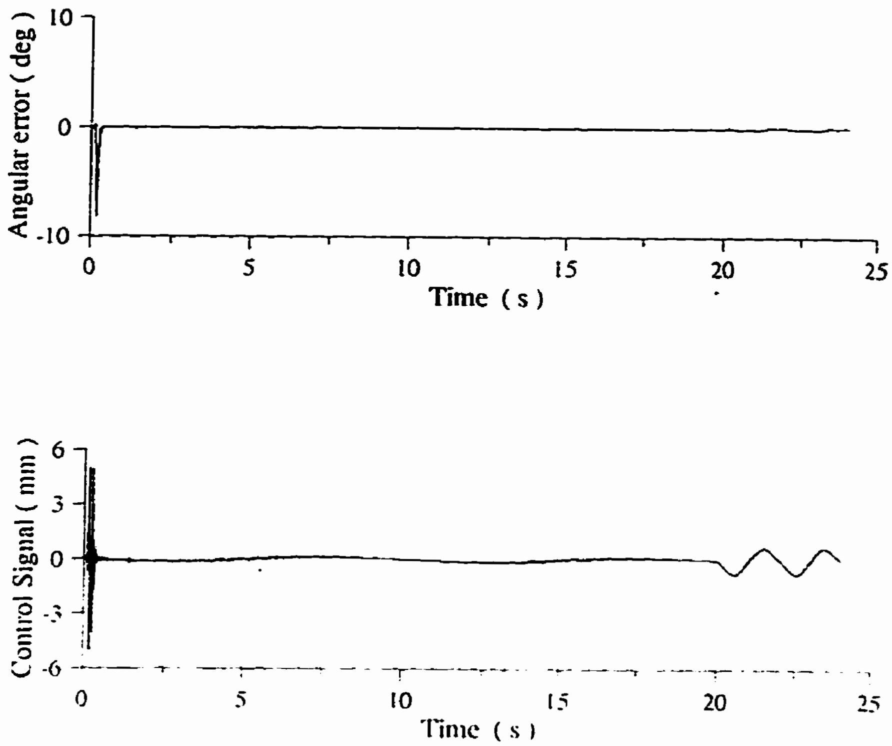

Fig. 4-13 Tracking error and control input for cosine input response.

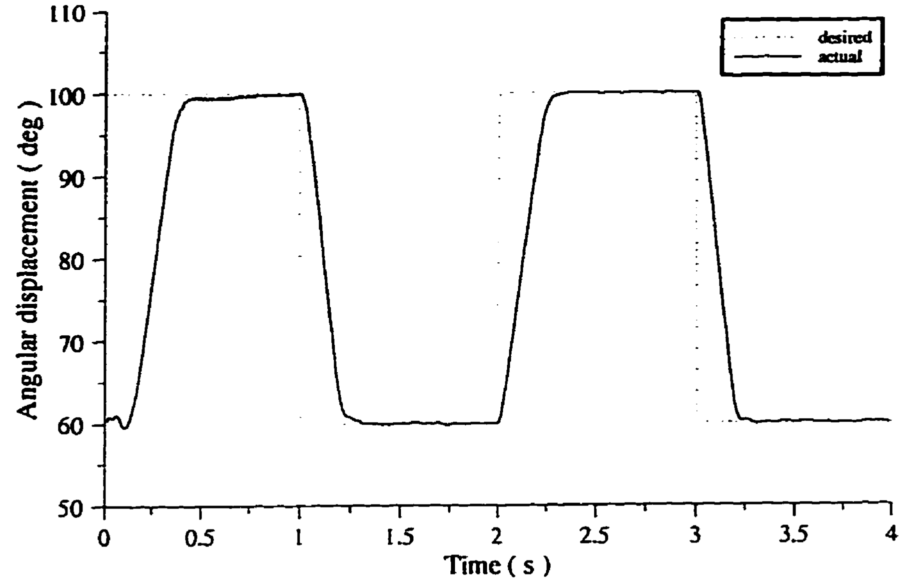

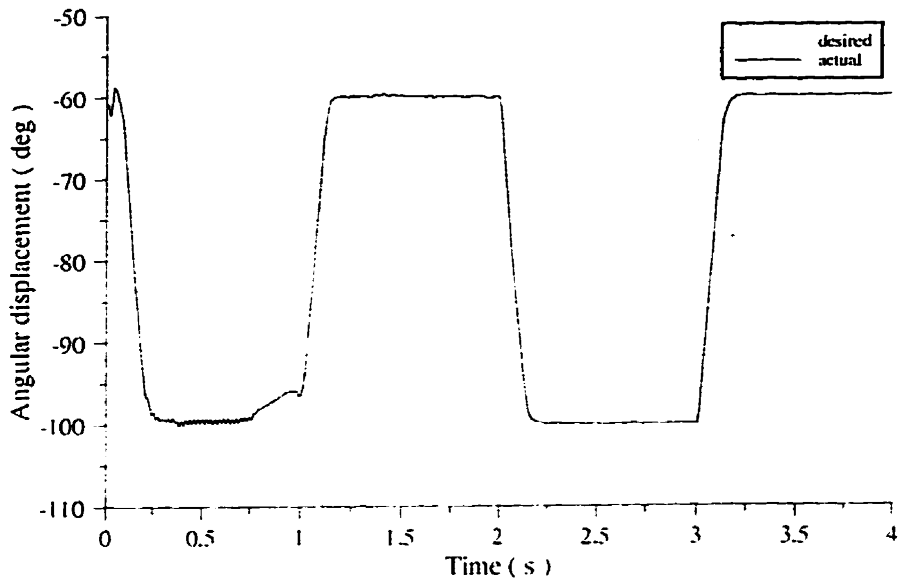

Fig. 4-14 Joint displacements when two links work together:
link 1(top): $N_1=1$, $N_2=60$, $N_u=1$, $\lambda_c=3000$, $\lambda_r=0.4$, $\lambda_f=0.99$:
link 2(bottom) : $N_1=1$, $N_2=40$, $N_u=1$, $\lambda_c=1000$, $\lambda_r=0.4$, $\lambda_f=0.99$).

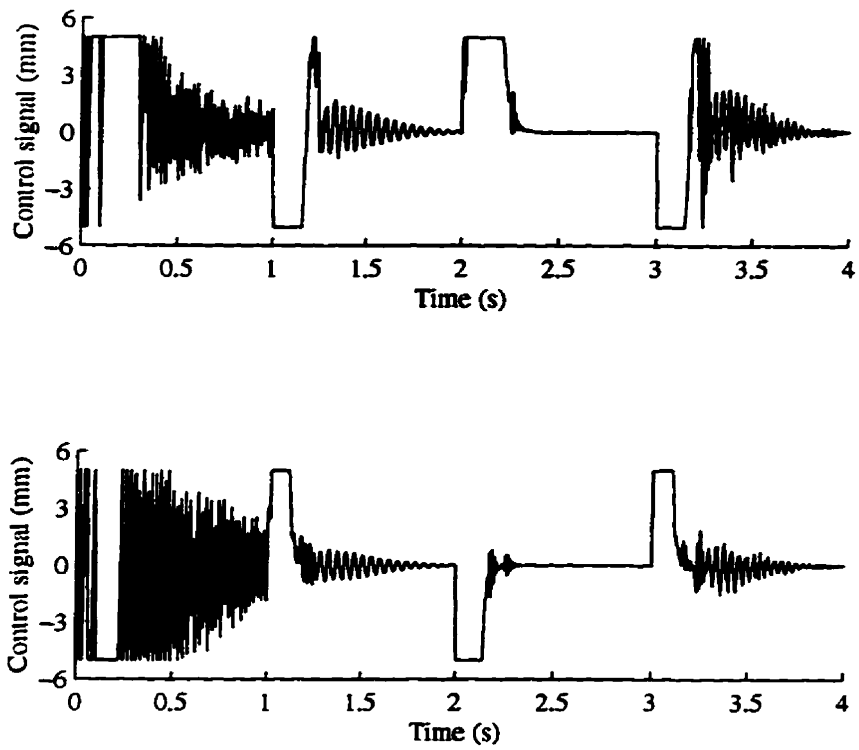

Fig. 4-15 Control inputs pertaining to Figure 4-14 (top: link1; bottom: link 2).

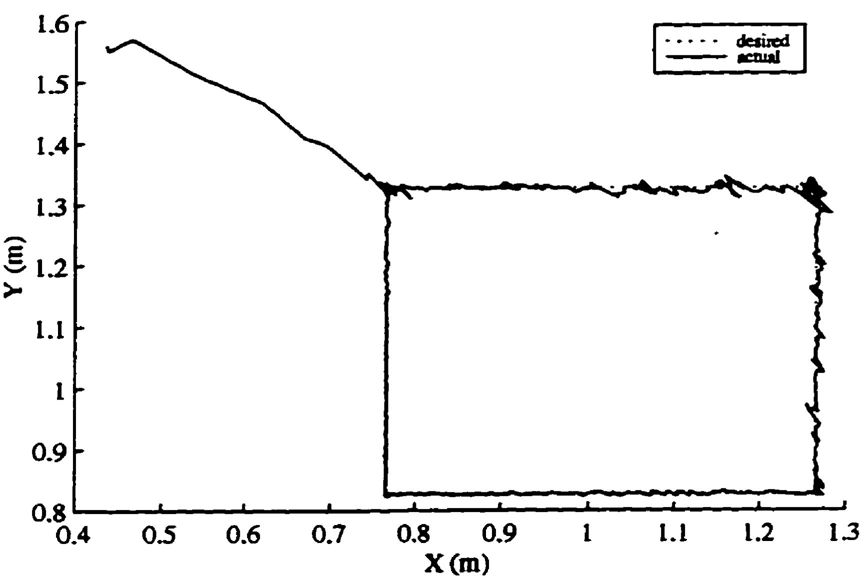

Fig. 4-16 End point response in Cartesian space.

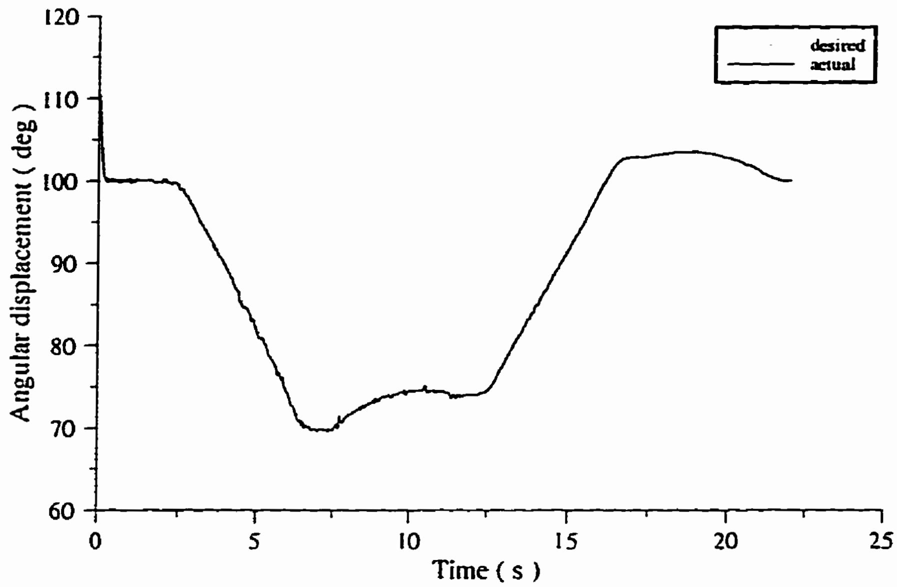

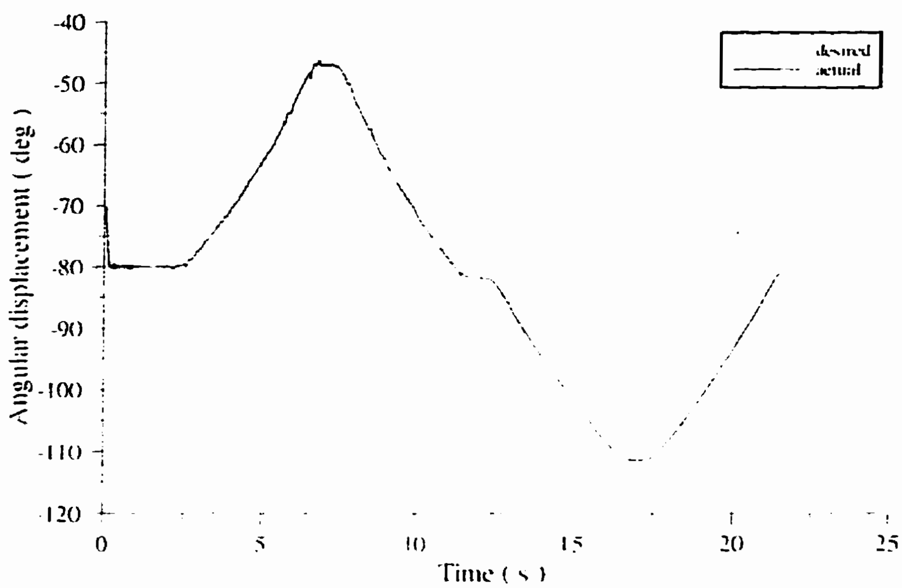

Fig. 4-17 Joint displacements pertaining to Figure 4-16 (top: link 1; bottom: link 2).

4.2.2 MVC Implementation

To be consistent with the previous work on this controller in references [7, 17], the relationship between joint velocity $\dot{\theta}_i$ and servovalve input voltage u_i is modeled instead of modeling joint displacement between θ_i and u_i. Figure 4-18 shows the control scheme.

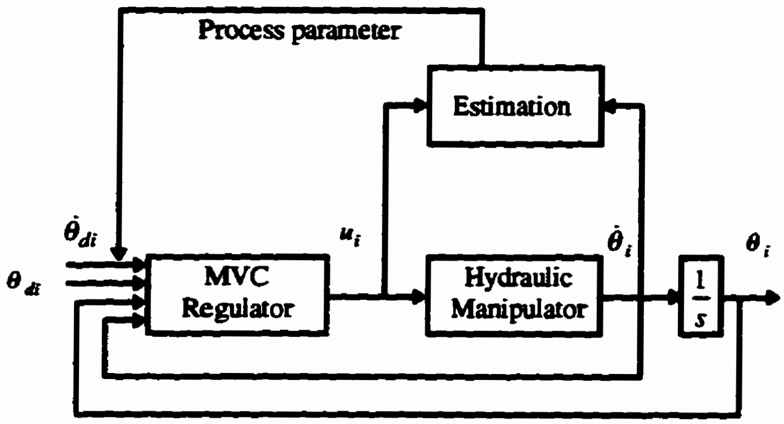

Fig. 4-18 Single link MVC system; position control.

The s-domain transfer function that represents the relationship between u_i and $\dot{\theta}_i$ was previously shown by equation (2-17) which is re-written here:

$$\frac{s\Theta_i(s)}{U_i(s)}=\frac{K_{ui}(A_{Ii}+A_{Oi})\hat{J}_i}{H_{ii}C_is^2+(\hat{J}_i^2d_iC_i+K_{pi}H_{ii})s+\hat{J}_i^2(d_iK_{pi}+A_{Ii}{}^2+A_{Oi}{}^2)} \tag{4-10}$$

Taking z-transform including zero order holder arrives at

$$\frac{\dot{\Theta}_i(z)}{u_i(z)} = \frac{b_{i0}z^{-1} + b_{i1}z^{-2}}{1 + a_{i1}z^{-1} + a_{i2}z^{-2}} \tag{4-11}$$

In other words, it is a second order system and the output in discrete time form is:

$$\dot{\theta}_i(t) = -a_{i1}\dot{\theta}_i(t-1) - a_{i2}\dot{\theta}_i(t-2) + b_{i0}u_i(t-1) + b_{i1}u_i(t-2) + h_i(t) \tag{4-12}$$

Here $h_i(t)$ is added as a forcing term to look after the nonlinear effects such as gravitational force. Therefore, in this case, five parameters in total are to be estimated on-line.

Together with equation (3-18), the control signal is determined by

$$u_i(t) = \frac{b_{i0}}{b_{i0}^{\;2} + b_{i0}^{*\,2}}[\dot{\theta}_{di}^*(t+1) + a_{i1}\dot{\theta}_i(t) + a_{i2}\dot{\theta}_i(t-1) - b_{i1}u_i(t-1) - h_i(t)] \tag{4-13}$$

where b_{i0}^* is the value of b_{i0} at last sampling instant t-1; $\dot{\theta}_{di}^*(t+1) = \dot{\theta}_{di}(t+1) + c_i[\theta_{di}(t-1) - \theta_i(t-1)]/T$, in which the last term with weighting factor c_i is expected to correct the position error at time t-1. T is the sampling time.

Similar to the implementation of a GPC, the control signal was kept within the range of [-5mm, 5mm]. The sampling time T=0.001s. Initially, link 1 and link 2 were set to 60 and -60 degrees, respectively. Then, only link 2 was controlled during the simulation while there was no control effort on link 1. The MVC controller has two parameters to be tuned: c_1 which corrects the position error, and the relaxing factor λ_r which is defined as $u_i = \lambda_r \times u_i$. Similar to GPC, the forgetting factor used in RLS estimator, λ_f, is also needed to be adjusted. The best performance was obtained with the following parameter values:

$$c_1=0.5,\ \lambda_r=0.0003,\ \lambda_f=0.98 \tag{4-14a}$$

The initial values of the plant model were:

$$a_1=0,\ a_2=0,\ b_0=1,\ b_1=0,\ h=0 \tag{4-14b}$$

where for the purpose of simplicity, a_{2i}, b_{2i} and h_2 are denoted as a_i, b_i and h, respectively.

Figure 4-19 shows the response with well-tuned gains. The response is very smooth without any overshoot, however, as compared with Fig. 4-2, it is much more sluggish. Fig. 4-20 shows the result of the test in which a load of 40kg is presented during 4th - 8th second. The response is quite oscillatory. The effect of changing hydraulic compliance was also tested, which is shown in Fig. 4-21. The results indicate that the MVC scheme is not capable to adapt to the changes as good as GPC scheme.

Figures 4-22 and 4-23 show the tracking errors and the control signals pertaining to the ramp and the cosine tracking shown in Fig. 4-11. The parameter settings were the same as (4-14). Note the steady state errors observed in the ramp response.

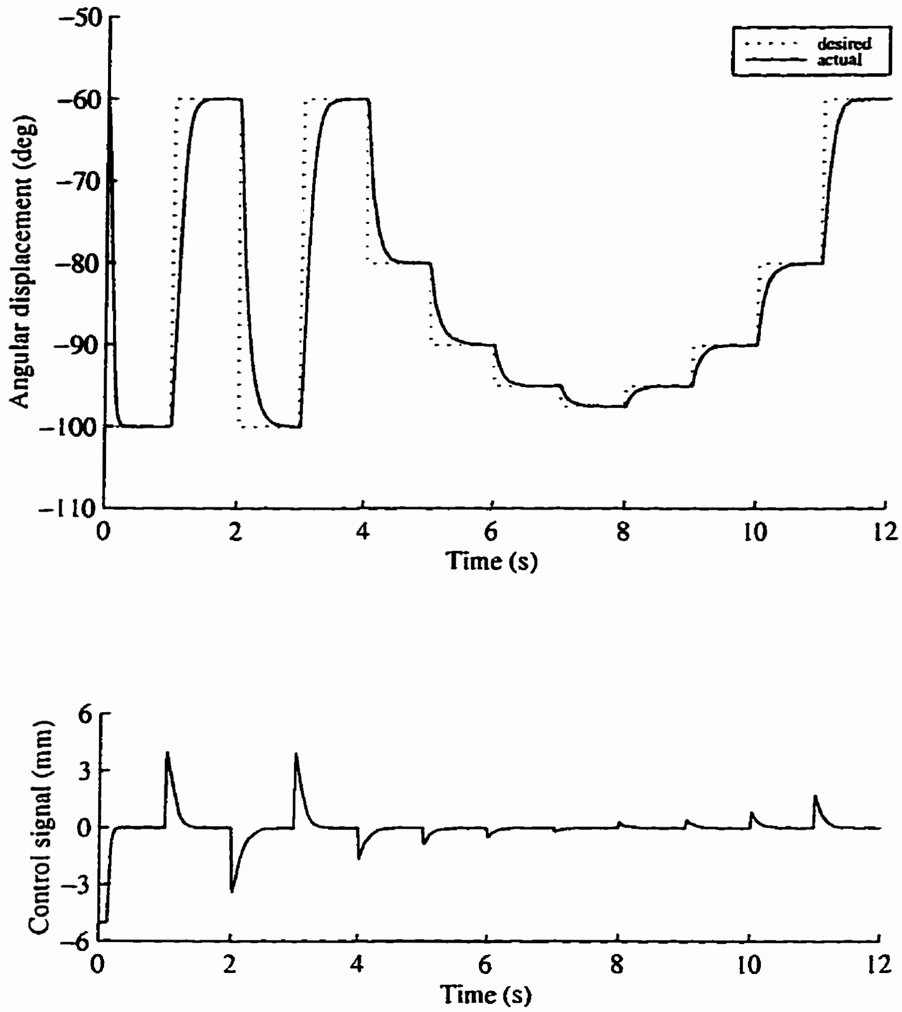

Fig. 4-19 Joint displacement and control input with c_1=0.5, λ_r=0.0003, λ_f=0.98.

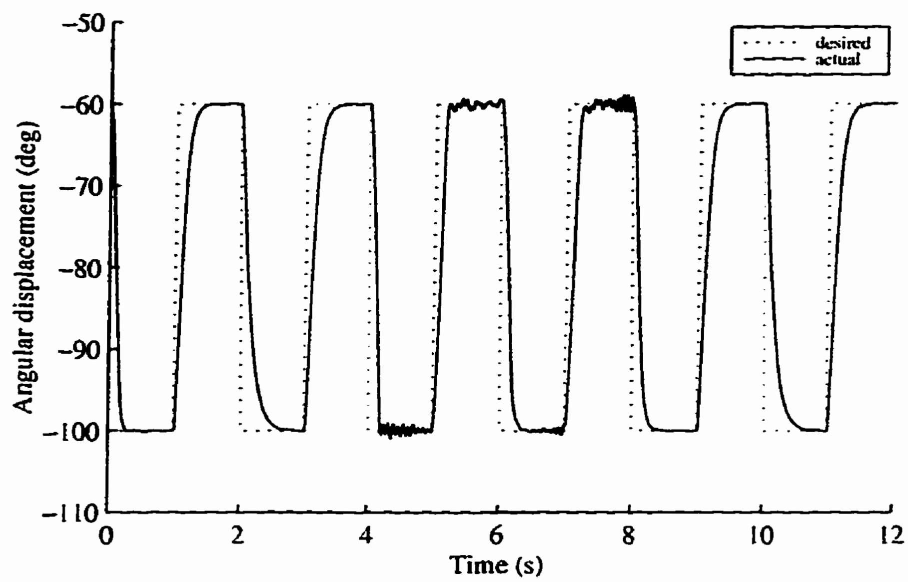

Fig. 4-20 Joint displacement responses with varying load.

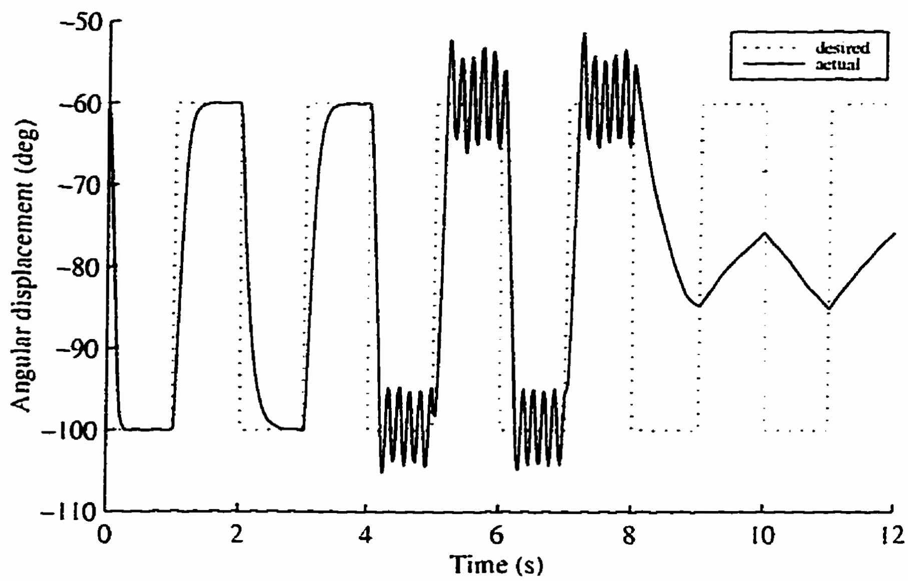

Fig. 4-21 Joint displacement responses with varying hydraulic compliance.

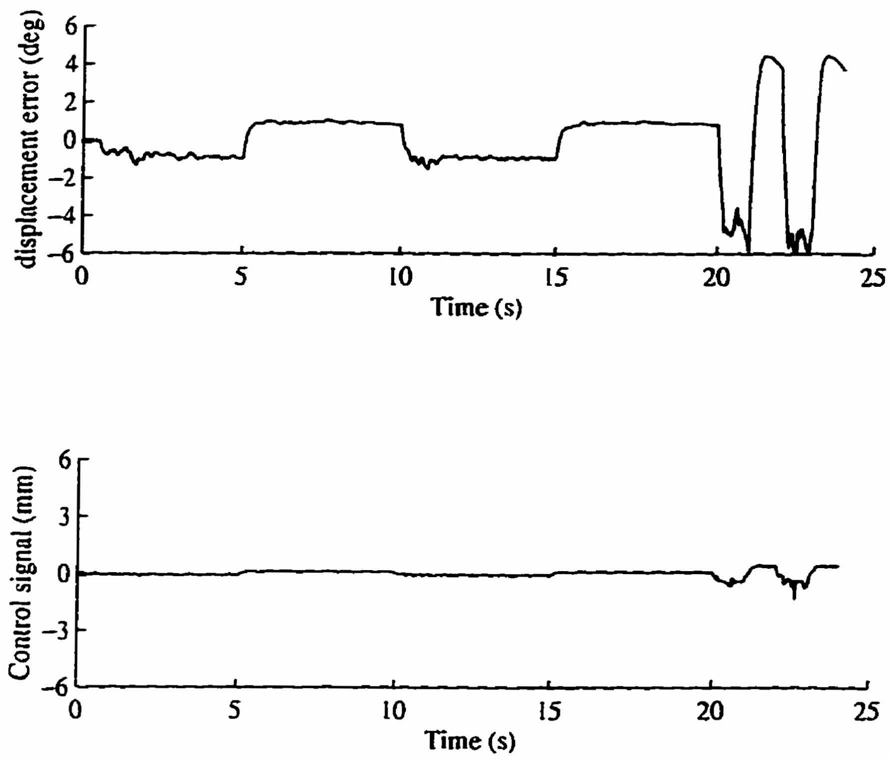

Fig. 4-22 Tracking error and control input during ramp tracking response.

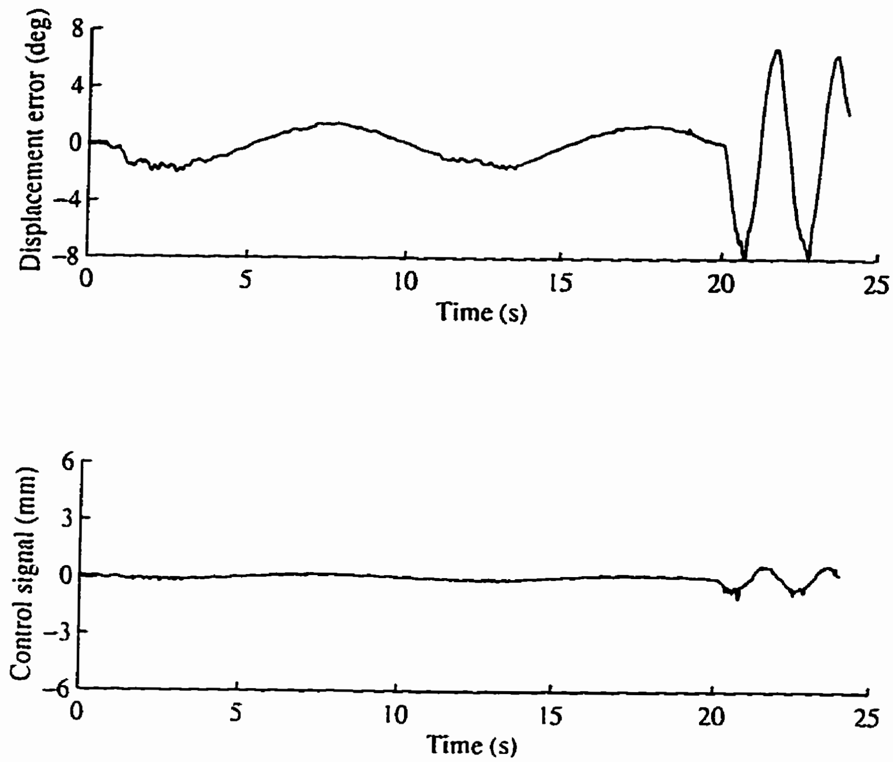

Fig. 4-23 Tracking error and control input during cosine tracking response.

4.3 MULTI-LINK GENERALIZED PREDICTIVE POSITION CONTROL

To better overcome the impact brought up by the interaction between links to the system performance, the dynamic coupling should be properly modeled. Since the manipulator has two degree-of-freedom, two variables are needed to determine the position of the endpoint. In this thesis, a straight forward way has been chosen, *i.e.*, using x an y in the task coordinate as position variables. Although other studies suggest that there exist alternative choices of variables for endpoint control which could lead to superior performance, such as using x and θ_2 in reference [21], adopting x and y has its own advantages. For instance, it is easy to specify the trajectory, and the need of inverse-kinematics-related computation is eliminated. Obviously, now the system has two inputs u_1 and u_2, and two outputs x and y. In this chapter, MIMO GPC is applied to this Cartesian-based position control approach.

The control scheme is drawn in Fig. 4-24. It is basically the same as the control scheme for SISO GPC algorithm shown in Fig. 4-2 except that the data flow is in a vector form.

The successful establishment of the s-domain transfer function from $[U_1, \ U_2]^T$ to $[X, \ Y]^T$, equation (2-43), enables the application of MIMO-GPC algorithm to the Cartesian motion control of a two-link manipulator.

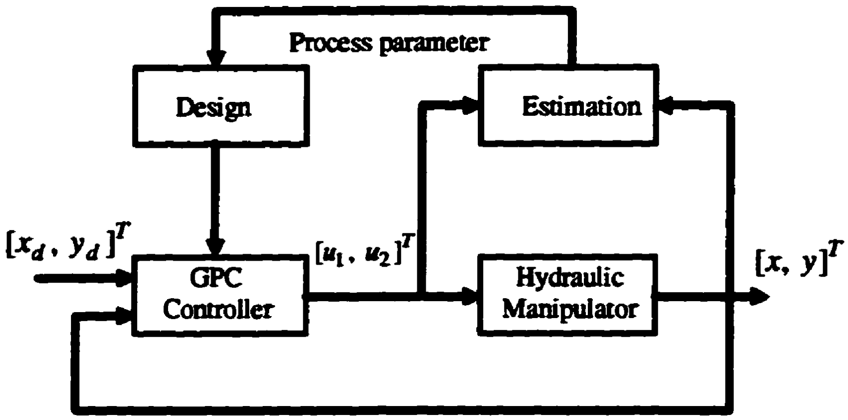

Fig. 4-24 MIMO GPC system block diagram.

Taking a z-transformation of equation (2-43) with a zero order holder arrives at:

$$\begin{bmatrix} X(z) \\ Y(z) \end{bmatrix} = \begin{bmatrix} K_1(z) & K_2(z) \\ K_3(z) & K_4(z) \end{bmatrix} \begin{bmatrix} U_1(z) \\ U_2(z) \end{bmatrix} \tag{4-15}$$

where $K_1(z) = \dfrac{b_{110}z^{-1} + b_{111}z^{-2} + b_{112}z^{-3} + b_{113}z^{-4} + b_{114}z^{-5}}{1 + a_{11}z^{-1} + a_{12}z^{-2} + a_{13}z^{-3} + a_{14}z^{-4} + a_{15}z^{-5}}$

$$K_2(z) = \frac{b_{120}z^{-1} + b_{121}z^{-2} + b_{122}z^{-3} + b_{123}z^{-4} + b_{124}z^{-5}}{1 + a_{11}z^{-1} + a_{12}z^{-2} + a_{13}z^{-3} + a_{14}z^{-4} + a_{15}z^{-5}}$$

$$K_3(z) = \frac{b_{210}z^{-1} + b_{211}z^{-2} + b_{212}z^{-3} + b_{213}z^{-4} + b_{214}z^{-5}}{1 + a_{11}z^{-1} + a_{12}z^{-2} + a_{13}z^{-3} + a_{14}z^{-4} + a_{15}z^{-5}}$$

$$K_4(z) = \frac{b_{220}z^{-1} + b_{221}z^{-2} + b_{222}z^{-3} + b_{223}z^{-4} + b_{224}z^{-5}}{1 + a_{21}z^{-1} + a_{22}z^{-2} + a_{23}z^{-3} + a_{24}z^{-4} + a_{25}z^{-5}}$$

From equation (4-15), the outputs in discrete time form can be written as following:

$$x(t) = -a_{11}x(t-1) - \cdots - a_{15}x(t-5) + b_{110}u_1(t-1) + \cdots + b_{114}u_1(t-5)$$

$$+b_{120}u_2(t-1)+\cdots+b_{124}u_2(t-5)+h_1 \qquad (4\text{-}16a)$$

$$y(t)=-a_{21}y(t-1)-\cdots-a_{25}y(t-5)+b_{210}u_1(t-1)+\cdots+b_{214}u_1(t-5)$$

$$+b_{220}u_2(t-1)+\cdots+b_{224}u_2(t-5)+h_2 \qquad (4\text{-}16b)$$

Equation (4-16a) is herewith called Channel x and (4-16b) Channel y.

Two RLS estimators are needed to find the best parameter sets $[a_{11} \ \cdots \ a_{15} \ \ b_{110} \ \cdots \ b_{114} \ \ b_{120} \ \cdots \ b_{124} \ \ h_1]$ and $[a_{21} \ \cdots \ a_{25} \ \ b_{210} \ \cdots \ b_{214} \ \ b_{220} \ \cdots \ b_{224} \ \ h_2]$ in equations (4-16a) and (4-16b), respectively.

The initial values of these parameters were set to:

Channel x: $a_{11}=\cdots=a_{15}=0$, $b_{110}=1$, $b_{111}=\cdots=b_{114}=0$, $b_{120}=1$, $b_{121}=\cdots=b_{124}=0$

Channel y: $a_{21}=\cdots=a_{25}=0$, $b_{210}=1$, $b_{211}=\cdots=b_{214}=0$, $b_{220}=1$, $b_{221}=\cdots=b_{224}=0$

The same trajectory tracking as in Fig. 4-18 was conducted to allow convincing comparison. The design parameters of the controller were tuned to be:

Channel x: $N_1=1$, $N_2=27$, $N_u=1$, $\lambda_c=1$, $\lambda_r=0.15$, $\lambda_f=0.99$

Channel y: $N_1=1$, $N_2=27$, $N_u=1$, $\lambda_c=1$, $\lambda_r=0.15$, $\lambda_f=0.99$

Figure 4-25 shows the excellent response of the end-point displacement. Joint displacement of each link is plotted in Fig. 4-26. Compared with Fig. 4-16, the response in Fig. 4-25 is much better, implying that the MIMO GPC strategy considerably eliminates the effects imposed by dynamic coupling between the linkages.

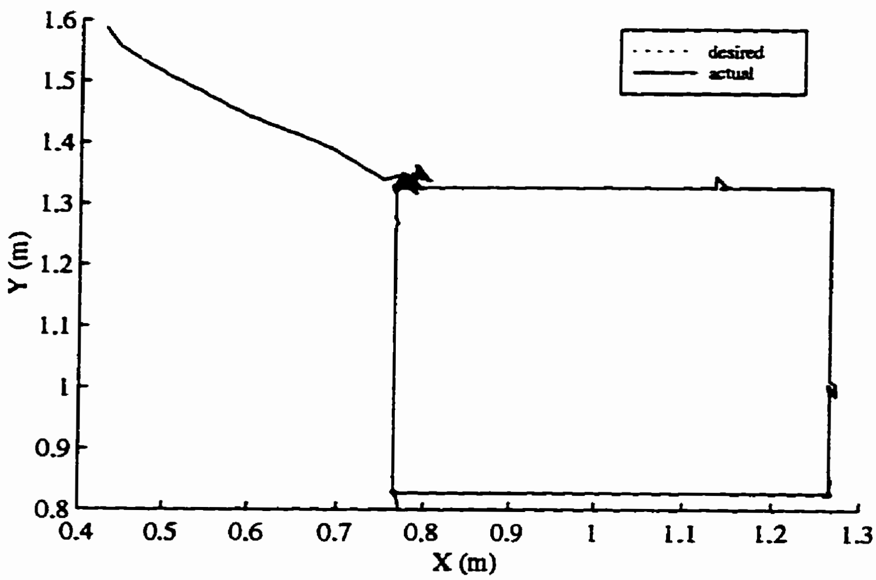

Fig. 4-25 End point response

(channel *x*: $N_1=1$, $N_2=27$, $N_u=1$, $\lambda_c=1$, $\lambda_r=0.15$, $\lambda_f=0.99$;

channel *y*: $N_1=1$, $N_2=27$, $N_u=1$, $\lambda_c=1$, $\lambda_r=0.15$, $\lambda_f=0.99$).

4.4 SUMMARY

In this chapter, the control performances of SISO GPC, SISO MVC and MIMO GPC were examined and compared on a two-link hydraulic manipulator. First, the effects of design parameters on the GPC performance have been studied. Second, the application of MVC and MIMO GPC schemes on the same manipulator have been carried out.

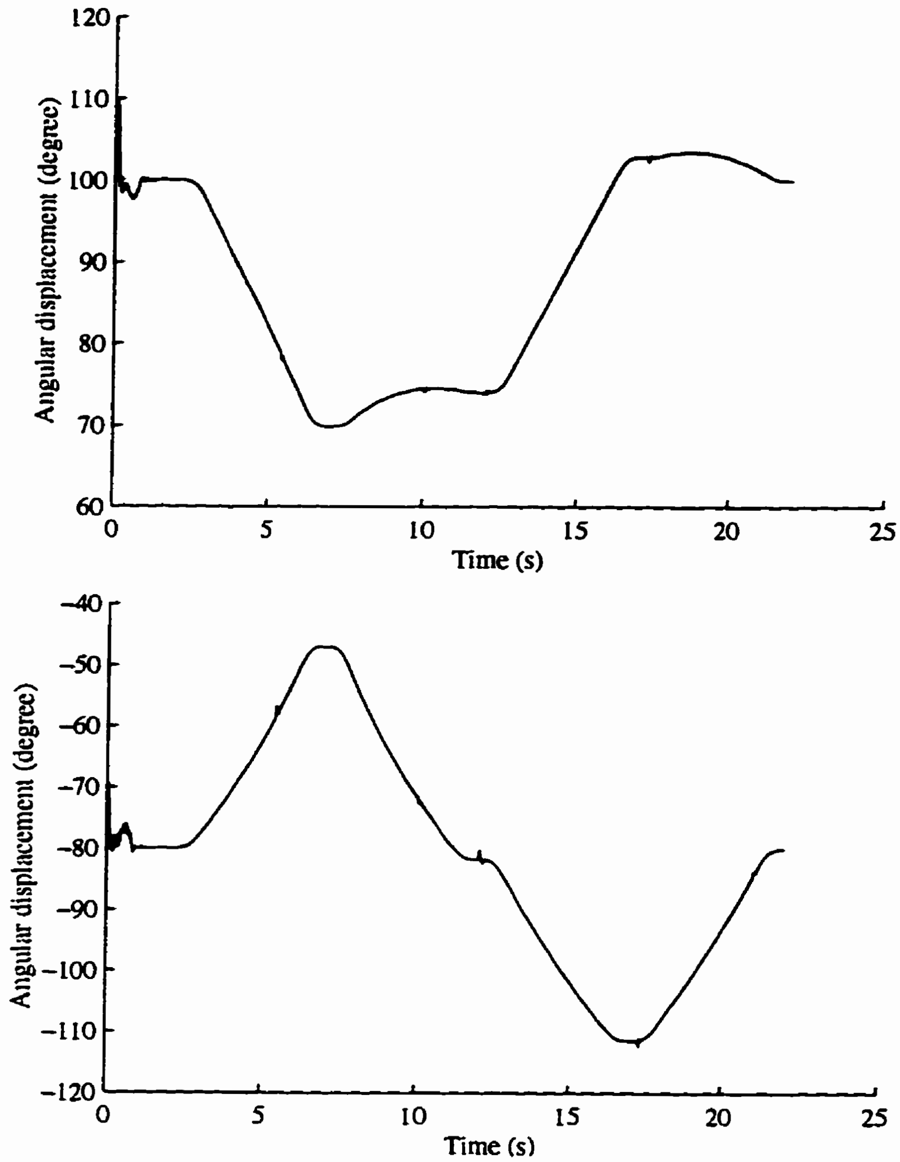

Fig. 4-26 Joint displacements pertaining to Figure 4-25 (top: link 1; bottom: link 2).

Although perfect response can be achieved by all the controllers, it is worth pointing out their performance differences in various aspects. The comparison between GPC and MVC can be summarized as below:

- GPC is more robust, while MVC can not adapt to load or hydraulic compliance changes as efficiently as GPC can.
- GPC has more design parameters to be tuned than MVC does, which is usually not preferred by engineers.
- GPC algorithm is computationally more expensive than MVC algorithm.
- Only position signal is required by the GPC, while the MVC strategy investigated here requires an additional measurement or calculation of the velocity.

The improvement of MIMO GPC over SISO GPC lies in the significant reduction of the effect that the dynamic coupling on the system's performance, though it is at the expense of tremendous increase in the number of the parameters to be estimated. The overall computation time was less because the **G** matrix to be manipulated was 54 by 54, compared with two **G** matrices having to be calculated in SISO GPC case, one of which was 60 by 60, the other 40 by 40.

CHAPTER FIVE

FORCE CONTROL OF A TWO-LINK HYDRAULIC MANIPULATOR

In this chapter, force control of hydraulic manipulators using adaptive GPC and MVC algorithms is addressed. This chapter consists of two parts. The first part discusses a single link force control. Both GPC and MVC algorithms are examined and compared through computer simulations. Second part discusses the multi-link force control case, in which the dynamics of both links are simultaneously taken into account along with the interaction with the environment.

5.1 SINGLE-LINK FORCE CONTROL

5.1.1 GPC Implementation

The control scheme of GPC implementation is shown in Fig. 5-1. u is the servovalve input voltage of the hydraulic actuator.

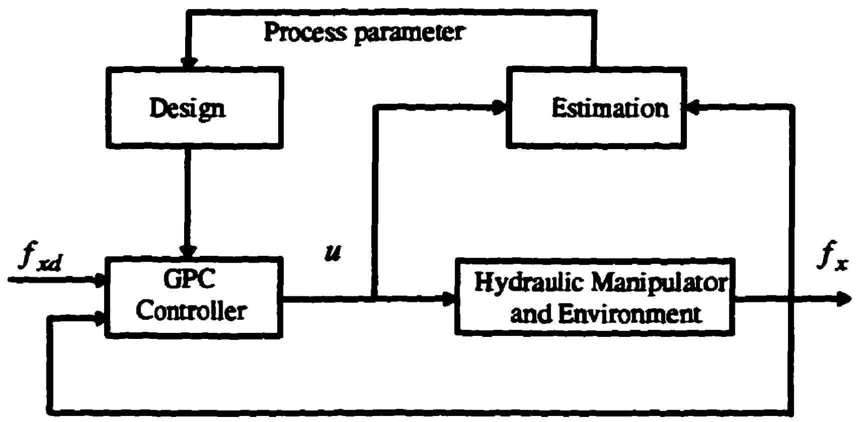

Fig. 5-1 Single link GPC system; force control.

The s-domain transfer function of the plant was found in equation (2-33). The z-transform of it with a zero order holder is

$$\frac{F_x(z)}{U_2(z)} = \frac{b_{20}z^{-1} + b_{21}z^{-2} + b_{22}z^{-3}}{1 + a_{21}z^{-1} + a_{22}z^{-2} + a_{23}z^{-3}} \tag{5-1}$$

and the output in discrete time form is:

$$f_x(t) = -a_{21}f_x(t-1) - a_{22}f_x(t-2) - a_{23}f_x(t-3)$$

$$+ b_{20}u_2(t-1) + b_{21}u_2(t-2) + b_{22}u_2(t-3) + h_2(t) \tag{5-2}$$

Here $h_2(t)$ is included as a forcing term to look after the effects of nonlinearity such as gravitational force.

The dynamics of the interaction between the end-effector and the environment has been added to the C-coded program that was used in position control to simulate the dynamics of the hydraulic actuators and the links of the manipulator. During the simulation only link 2 was controlled while link 1 was fixed at 70 degree. Dynamics of the environmental interaction was assumed as a mass-damper-spring system depicted in Fig. 2-3 with $m_e = 0\ \text{kg}$, $d_e = 80\ \text{N}\cdot\text{s/m}$ and $k_e = 5000\ \text{N/m}$. The spool displacement (control signal) was kept within the range of [-5mm, 5mm]. The sampling time T was chosen to be 0.001s.

Referring to equation (5-2) seven parameters are to be estimated. The values of these parameters were initially obtained mathematically by taking a z-transformation of (2-33) and a knowledge of the value of its coefficients. As a matter of fact, in computer simulation case the parameters can be found easily given the operating point. Through computer simulation, the initial position of link 2 was -100 degree with link 1 fixed at 70 degree. It was found that around such an operating point ($\theta_1 = 70°$, $\theta_2 = -100°$) the spool displacement was 0mm, the supply line pressure was $2.6962 \times 10^6\,\text{Pa}$ and the return line pressure was $3.0140 \times 10^6\,\text{Pa}$. Knowing these, all the parameters can be calculated as in Table 5-1.

Using the values in Table 5-1, equation (2-33) is re-written as:

$$\frac{F_x(s)}{U_2(s)} = \frac{0.89006 + 0.014241s}{1.4467 \times 10^{-11} s(15248 + 50.588s + s^2)} \tag{5-3}$$

Table 5-1 Parameter values in *s*-domain transfer function

Parameters	Values	Source
A_{I2}	$1.90\times10^{-3}\ \mathrm{m}^2$	Table 4-1
A_{O2}	$1.40\times10^{-3}\ \mathrm{m}^2$	Table 4-1
$\hat{J}_2$	0.19914 m/rad	Equation (2-6)
P_{12}	0.5 m	Equation (2-26)
K_{u2}	$0.54176\ \mathrm{m}^4/\mathrm{s}$	Equation (2-10c)
K_{p2}	$0.0\ \mathrm{m}^5/\mathrm{N}\cdot\mathrm{s}$	Equation (2-10c)
k_2	$6.6667\ \mathrm{kg}\cdot\mathrm{m}^2$	Equation (2-24b)
C_2	$2.2\times10^{-12}\ \mathrm{m}^5/\mathrm{N}$	Table 4-1
d_2	$8000.0\ \mathrm{N}\cdot\mathrm{s/rad}$	Table 4-1
m_{ex}	0.0 kg	Simulation setup
d_{ex}	$80.0\ \mathrm{N}\cdot\mathrm{s/m}$	Simulation setup
k_{ex}	5000.0 N/m	Simulation setup

Taking a z-transformation of the above equation including a zero order holder will lead to the following relation:

$$\frac{F_x(z)}{u_2(z)} = \frac{487.76z^{-1} + 32.458z^{-2} - 460.93z^{-3}}{1 - 2.9419z^{-1} + 2.8983z^{-2} - 0.9564z^{-3}} \tag{5-4}$$

Therefore,

$$a_1 = -2.9358,\ a_2 = 2.8865,\ a_3 = -0.9507,\ b_0 = 485.41,\ b_1 = 31.439,\ b_2 = -457.74 \tag{5-5}$$

Here, for simplicity a_{2i} and b_{2i} are denoted as a_i and b_i, respectively.

These values were only used later for the verification of the on-line estimation. The initial values used during the simulation were assigned as:

$$a_1 = 0,\ a_2 = 0,\ a_3 = 0,\ b_0 = 1,\ b_1 = 0,\ b_2 = 0,\ h = 0 \tag{5-6a}$$

The best performing step response was achieved with the following parameter setting for link 2 (see Fig. 5-2):

$$N_1 = 1,\ N_2 = 60,\ N_u = 1,\ \lambda_c = 1,\ \lambda_r = 0.06,\ \lambda_f = 0.99 \tag{5-6b}$$

Figure 5-3 shows the performance of the on-line estimator, which is consistent with the values obtained in (5-5). The parameters converged after ≈ 1.1second and roughly remained constant, due to the nonlinearities that could not be represented as a fixed-parameter linear model. Before the model was correctly established, the response was oscillatory, which clearly shows how the on-line estimation helped the controller performance.

Using (5-6) as the standard parameter setting, tests were also carried out to study the effects of the design parameters on the controller performance. Table 5-2 summarizes the findings. N_1 was set to 1 because it was assumed that no knowledge about the delay of the system was available.

Table 5-2 Step response with different system design parameter settings

Figure number	**Parameter setting**	**Remarks**
Fig. 5-2/5-3	Standard (5-6)	Fast response, no overshoot, no steady state error.
Fig. 5-4	Standard (5-6) with 2.5 times bigger set-point	A little deteriorated response with slight overshoots.
Fig. 5-5	N_2 changed to 30	Smaller N_2 resulted in a faster response with overshoot.
Fig. 5-6	N_u changed to 2	Faster response and larger error due to high environment stiffness.
Fig. 5-7	λ_c changed to 5×10^{11}	Larger λ_c resulted in a response with overshoot and oscillation.
Fig. 5-8	λ_r changed to 0.12	Larger λ_r led to strong control actions which worsened the response while the plant model was insufficiently modeled.
Fig. 5-9	λ_f changed to 0.98	Smaller λ_f made the parameter converge faster and the response more sensitive to error.

GPC also demonstrated good capability to track a specified the trajectory. Figures 5-10 to 5-14 show the simulation results of ramp and cosine set-points. Due to the inherent integral action of GPC, there was no steady state error observed for the ramp tracking test.

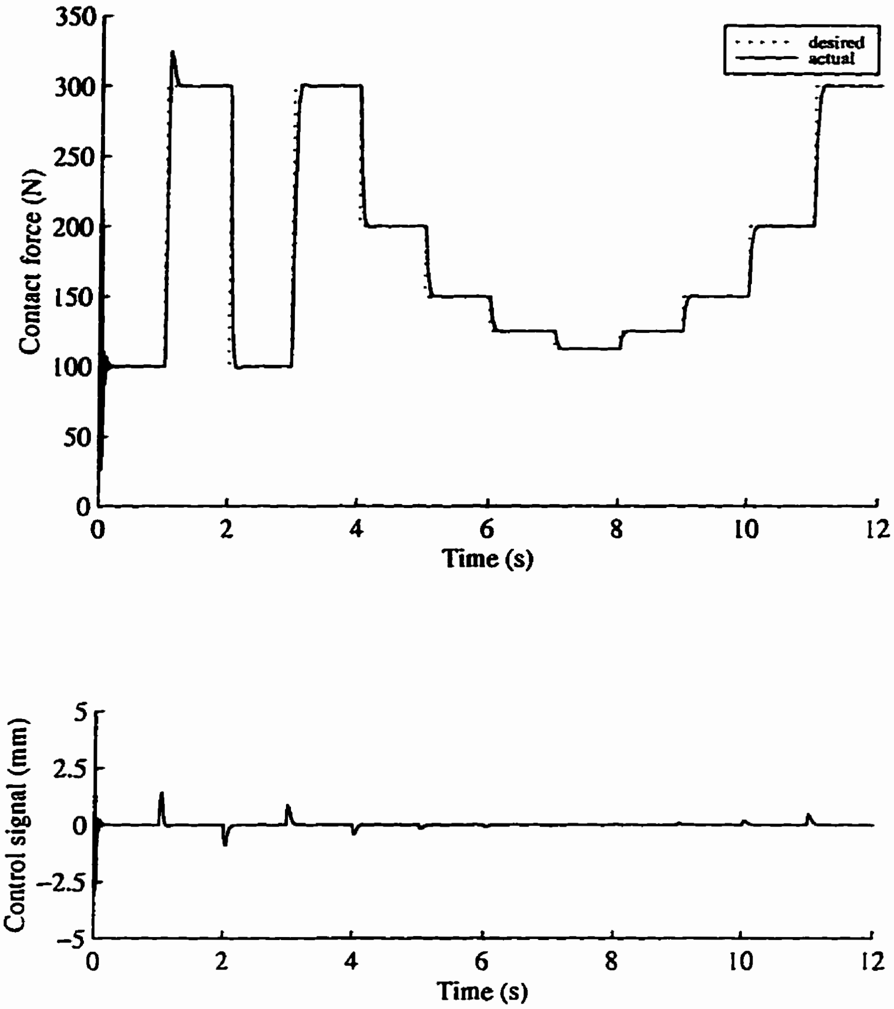

Fig. 5-2 Contact force and control input with

$N_1=1$, $N_2=60$, $N_u=1$, $\lambda_c=1$, $\lambda_r=0.06$, $\lambda_f=0.99$.

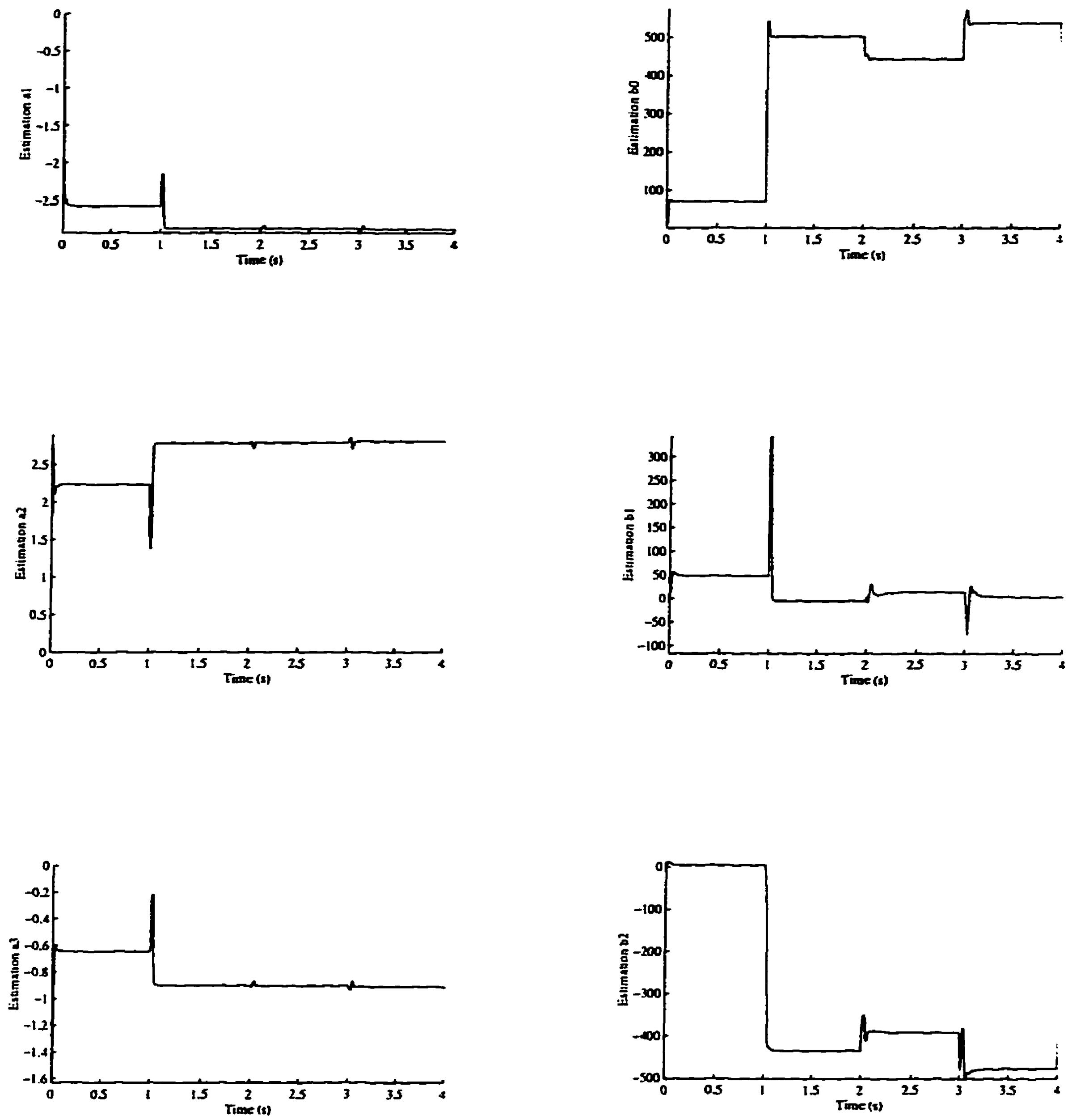

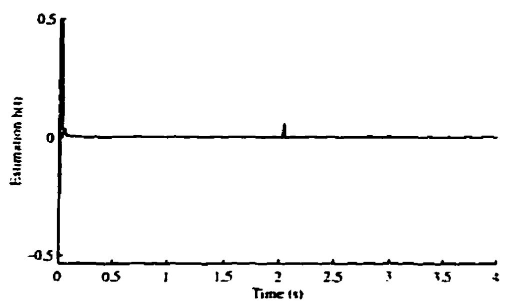

Fig. 5-3 Parameter estimation pertaining to Fig. 5-2.

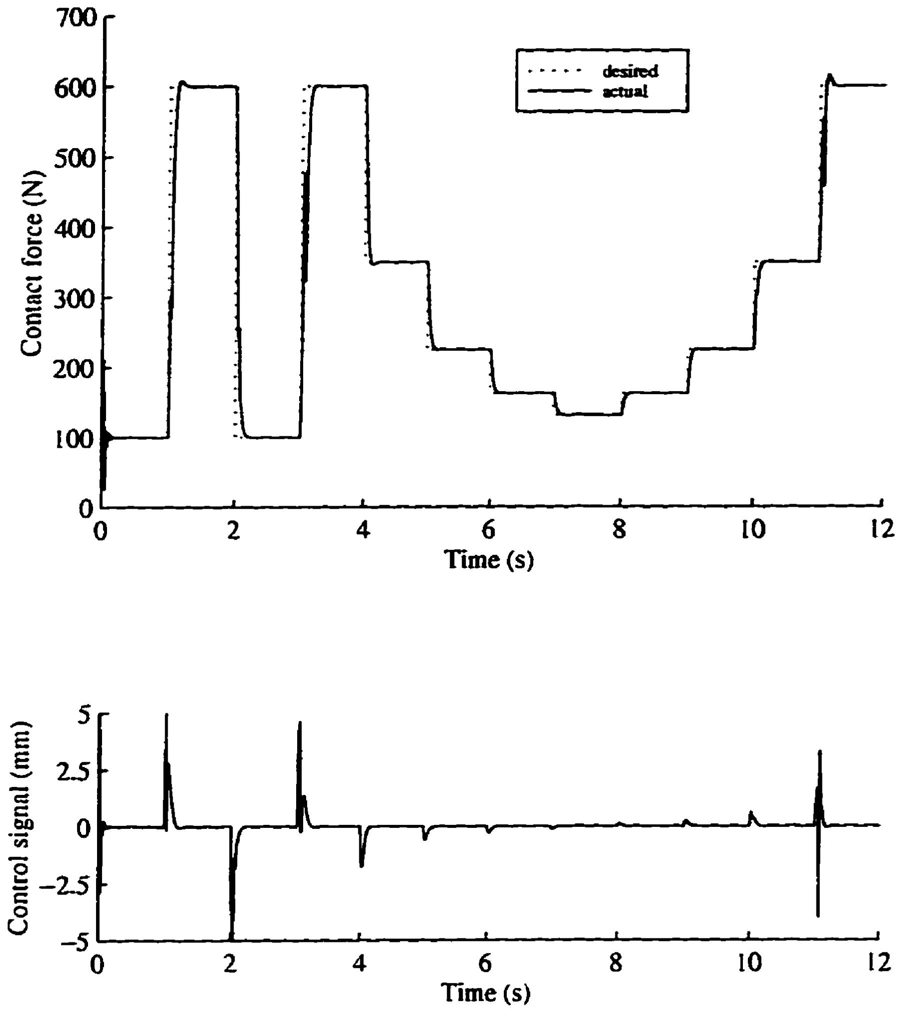

Fig. 5-4 Contact force and control input with large step set-points.

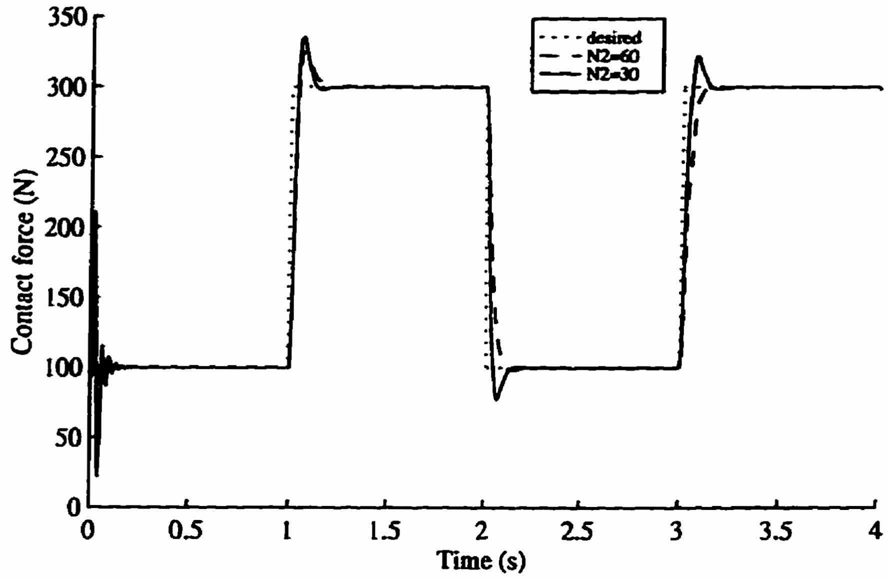

Fig. 5-5 Contact force response with $N_2 = 30$.

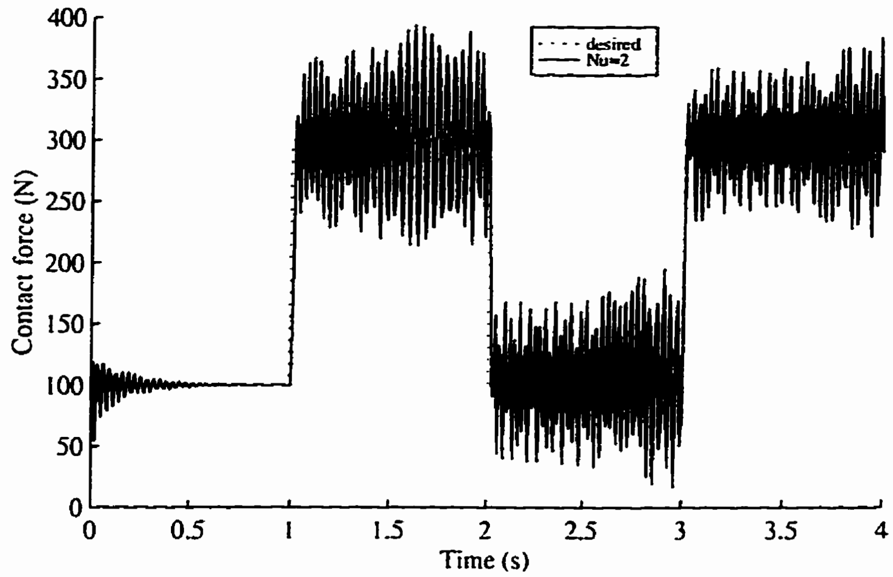

Fig. 5-6 Contact force response with $N_u = 2$.

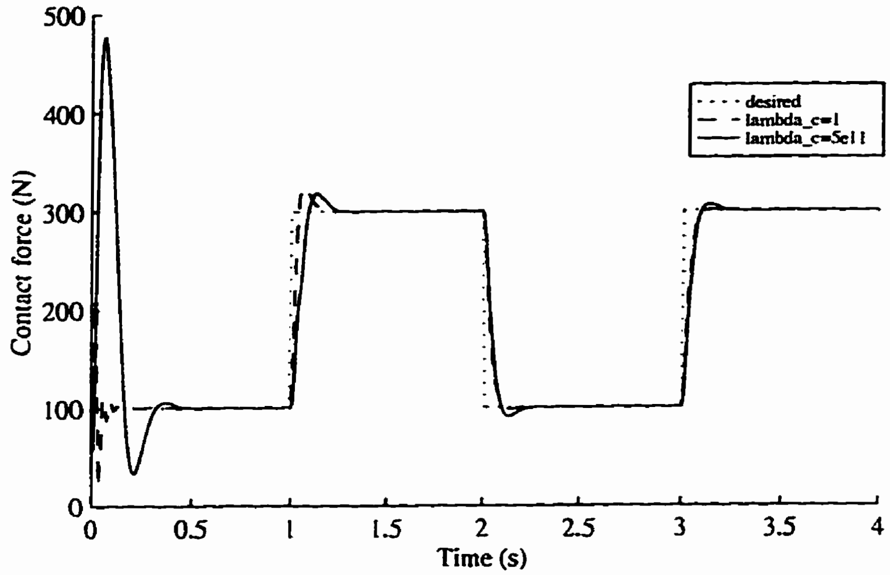

Fig. 5-7 Contact force response with $\lambda_c = 5\times 10^{11}$.

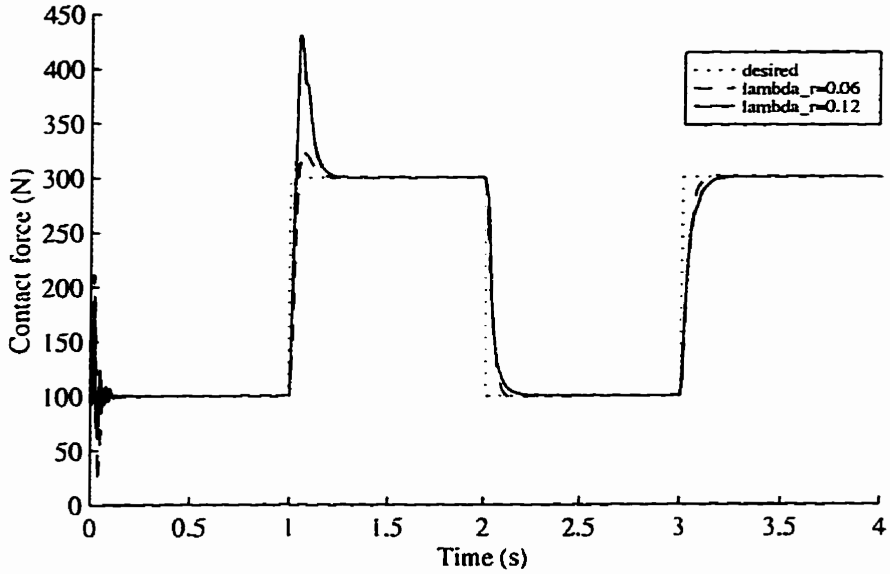

Fig. 5-8 Contact force response with $\lambda_r = 0.12$.

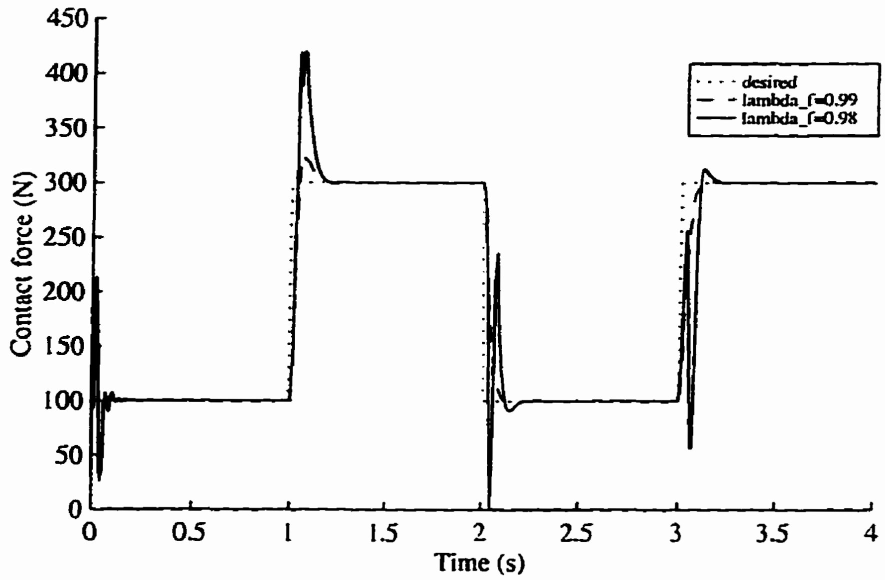

Fig. 5-9 Contact force response with $\lambda_f = 0.98$.

Further, in order to verify the robustness of the GPC force controller, the simulation started with the design parameter setting given in (5-6) and with $m_{ex} = 0\ \text{kg}$, $d_{ex} = 80\ \text{N}\cdot\text{s/m}$ and $k_{ex} = 5000\ \text{N/m}$ on the environment side. The stiffness of the environment was then suddenly quadrupled to $k_{ex} = 20000\ \text{N/m}$ at $t = 4.5$ second. Referring to Fig. 5-15, it took the controller almost 1 second to stabilize the response. At the $t = 8.5$ second, the second environment parameter, *i.e.*, the damping ratio, was changed to $d_{ex} = 20\ \text{N}\cdot\text{s/m}$. The change had no significant impact on the system output.

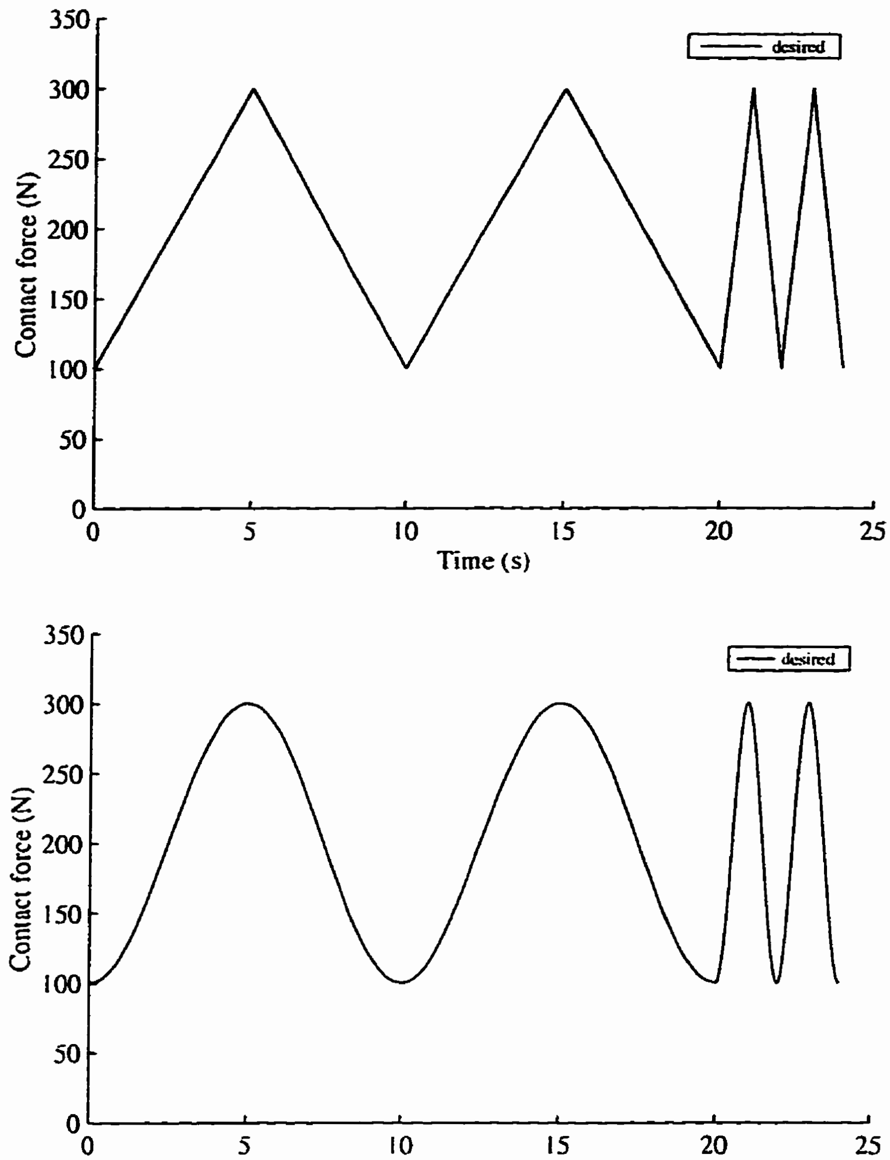

Fig. 5-10 Ramp and cosine force tracking inputs.

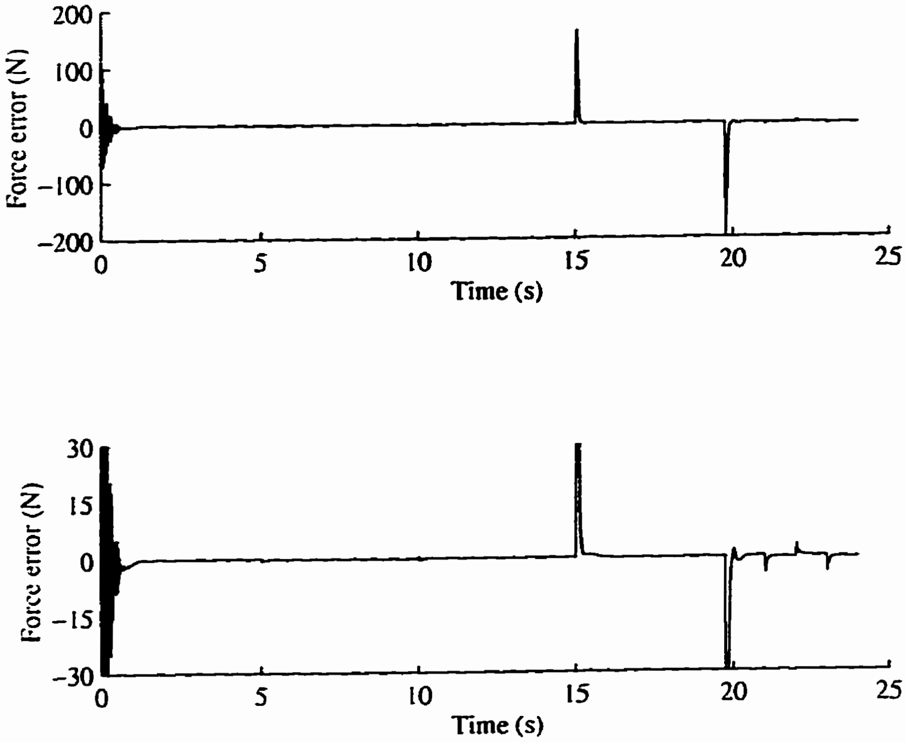

Fig. 5-11 Force tracking error to a ramp input.

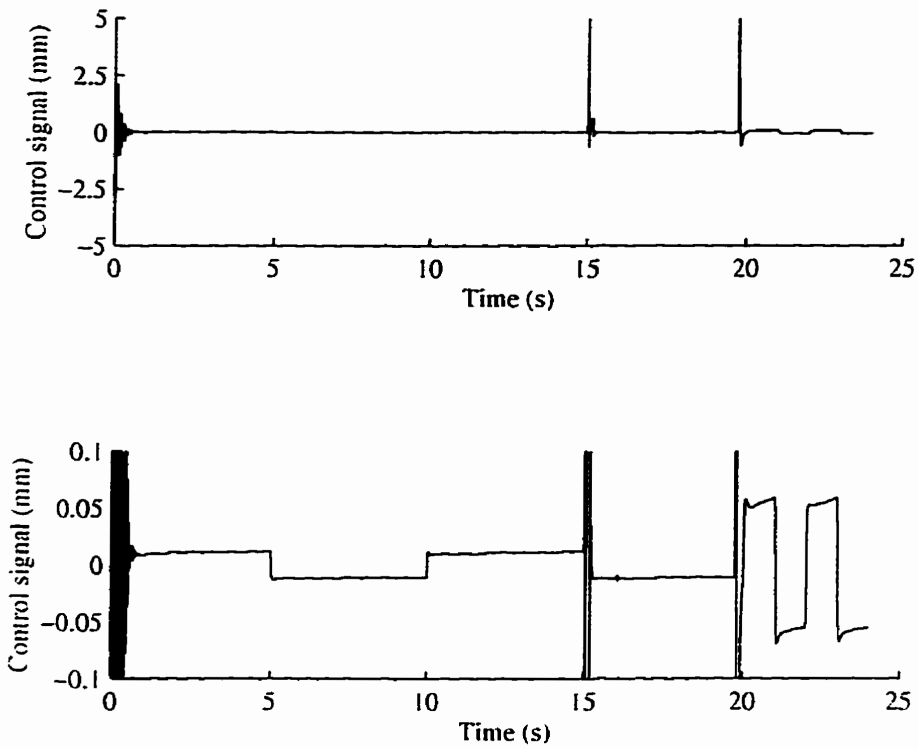

Fig. 5-12 Control input pertaining to Figure 5-11.

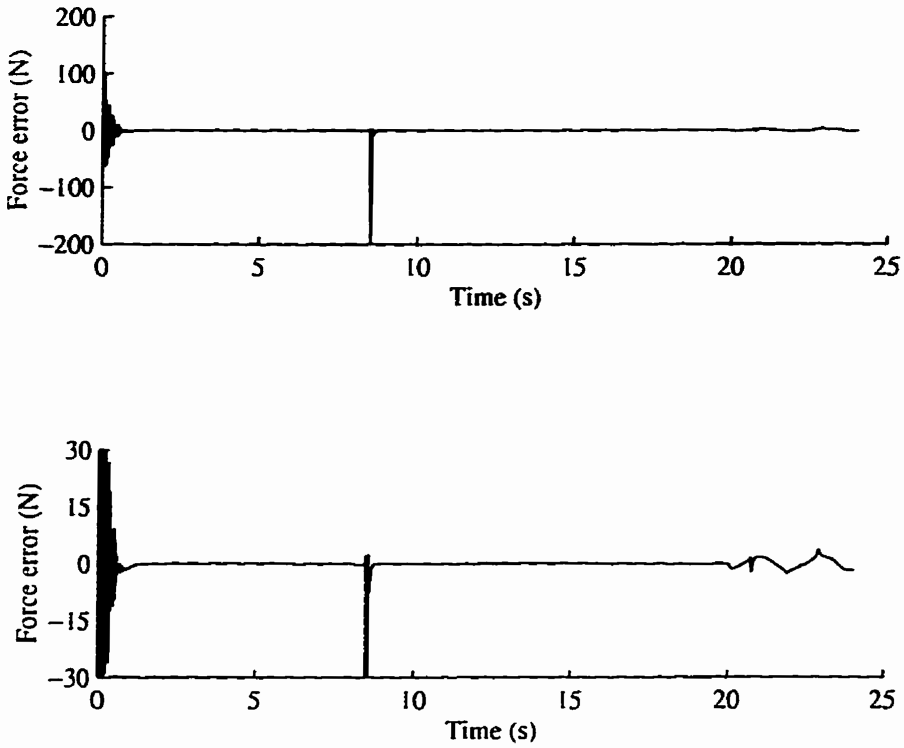

Fig. 5-13 Force tracking error to a cosine input.

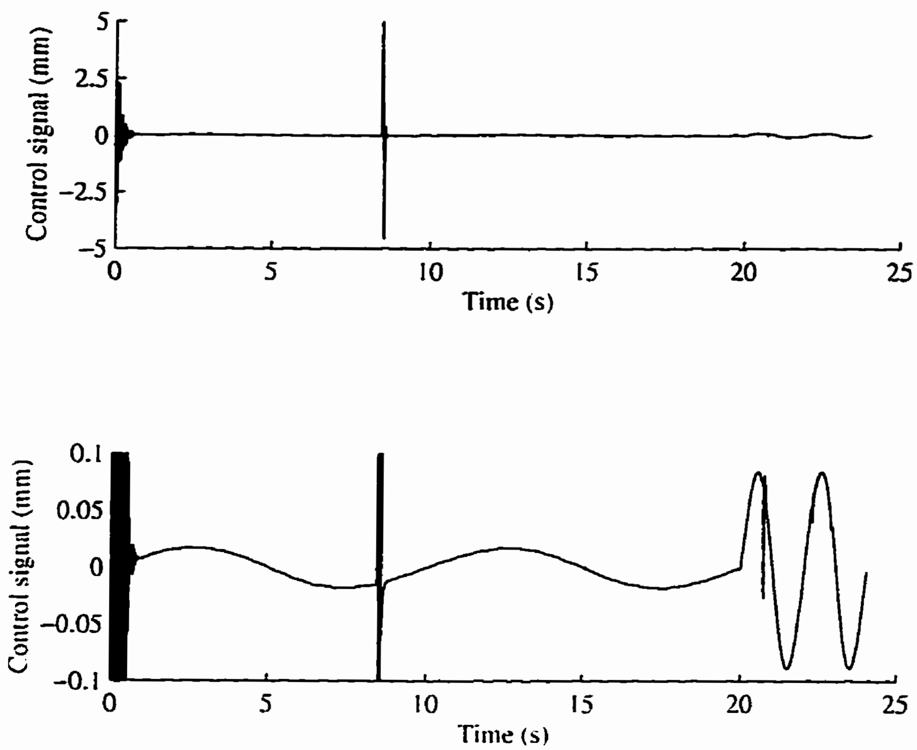

Fig. 5-14 Control input pertaining to Figure 5-13.

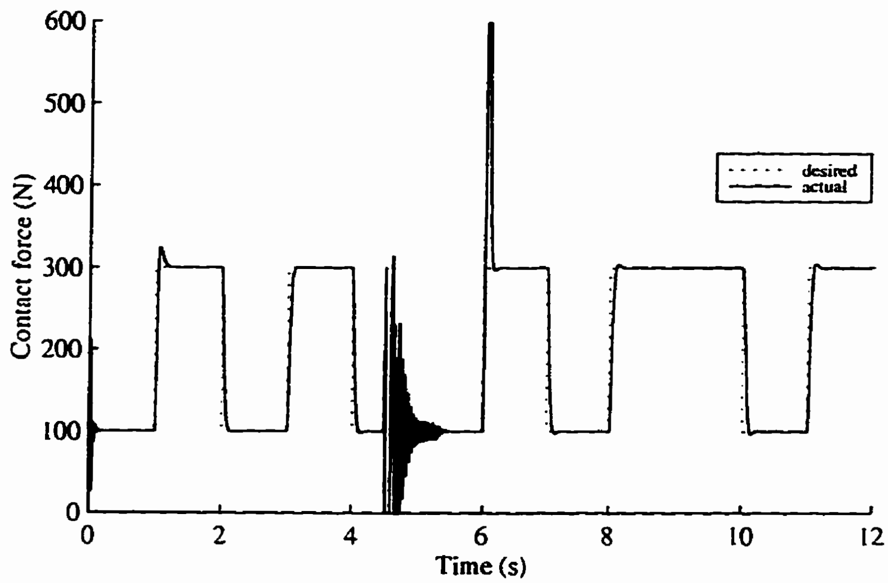

Fig. 5-15 Contact force response with varying environment.

5.1.2 MVC Implementation

In Chapter 4, the relationship between joint velocity $\dot{\theta}_i$ (time derivative of joint angle) and the input control signal u_i was modeled as a second order system. By using the transfer function of $\dot{\theta}_i$ over u_i, the order of the system was reduced from 3 to 2. With respect to force control, equation (2-33) was used. This is due to two reasons. First, the derivative of the force usually is not measurable; instead, it is obtained by calculation based on the measured forces. In fact, the measurement of force itself is very noisy due to the hardware limitations, which leads to inaccurate derivatives. Secondly, with reference to equation (2-33), one can write the transfer function from u_2 to $\dot{f}_x$ as following:

$$\frac{sF_x}{U_2}=\frac{J_2P_{12}K_{u2}(A_{I2}+A_{O2})(m_es^2+d_es+k_e)s}{(K_{p2}+C_2s)[a_2s^2+J_2^2d_2s-P_{12}^2(m_es^2+d_es+k_e)]+J_2^2(A_{I2}^2+A_{O2}^2)s}$$

(5-7)

which indicates that in the force control the order of the system can not be reduced by using the transfer function from u_2 to $\dot{f}_x$.

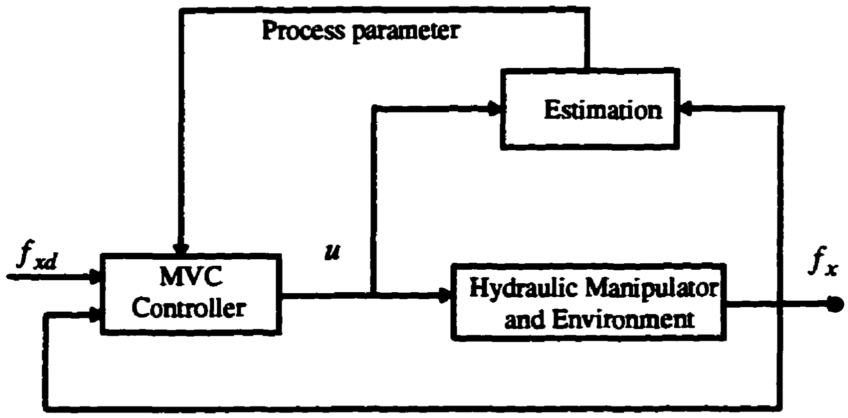

Fig. 5-16 Single link MVC system; force control.

Figure 5-16 shows the control scheme. Recalling equation (3-18), together with (5-2), the control signal is determined by

$$u_2(t)=\frac{b_{20}}{b_{20}{}^2+b_{20}^{*\,2}}[f_{xd}(t+1)+a_{21}f_x(t)+a_{22}f_x(t-1)$$

$$-a_{23}f_x(t-2)-b_{21}u_2(t-1)-b_{22}u_2(t-2)-h_2(t)] \qquad (5\text{-}8)$$

where b_{20}^* is the value of b_{20} at last sampling instant t-1.

According to equation (5-2) seven parameters were to be estimated. Their initial values were set to:

$$a_1 = 0,\ a_2 = 0,\ a_3 = 0,\ b_0 = 1,\ b_1 = 0,\ b_2 = 0,\ h = 0 \tag{5-9a}$$

For the purpose of simplicity, a_{2i}, b_{2i} and h_2 are denoted as a_i, b_i and h, respectively.

Figure 5-17 shows the best performing response that could be achieved. The design parameters in this case were:

$$\lambda_r = 0.01 \text{ and } \lambda_f = 0.99 \tag{5-9b}$$

The response is smooth without any overshoot, however, compared with the response of the GPC, shown in Fig. 5-2, it is more sluggish. Fig. 5-18 shows the response when the set-point magnitude was increased 2.5 times.

Figures 5-19 to 5-22 show the simulation results of tracking trajectories, which can be compared with those belonging to GPC scheme.

A similar robustness test, as in GPC implementation, was also performed on the minimum variance force controller. The simulation started with the design parameter setting given in (5-9) and with $m_e = 0\ \mathrm{kg}$, $d_e = 80\ \mathrm{N \cdot s / m}$ and $k_e = 5000\ \mathrm{N / m}$. At $t = 4.5$ second, k_e suddenly changed to $20000\ \mathrm{N / m}$, and at the $t = 8.5$ second, d_e changed to $20\ \mathrm{N \cdot s / m}$. Figure 5-23 shows the response. It is seen that minimum variance force control scheme could not adapt to the changes in the environment as well as generalized predictive force controller did.

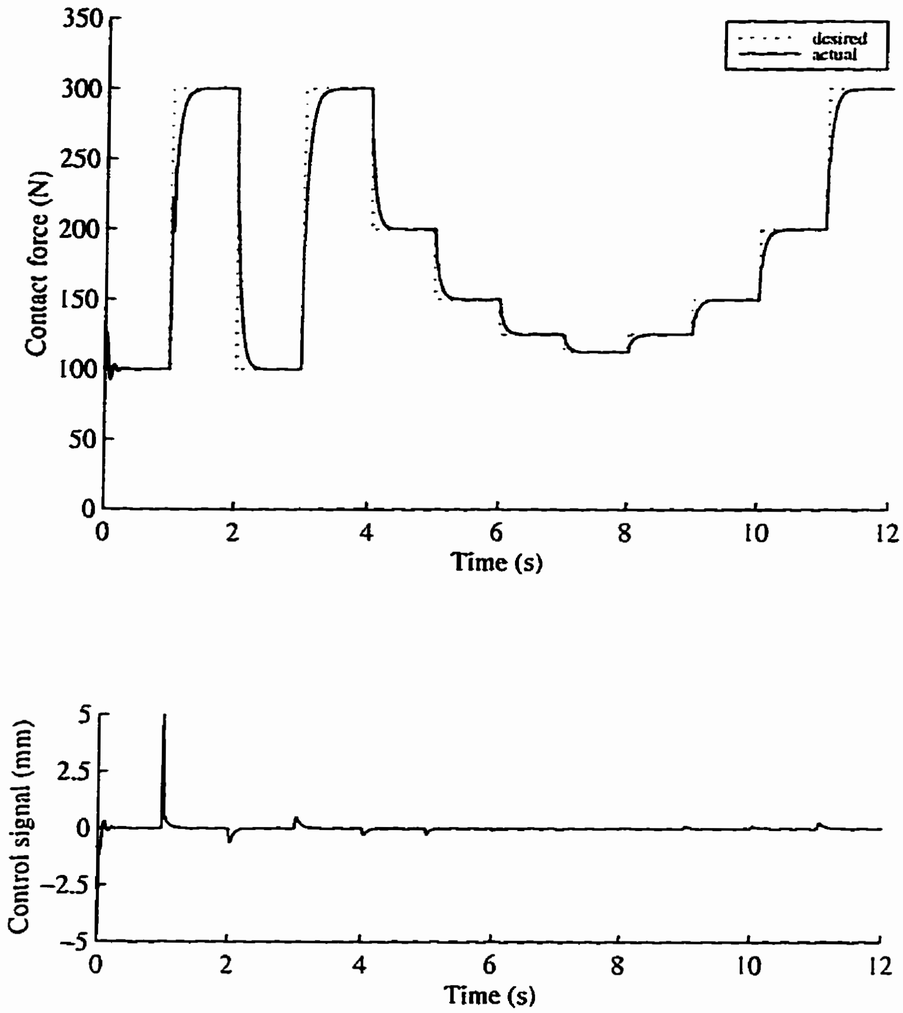

Fig. 5-17 Contact force and control input with λ_r=0.01 and λ_f=0.99.

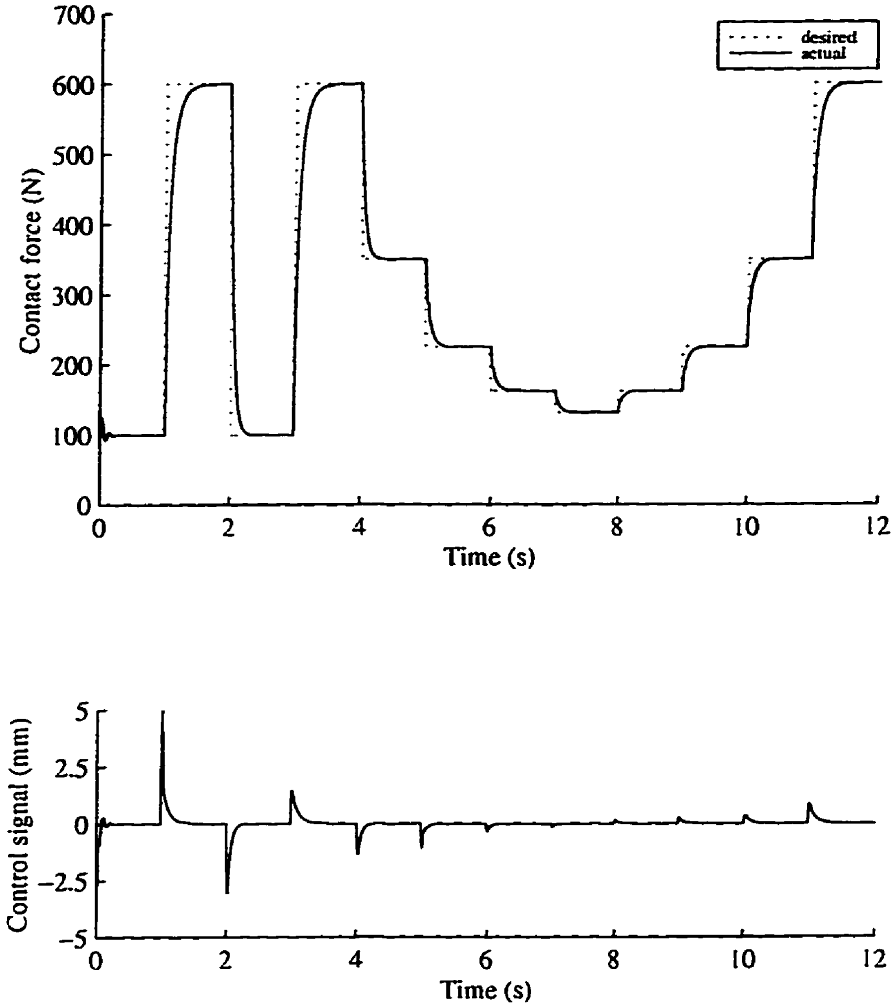

Fig. 5-18 Contact force and control input with large step set-point.

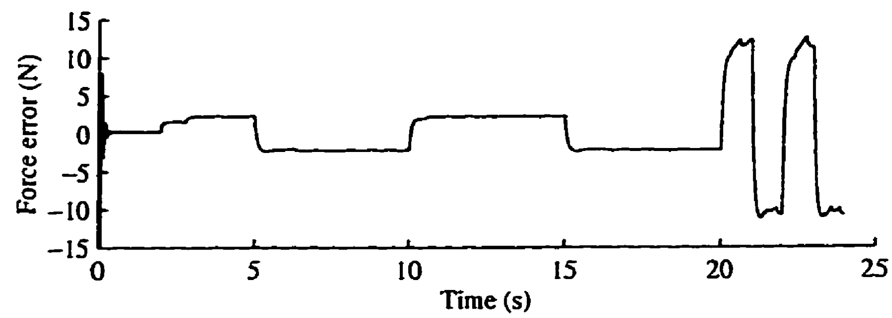

Fig. 5-19 Force tracking error to a ramp input.

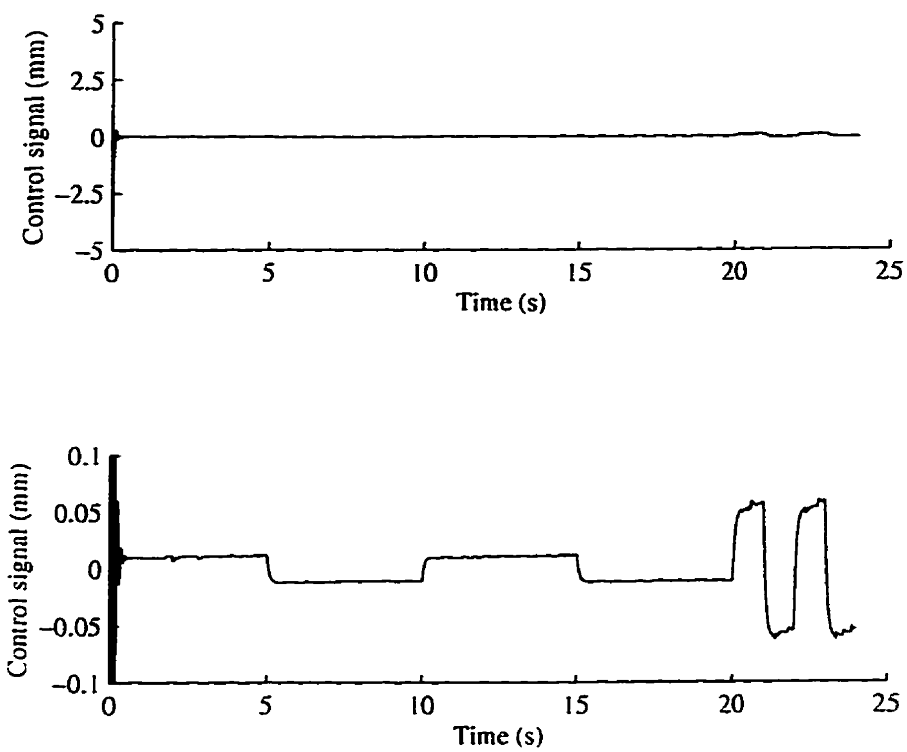

Fig. 5-20 Control input pertaining to Figure 5-19.

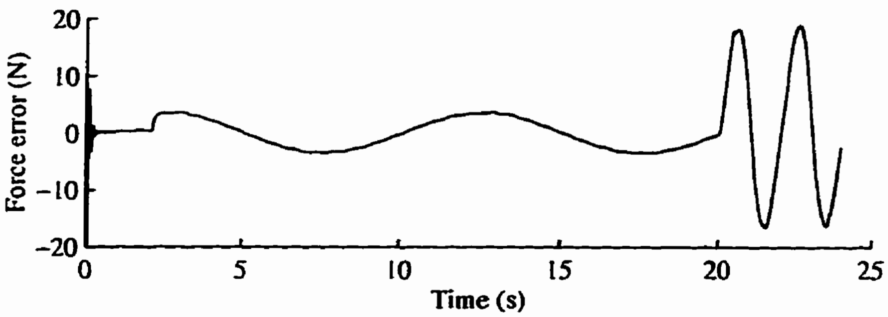

Fig. 5-21 Force tracking error to a cosine input.

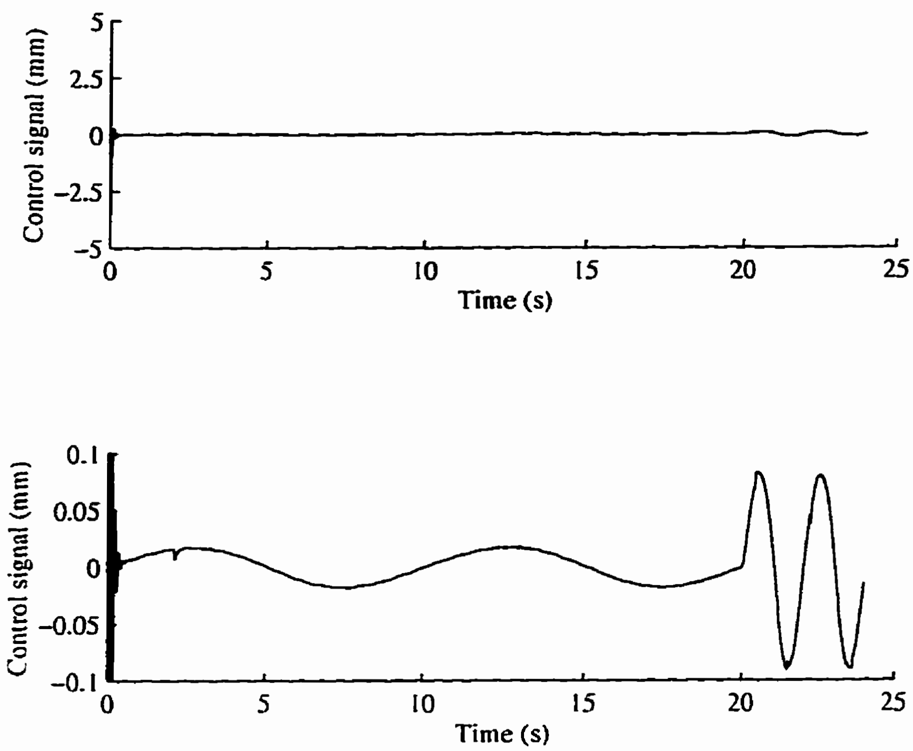

Fig. 5-22 Control input pertaining to Figure 5-21.

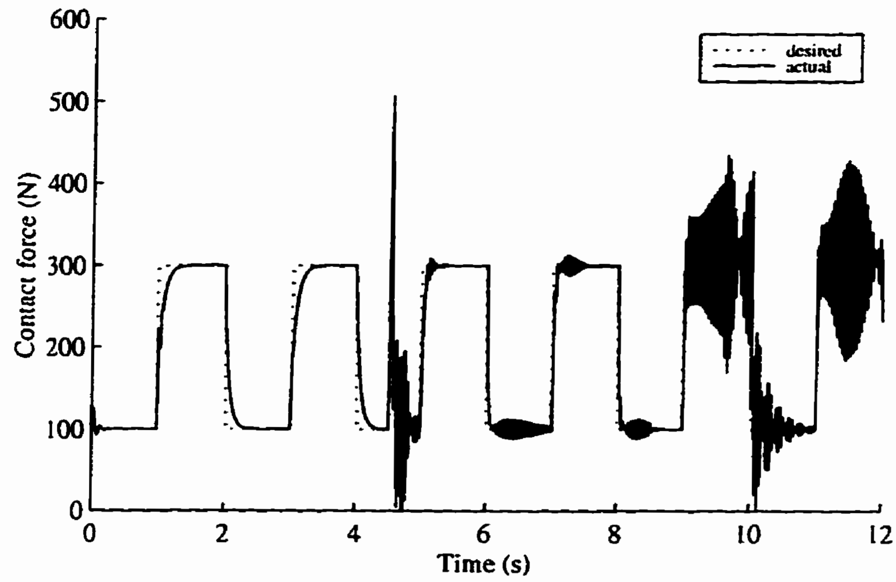

Fig. 5-23 Contact force response with varying environment stiffness.

5.2 MULTI-LINK GENERALIZED PREDICTIVE FORCE CONTROL

This section examines the case in which both links of the two-link hydraulic manipulator are simultaneously controlled using multiple-input multiple-output GPC algorithm. Two situations are considered: one is that the end-effector is force controlled in two orthogonal directions; the other one is when the force control is only required in one direction while the other direction is position controlled.

5.2.1 Cartesian Force Control

Figure 2-5 depicts the scenario that the end-effector is to be controlled in both x and y directions. Figure 5-24 shows the block diagram of force control applied at the end-effector of a two-link manipulator using a MIMO GPC scheme.

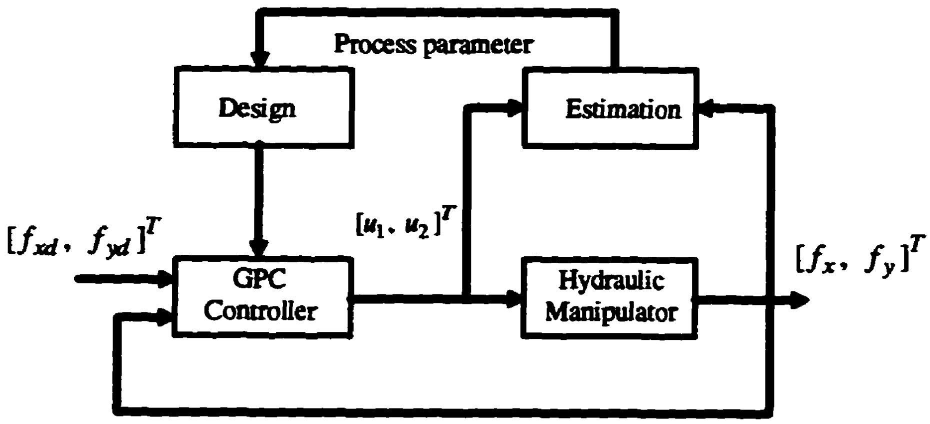

Fig. 5-24 MIMO GPC system block diagram.

The s-domain transfer function relating $[U_1,\ \ U_2]^T$ to $[F_x,\ \ F_y]^T$ was found in equation (2-46). With a zero order holder, the z-transformation of equation (2-46) is:

$$\begin{bmatrix} F_x(z) \\ F_y(z) \end{bmatrix} = \begin{bmatrix} K_1(z) & K_2(z) \\ K_3(z) & K_4(z) \end{bmatrix} \begin{bmatrix} u_1(z) \\ u_2(z) \end{bmatrix} \tag{5-10}$$

where

$$K_1(z)=\frac{b_{110}z^{-1}+b_{111}z^{-2}+b_{112}z^{-3}+b_{113}z^{-4}+b_{114}z^{-5}+b_{115}z^{-6}}{1+a_{11}z^{-1}+a_{12}z^{-2}+a_{13}z^{-3}+a_{14}z^{-4}+a_{15}z^{-5}+a_{16}z^{-6}}$$

$$K_2(z)=\frac{b_{120}z^{-1}+b_{121}z^{-2}+b_{122}z^{-3}+b_{123}z^{-4}+b_{124}z^{-5}+b_{125}z^{-6}}{1+a_{11}z^{-1}+a_{12}z^{-2}+a_{13}z^{-3}+a_{14}z^{-4}+a_{15}z^{-5}+a_{16}z^{-6}}$$

$$K_3(z)=\frac{b_{210}z^{-1}+b_{211}z^{-2}+b_{212}z^{-3}+b_{213}z^{-4}+b_{214}z^{-5}+b_{215}z^{-6}}{1+a_{11}z^{-1}+a_{12}z^{-2}+a_{13}z^{-3}+a_{14}z^{-4}+a_{15}z^{-5}+a_{16}z^{-6}}$$

$$K_4(z)=\frac{b_{220}z^{-1}+b_{221}z^{-2}+b_{222}z^{-3}+b_{223}z^{-4}+b_{224}z^{-5}+b_{225}z^{-6}}{1+a_{21}z^{-1}+a_{22}z^{-2}+a_{23}z^{-3}+a_{24}z^{-4}+a_{25}z^{-5}+a_{26}z^{-6}}$$

With h_1 and h_2 added as the terms to take care of nonlinear effects, the outputs in discrete time form are:

$$f_x(t)=-a_{11}f_x(t-1)-\cdots-a_{16}f_x(t-6)+b_{110}u_1(t-1)+\cdots+b_{115}u_1(t-6)$$
$$+b_{120}u_2(t-1)+\cdots+b_{125}u_2(t-6)+h_1(t) \quad \text{(5-11a)}$$

$$f_y(t)=-a_{21}f_y(t-1)-\cdots-a_{26}f_y(t-6)+b_{210}u_1(t-1)+\cdots+b_{215}u_1(t-6)$$
$$+b_{220}u_2(t-1)+\cdots+b_{225}u_2(t-6)+h_2(t) \quad \text{(5-11b)}$$

Equation (5-11a) is herewith called Channel x and (5-11b) Channel y.

Two RLS estimators are needed to find the parameter sets $[a_{11} \;\cdots\; a_{16} \;\; b_{110} \;\cdots\; b_{115} \;\; b_{120} \;\cdots\; b_{125} \;\; h_1]$ and $[a_{21} \;\cdots\; a_{26} \;\; b_{210} \;\cdots\; b_{215} \;\; b_{220} \;\cdots\; b_{225} \;\; h_2]$. In the computer simulation, the initial values of these parameters were set to:

Channel x: $a_{11}=\cdots=a_{16}=0$, $b_{110}=1$, $b_{111}=\cdots=b_{115}=0$, $b_{120}=1$, $b_{121}=\cdots=b_{125}=0$

Channel y: $a_{21} = \cdots = a_{26} = 0$, $b_{210} = 1, b_{211} = \cdots = b_{215} = 0$, $b_{220} = 1, b_{221} = \cdots = b_{225} = 0$

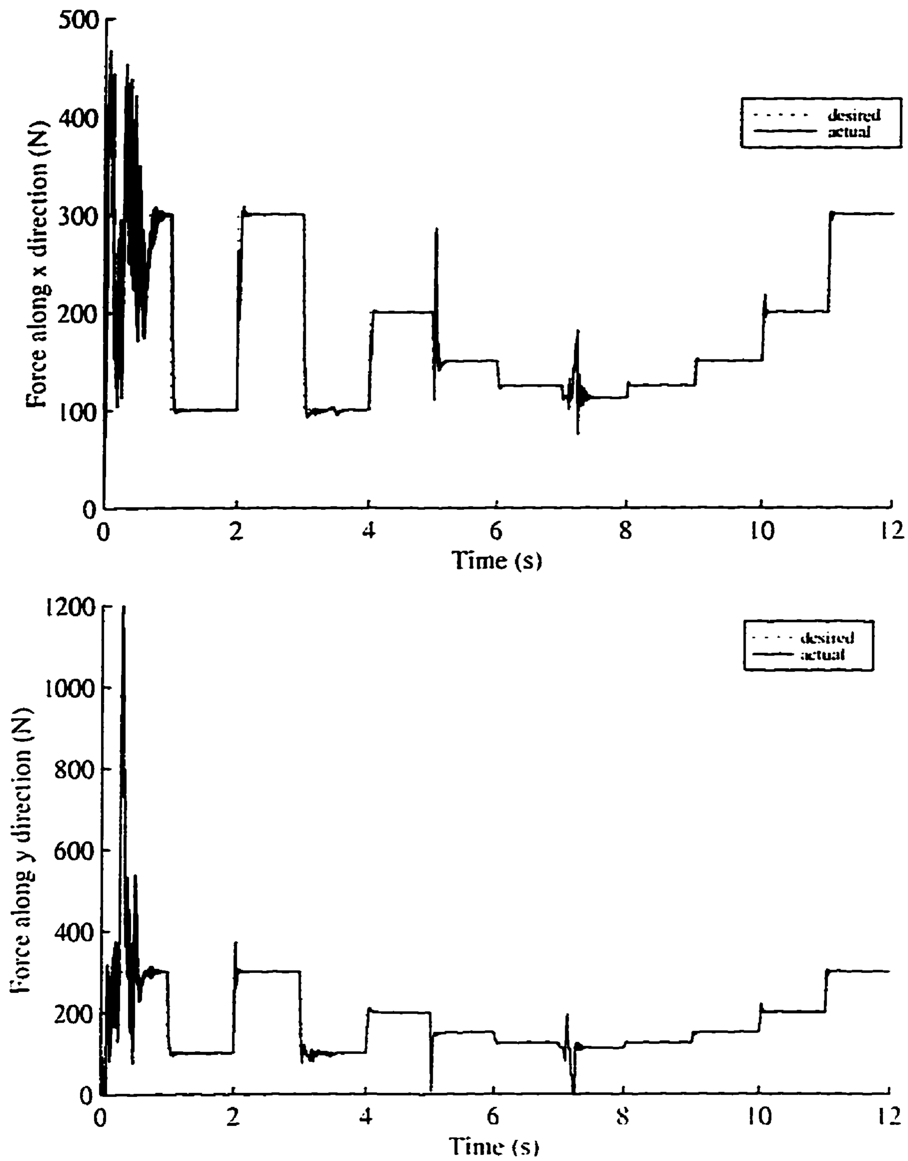

Fig. 5-25 Contact force responses along x and y directions (channel x: $N_1=1$, $N_2=17$, $N_u=1$, $\lambda_c=1$, $\lambda_r=0.35$, $\lambda_f=0.99$; channel y: $N_1=1$, $N_2=17$, $N_u=1$, $\lambda_c=1$, $\lambda_r=0.35$, $\lambda_f=0.99$).

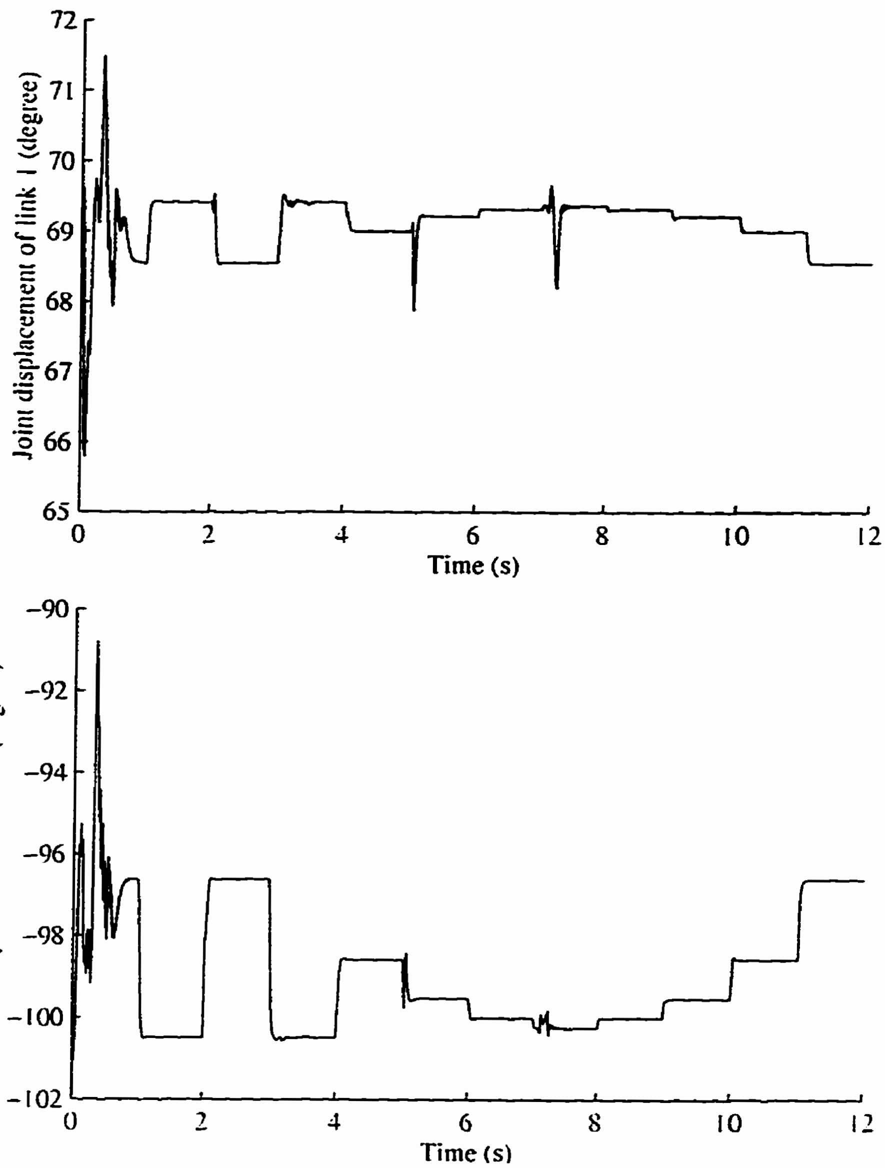

Fig. 5-26 Joint displacements pertaining to Figure 5-25 (top: link 1: bottom: link 2).

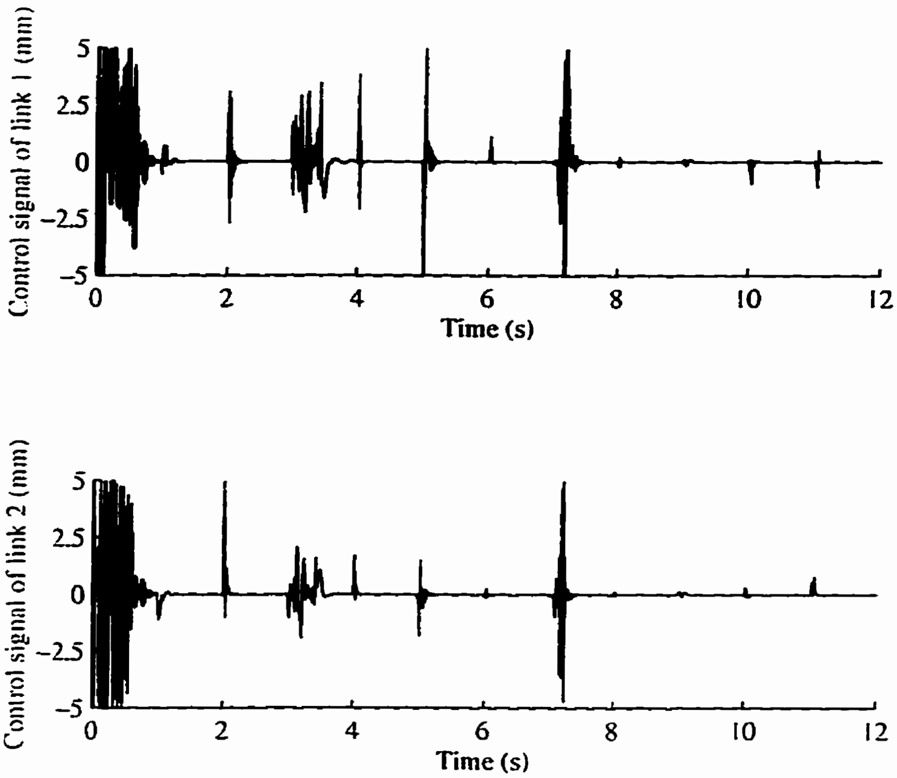

Fig. 5-27 Control inputs pertaining to Figure 5-25 (top: link 1; bottom: link 2).

On the environment side, $m_{ex} = m_{ey} = 0$ kg, $d_{ex} = d_{ey} = 80$ N·s/m and $k_{ex} = k_{ey} = 5000$ N/m.

To achieve the best response to step inputs along both axes, the design parameters of the controller were tuned to be:

Channel x: N_1=1, N_2=17, N_u=1, λ_c=1, λ_r=0.35, λ_f=0.99

Channel y: N_1=1, N_2=17, N_u=1, λ_c=1, λ_r=0.35, λ_f=0.99

Figure 5-25 shows the force responses along the x and y axis. There was large overshoot at the beginning because no prior knowledge about the values of the plant model parameters was given. The overshoot can be avoided if some prior information was incorporated into the controller. For instance, the initial values of the parameter could have been obtained by off-line estimation. Figures 5-26 and 5-27 show the joint displacement and the control signal, respectively.

Figure 5-28 shows the force response of another test with step and ramp set-points. At $t =$ 15second, the stiffness of the environment suddenly doubled to $k_e = 10000\ \mathrm{N/m}$. Again, generalized predictive force controller demonstrated its adaptability to stiffness change. The control signal was shown in Fig. 5-29.

5.2.2 Hybrid Position/Force Control

This section involves the development of an algorithm capable of handling hybrid position/force control tasks depicted in Fig. 2-6.

Suppose the implement of a two-link manipulator is commanded to apply a certain force along x direction to the environment. At the same time, it is to travel along y direction on the environment surface following a specified trajectory. Reference [3] suggested that the force in x-direction, f_x, and the position in y direction, y, could be controlled independently since x and y are orthogonal, which made the hybrid force/position control valid in theory. The idea is adopted in this thesis, and the adaptive MIMO GPC algorithm is applied to perform the task.

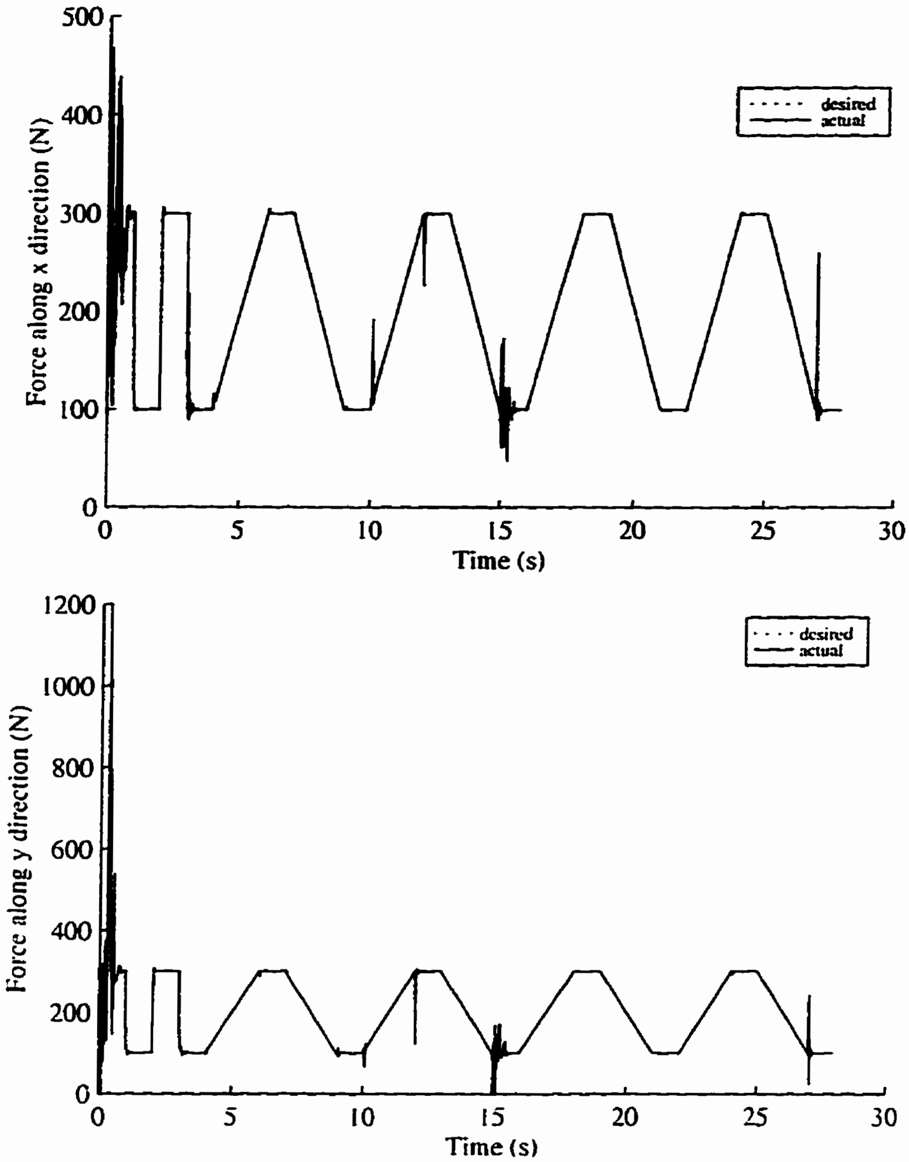

Fig. 5-28 Contact forces responses to a ramp input.

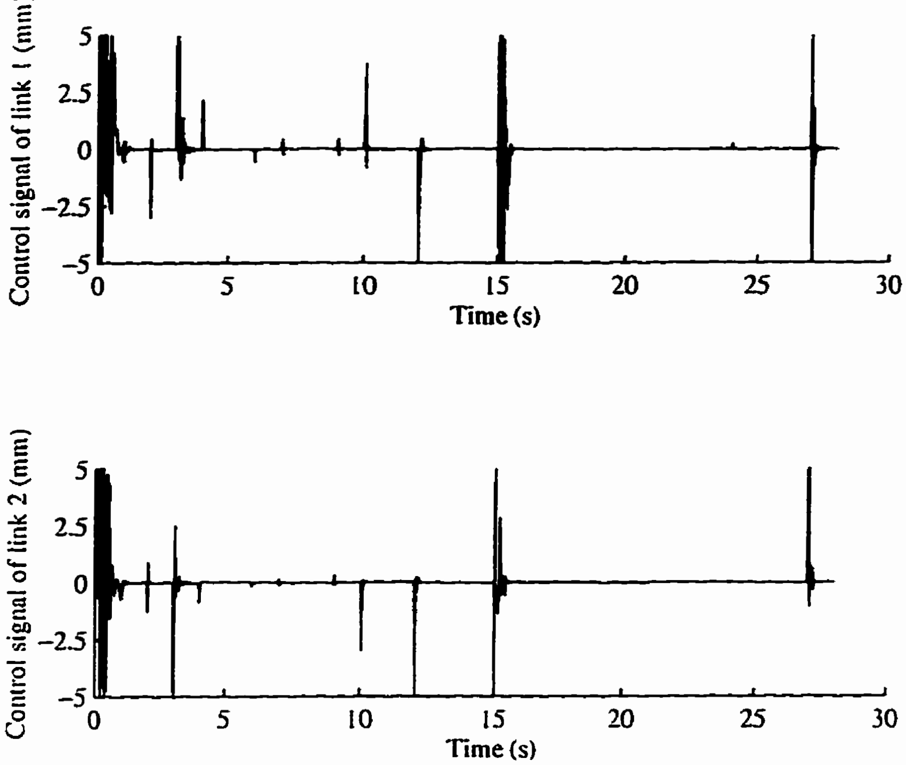

Fig. 5-29 Control inputs pertaining to Figure 5-28.

Fig. 5-30 shows the hybrid position/force control scheme using MIMO GPC algorithm.

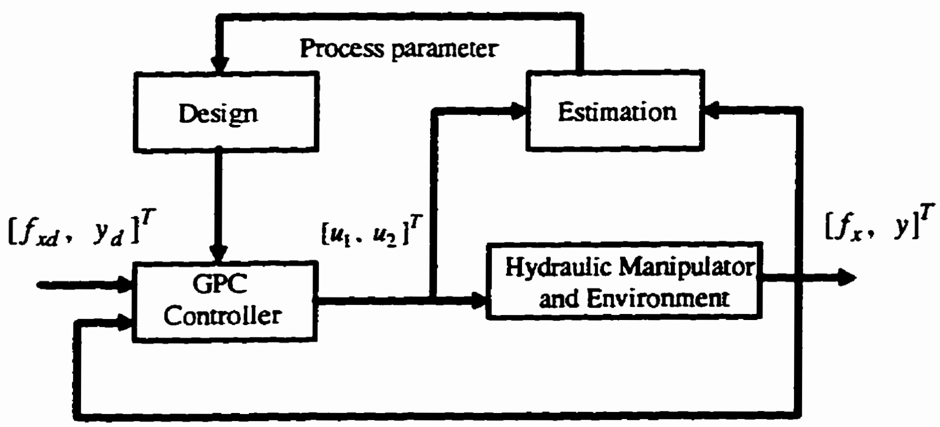

Fig. 5-30 Hybrid position/force MIMO GPC system.

The s-domain transfer function was previously found in equation (2-51). With a zero order holder, the z-transformation is similar to equation (5-10).

With $h_1(t)$ and $h_2(t)$ added as the terms to take care of nonlinear effects, the outputs in discrete time form are therefor,

$$f_x(t) = -a_{11}f_x(t-1) - \cdots - a_{16}f_x(t-6) + b_{110}u_1(t-1) + \cdots + b_{115}u_1(t-6)$$
$$+ b_{120}u_2(t-1) + \cdots + b_{125}u_2(t-6) + h_1(t) \quad \text{(5-12a)}$$

$$y(t) = -a_{21}y(t-1) - \cdots - a_{26}y(t-6) + b_{210}u_1(t-1) + \cdots + b_{215}u_1(t-6)$$
$$+ b_{220}u_2(t-1) + \cdots + b_{225}u_2(t-6) + h_2(t) \quad \text{(5-12b)}$$

The parameter sets $[a_{11} \ \cdots \ a_{16} \ b_{110} \ \cdots b_{115} \ b_{120} \ \cdots \ b_{125} \ h_1]$ and $[a_{21} \ \cdots \ a_{26} \ b_{210} \ \cdots \ b_{215} \ b_{220} \ \cdots \ b_{225} \ h_2]$ are to be estimated by two RLS estimators respectively.

In the computer simulation, the initial values of these parameters were set to:

$$a_{11} = \cdots = a_{16} = 0,\ b_{110} = 1,\ b_{111} = \cdots = b_{115} = 0,\ b_{120} = 1,\ b_{121} = \cdots = b_{125} = 0$$

$$a_{21} = \cdots = a_{26} = 0,\ b_{210} = 1,\ b_{211} = \cdots = b_{215} = 0,\ b_{220} = 1,\ b_{221} = \cdots = b_{225} = 0$$

The sampling time was chosen to be 0.001s and $m_{ex} = 0\ \text{kg}$, $d_{ex} = 0\ \text{N}\cdot\text{s/m}$ and $k_{ex} = 1\times10^4\ \text{N/m}$ to model a stiff environment.

In the simulation, the environment was placed along $x = 0.61116\text{m}$ while the end point was initially placed at point $x = 0.81116\text{m}$ and $y = 1.15846\text{m}$, which generated an initial force of 1500N due to the deformation of the environment. During the first 5 seconds, the end point was set to stay at its initial position. It was then commanded to follow a pre-specified trajectory along the y direction. Meanwhile, the manipulator was trying to keep a constant force of 1500N against the surface of the environment along the x direction.

The best response was obtained by using the following parameter setting:

Channel x: N_1=1, N_2=17, N_u=1, λ_c=1, λ_r=0.3, λ_f=0.999

Channel y: N_1=1, N_2=17, N_u=1, λ_c=1, λ_r=0.3, λ_f=0.999

Figure 5-31 shows the force and position responses along the x and y axes, respectively. The largest overshoot for the force occurred at the very beginning when the controller was learning the system's dynamics. The response after this period was very good. The contact force was kept at the desired 1500N with the maximum error of 20N or 1.33% of the desired value (see Fig. 5-32). The position tracking along the y direction, shown in Fig. 5-33, was also acceptable with the maximum error of only 1mm.

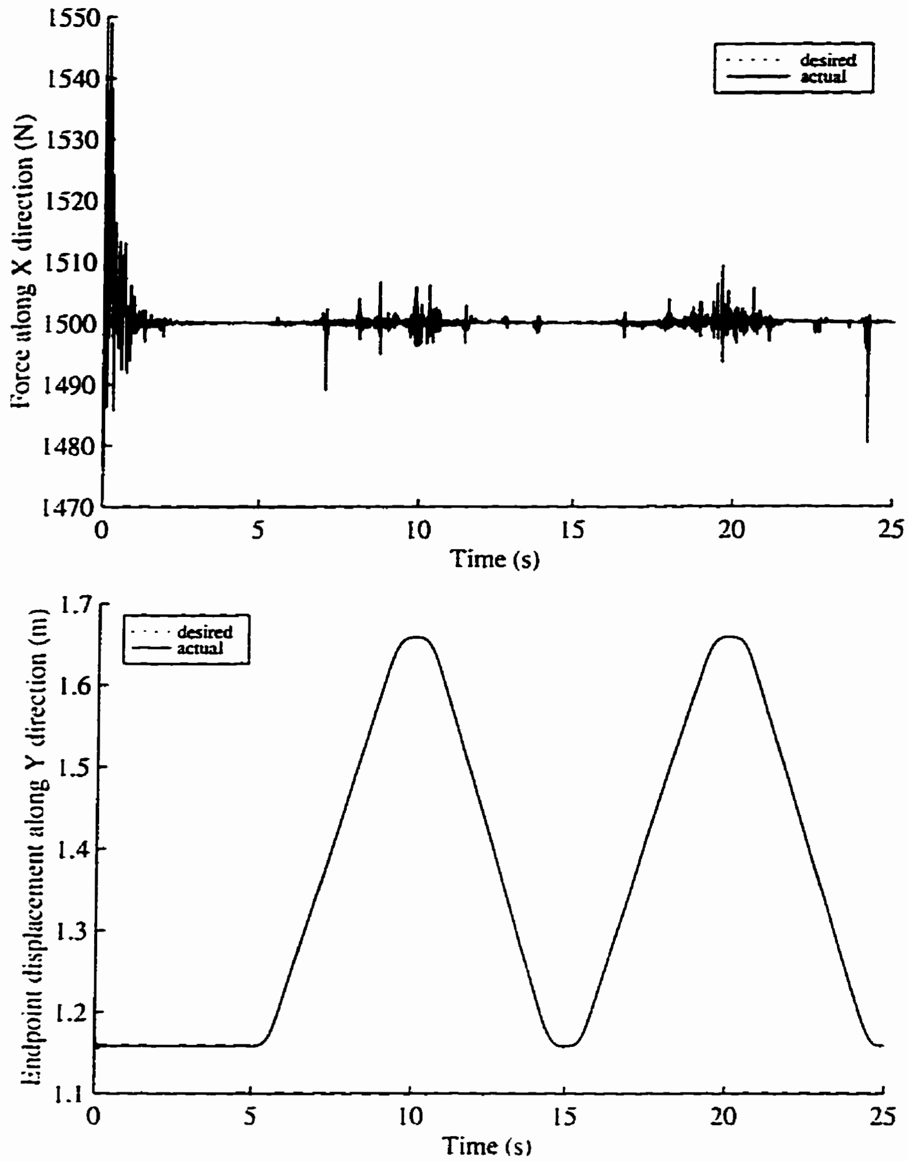

Fig. 5-31 Contact force along x direction and end point position along y direction (channel x: $N_1=1$, $N_2=17$, $N_u=1$, $\lambda_e=1$, $\lambda_r=0.3$, $\lambda_f=0.999$; channel y: $N_1=1$, $N_2=17$, $N_u=1$, $\lambda_e=1$, $\lambda_r=0.3$, $\lambda_f=0.999$).

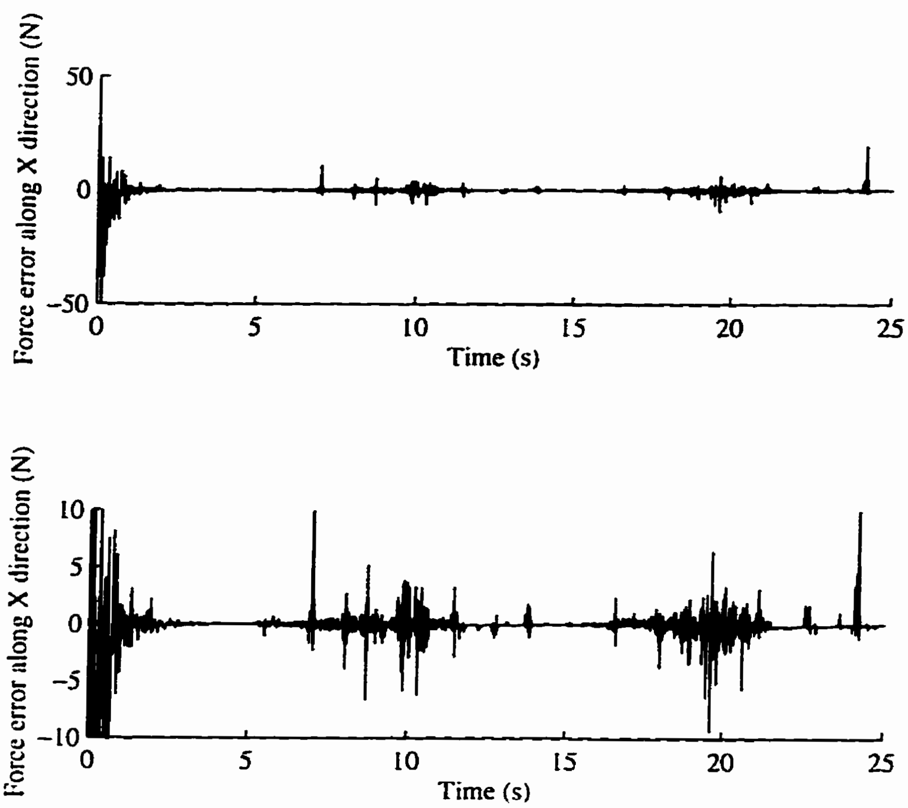

Fig. 5-32 Force tracking error pertaining to Figure 5-31.

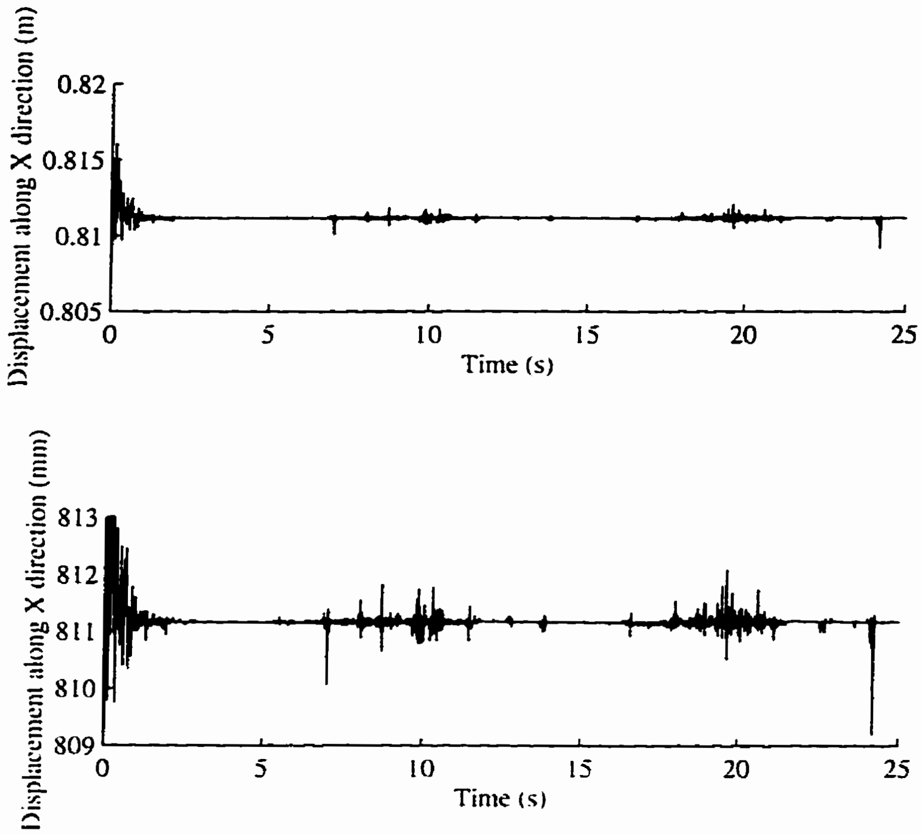

Fig. 5-33 Position tracking error pertaining to Figure 5-32.

5.3 SUMMARY

In this chapter, the performances of SISO-GP, SISO-MV and MIMO-GP force controllers were carefully examined as they were applied to a two-link hydraulic manipulator. The results demonstrate the strength and the weakness of each controller. SISO-GPC outperformed SISO-MVC in the speed of response and, more importantly, in the adaptability to the environmental changes. Regarding the comparison between SISO- and MIMO-GPC's, the introduction of MIMO-GPC algorithm to the force control did not bring significant improvement to the system performance; however, MIMO-GPC did considerably reduce the computational burden compared with the SISO-GPC algorithm. The index of computational expense is the *maximum output horizon* N_2. For each channel of the MIMO GPC algorithm, set N_2 to 17 is enough to get an excellent response. For SISO GPC controller, the best response was obtained after increasing N_2 to 60. Computational expense is among the top problems that have to be addressed before GPC algorithm can fully enter the practice in robotic control. However, there will be a significant increment of the number of the parameters to be estimated on-line as the number of linkages increases. Actually, for each channel, the number is roughly equal to the order of the system multiplied by the number of the inputs. The situation for a 2-link manipulator is still acceptable, but, for a general n-link manipulator with n being a larger value, the large number of parameters to be identified may lead to inaccurate estimation and therefore, unsatisfying system performance.

CHAPTER SIX

EXPERIMENTAL OBSERVATION

The chapter presents the verification of the adaptive control of hydraulic manipulators using Generalized Predictive and Minimum Variance Control algorithms by means of experimentation. The experiments were performed on a hydraulic actuator which has all the nonlinear characteristics that a multi-link hydraulic manipulator possesses except for the kinematics terms. Both position control and force control were experimented.

6.1 POSITION CONTROL

6.1.1 Experimental Setup

Figure 6-1 shows the test station on which all position control experiments have been carried out. The test station consists of a hydraulic actuator unit, a micro-computer with an analog/digital (A/D) conversion card, and a load. The hydraulic actuator unit has a pump, a servovalve and a cylinder. The pump is set to provide a constant operational supply pressure of $\approx$7000kPa. The servovalve is a closed-center four-way valve. The cylinder is fixed on a frame, and the load is attached to the actuator piston through steel cables. The load could help or oppose the motion of the piston depending on whether it extends or retracts. Three pressure transducers read supply pump pressure, supply line pressure and return line pressure. The displacement of the cylinder piston is read by an incremental transducer. The computer (66Hz CPU and 8M RAM) then compares the digitized position signal with the set-point, and generates a control signal. The control signal is converted to an analog signal by the A/D card, and is transmitted to the hydraulic servovalve.

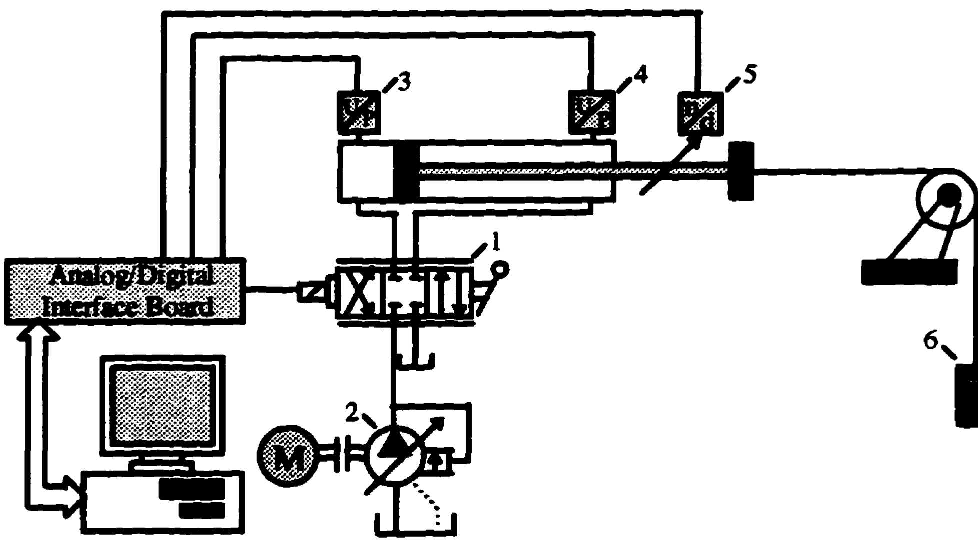

1- Servovalve 3- Supply Line Pressure Transducer 5- Incremental Encoder
2- Pump 4- Return Line Pressure Transducer 6- Load

Fig. 6-1 Schematic of the experimental test station for position control.

The servovalve operation is linear when the control signal is within [-1.8volt, 1.8volt]. Therefore, in the experiments the control signal is limited within this range to ensure acceptable performance. The servovalve also has a dead-band of [-0.4volt, 0.4volt]. A sampling time of 0.01 second was chosen for the experiments.

6.1.2 System Analysis

Figure 6-2 depicts the configuration of the hydraulic actuator with almost all variables being defined before, except for *m* stands for the mass of the rod plus piston. *m* was neglected in the previous chapters because it was far smaller than the link being actuated.

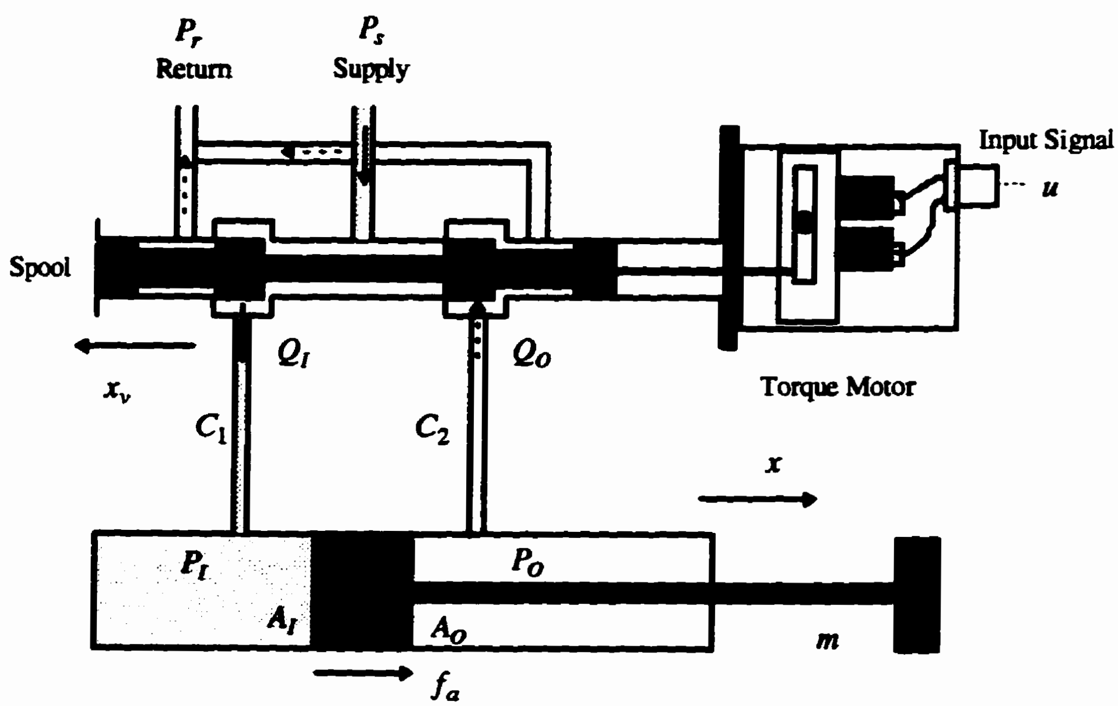

Fig. 6-2 Hydraulic actuator in free motion.

From Chapter 2 it is known that the linearized dynamics equation of a hydraulic actuator in s-domain are:

$$Q_I = K_u U - K_p P_I \tag{6-1a}$$

$$Q_O = K_u U + K_p P_O \tag{6-1b}$$

where $K_u = Kw\sqrt{\frac{P_s - P_l}{2}}$, $K_p = \frac{Kwx}{\sqrt{2(P_s - P_l)}}$ and $P_l = P_I - P_O$.

The pipe dynamics equations in s-domain are:

$$Q_I = CP_I s + A_I Xs \tag{6-2a}$$

$$Q_O = -CP_O s + A_O Xs \tag{6-2b}$$

Note it is assumed that $C_1 = C_2 = C$.

Equating equations (6-1) and (6-2) to remove Q_I and Q_O arrives:

$$P_I = \frac{K_u U - A_I Xs}{K_p + Cs} \tag{6-3a}$$

$$P_O = \frac{-K_u U + A_O Xs}{K_p + Cs} \tag{6-3b}$$

The actuating force is:

$$F_a = P_I A_I - P_O A_O \tag{6-4}$$

F_a overcomes the viscous friction and the Coulomb friction, and moves the rod, the piston and the load. Hence, F_a can be expressed as:

$$F_a = mXs^2 + dXs \tag{6-5}$$

Substituting (6-3) into (6-4) and comparing the result with (6-5) gives:

$$\frac{X(s)}{U(s)} = \frac{K_u(A_I + A_O)}{s[(ms+d)(Cs+K_p)+(A_I^2 + A_O^2)]} \tag{6-6}$$

and

$$\frac{V(s)}{U(s)} = \frac{K_u(A_I + A_O)}{[(ms+d)(Cs+K_p)+(A_I^2 + A_O^2)]} \tag{6-7}$$

where $V(s)$ represents the velocity of the actuator.

Equation (6-6) is a third order system, and its z-transform including a zero order holder is in the form of:

$$\frac{X(z)}{U(z)} = \frac{b_0 z^{-1} + b_1 z^{-2} + b_2 z^{-3}}{1 + a_1 z^{-1} + a_2 z^{-2} + a_3 z^{-3}} \tag{6-8}$$

Therefore the discrete form of the output $x(t)$ is:

$$\begin{aligned} x(t) = &-a_1 x(t-1) - a_2 x(t-2) - a_3 x(t-3) \\ &+ b_0 u(t-1) + b_1 u(t-2) + b_2 u(t-3) + h(t) \end{aligned} \tag{6-9}$$

Again, $h(t)$ is added as a forcing term to look after the effects of unmodeled dynamics such as loading. The above equation will be used for GPC algorithm.

Equation (6-7) is a second order system, and its z-transform including a zero order holder is in the form of:

$$\frac{V(z)}{U(z)} = \frac{b_0 z^{-1} + b_1 z^{-2}}{1 + a_1 z^{-1} + a_2 z^{-2}} \tag{6-10}$$

The discrete form of the output $v(t)$ can be written as:

$$v(t) = -a_1 v(t-1) - a_2 v(t-2) + b_0 u(t-1) + b_1 u(t-2) + h(t) \tag{6-11}$$

$h(t)$ is added as a forcing term to look after the effects of unmodeled dynamics such as loading. Equation (6-11) will be used for the MVC algorithm.

6.1.3 Results

6.1.3.1 GPC Implementation

Unlike the computer simulation study where no *prior* information of the values of the plant model parameters was given to the controller, here, in order to avoid possible large overshoots that could damage the equipment, the initial values of those parameters were needed to be carefully assigned. The data could not be obtained by taking a z-transformation of equation (6-6) because certain parameters were not accessible, such as m and d. An off-line estimation was therefore performed by removing the feedback path in Fig. 6-1 and, replacing the controller with a signal generator. Figure 6-3 shows the block diagram for the off-line parameter estimation in which u is the control signal and x

the displacement of the hydraulic actuator. The control input used for off-line estimation is shown in Fig. 6-4. Also shown in Fig. 6-4 is the response of piston displacement to the input. Figure 6-5 shows the off-line estimation results. The data obtained are:

$$a_1 = -2.3,\ a_2 = 1.82,\ a_3 = -0.48,\ b_0 = 0.00011,\ b_1 = 0.00025,\ b_2 = 0.00018,\ h = 0.0 \tag{6-12}$$

These values were then used as initial values of those parameters when on-line estimation was performed.

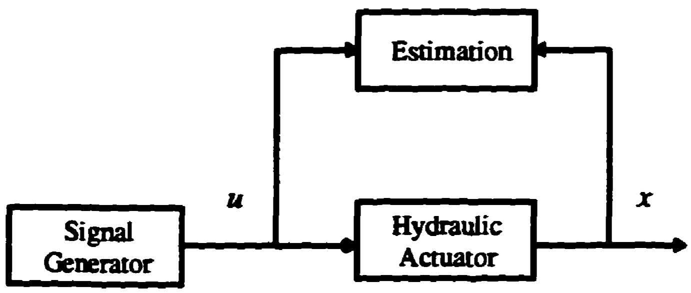

Fig. 6-3 Configuration of off-line estimation for the GPC system.

Additionally, to prevent the parameters from drifting when there was no sufficient excitation in the control signal during the on-line estimation, the following procedures were performed. First, when the control signal dropped into the dead-band with the range [-0.4volt, 0.4volt], the estimation was simply switched off. Second, both the diagonal matrix **D** and the upper triangular matrix **U** were bounded as follows :

the sum of elements in **D** was bounded within [10, 100],

the sum of elements in **U** was bounded within [0, 1.2].

The values of the boundaries were initially chosen according to the off-line identification and then were tuned experimentally, *i.e.*, they were adjusted by observing the parameter drifting during the experiments. According to L. Ljung [18], it would be sufficient to set

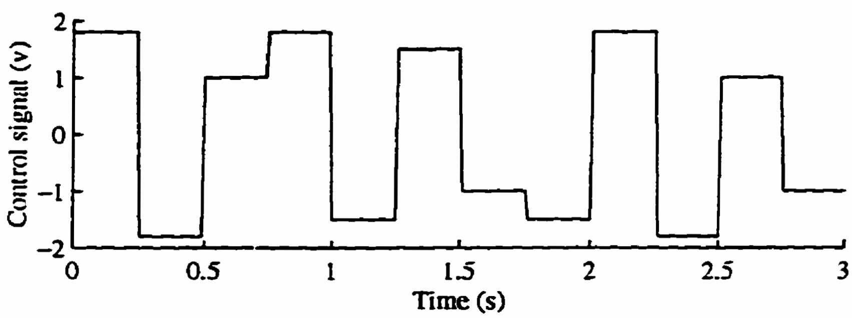

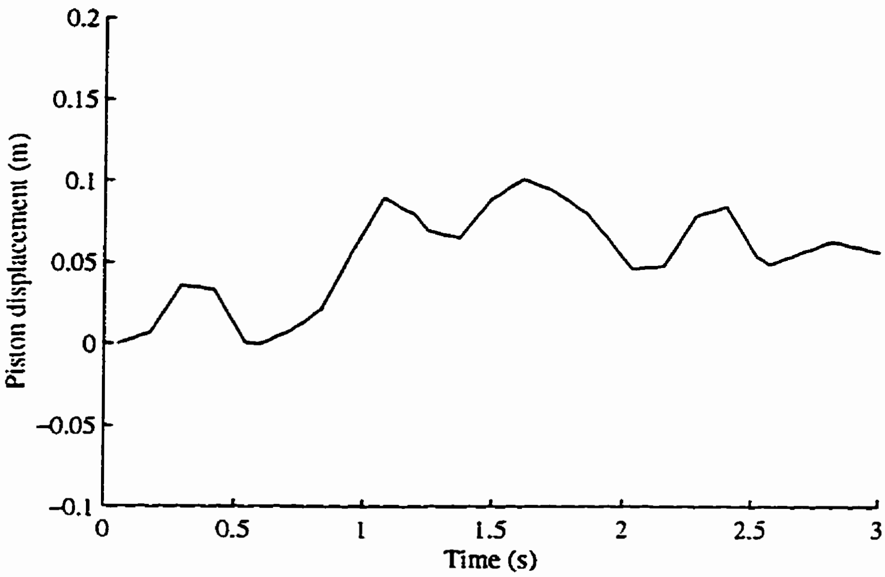

Fig. 6-4 Control input and piston displacement for off-line estimation.

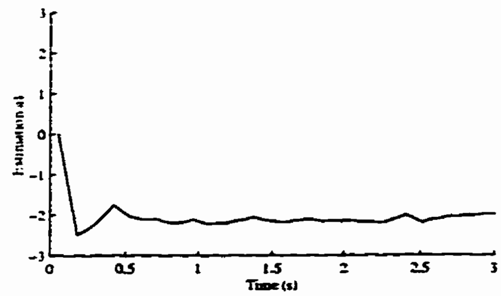

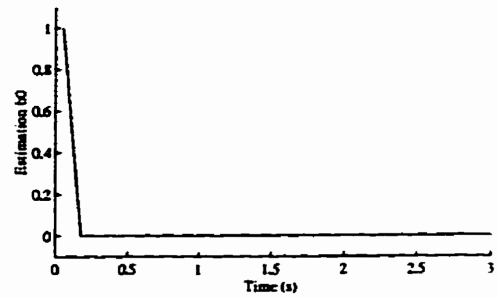

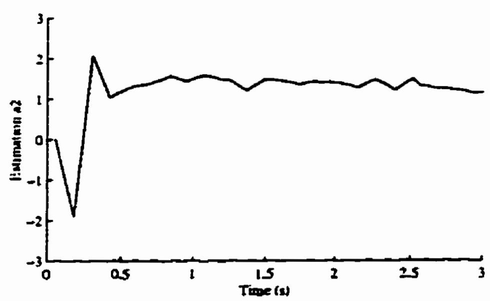

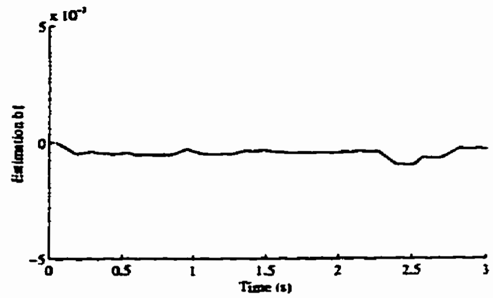

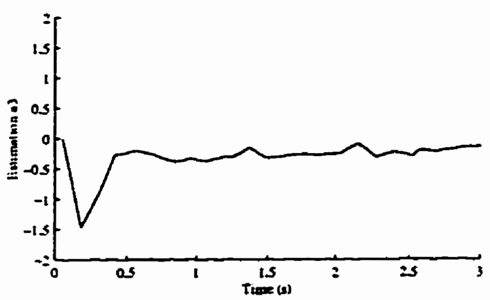

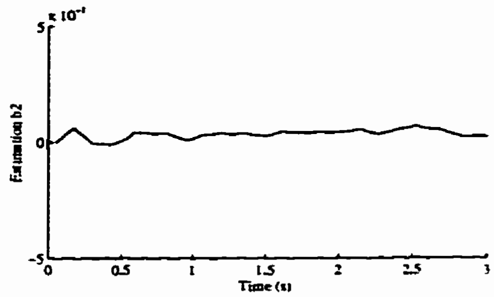

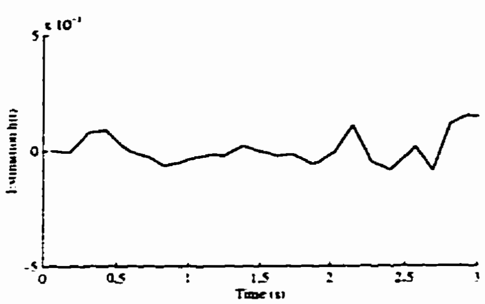

Fig. 6-5 Off-line estimation results.

only lower boundaries. However, in the experiments, it was found that the upper boundaries also affected the success of estimation. The sums of the elements were bounded instead of each element. This is because there were 7 elements in **D** and 42 elements in **U** and therefore it was difficult to set boundary for each element correctly. Nevertheless, fairly good results were obtained by bounding the sums.

The system was tested first with step inputs. The best response was obtained with the following parameter setting:

$$N_1=1,\ N_2=22,\ N_u=1,\ \lambda_c=0.005,\ \lambda_r=1.0,\ \lambda_f=0.99 \tag{6-13}$$

Figure 6-6 shows the response of piston displacement and the control signal. There was an overshoot at the very beginning during the identification of proper values of parameters. The response afterwards was excellent. It was fast, with no overshoot at all and steady-state error free. From the control signal, the integrating action of the controller in the dead-band area can be clearly seen. Fig. 6-7 shows the parameter estimation without significant drifting. The supply pressure, which was supposed to keep constant at 7000kPa, as well as the pressures of supply line and return line, P_I and P_O, are shown in Fig. 6-8.

Figure 6-9 shows the effect of varying N_2 on the response. When N_2 was increased to 32, the response became sluggish. When N_2 was decreased to 12, the response became slightly oscillatory. These observations agree with the simulation results.

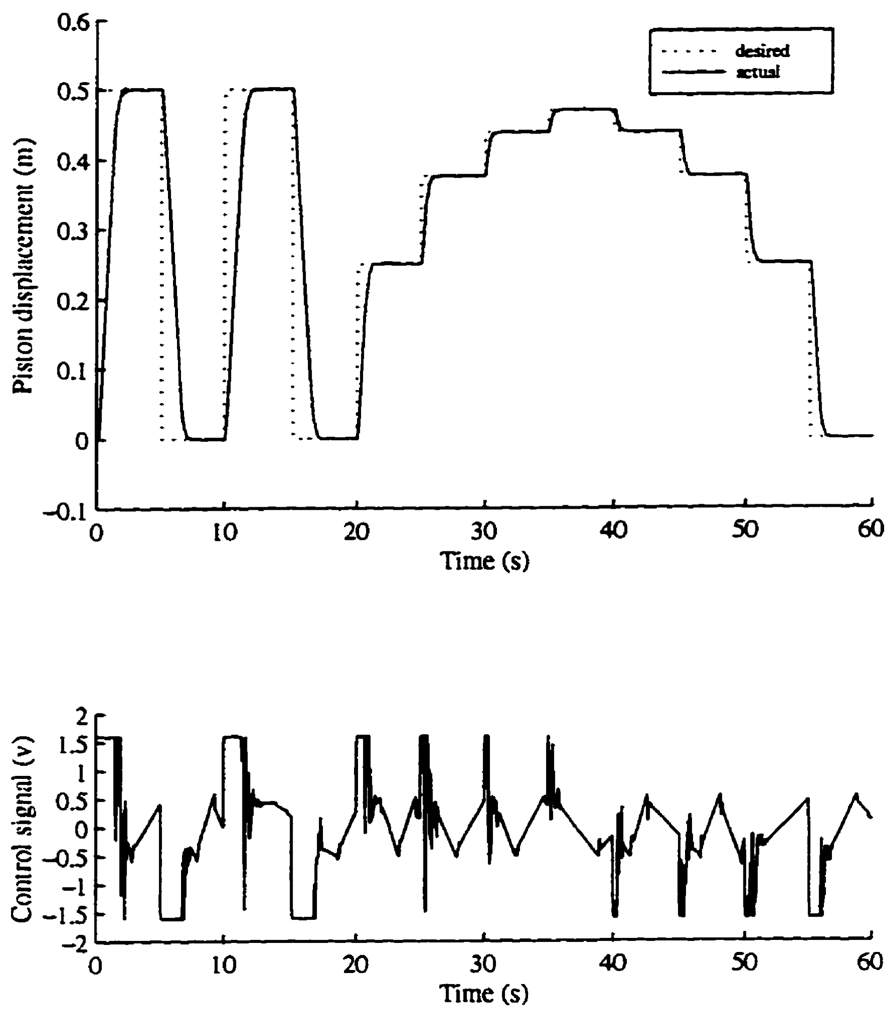

Fig. 6-6 Piston displacement and control input with

N_1=1, N_2=22, N_u=1, λ_c=0.005, λ_r=1.0, λ_f=0.99.

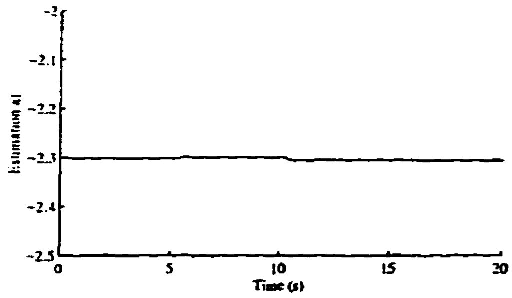

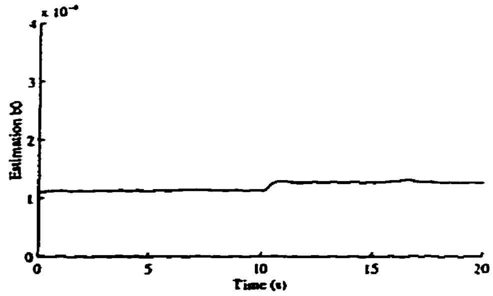

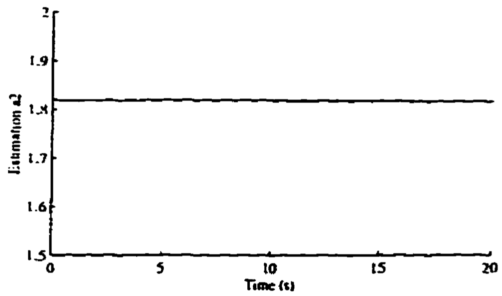

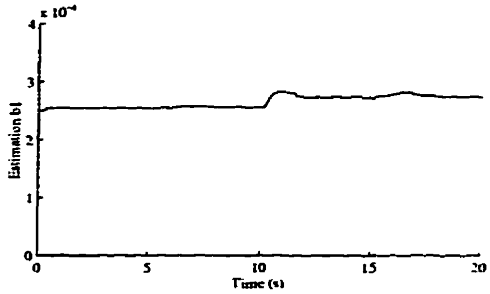

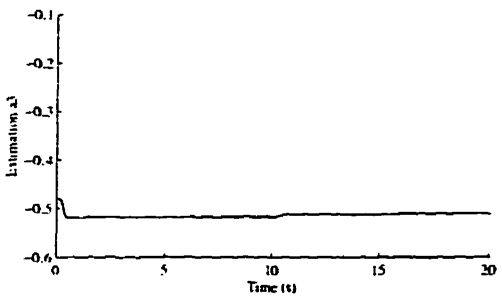

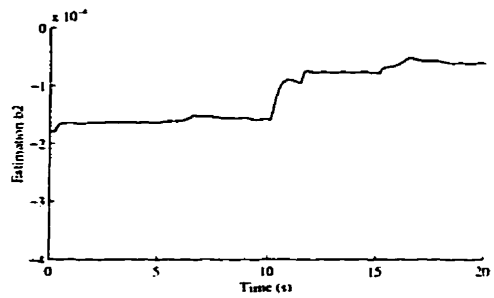

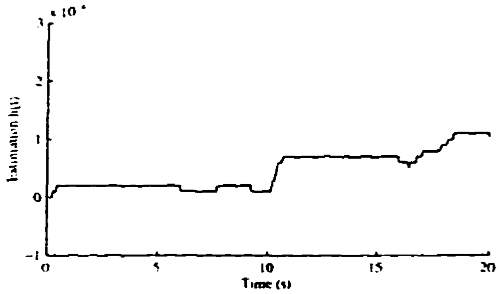

Fig. 6-7 Parameter estimation pertaining to Fig. 6-6.

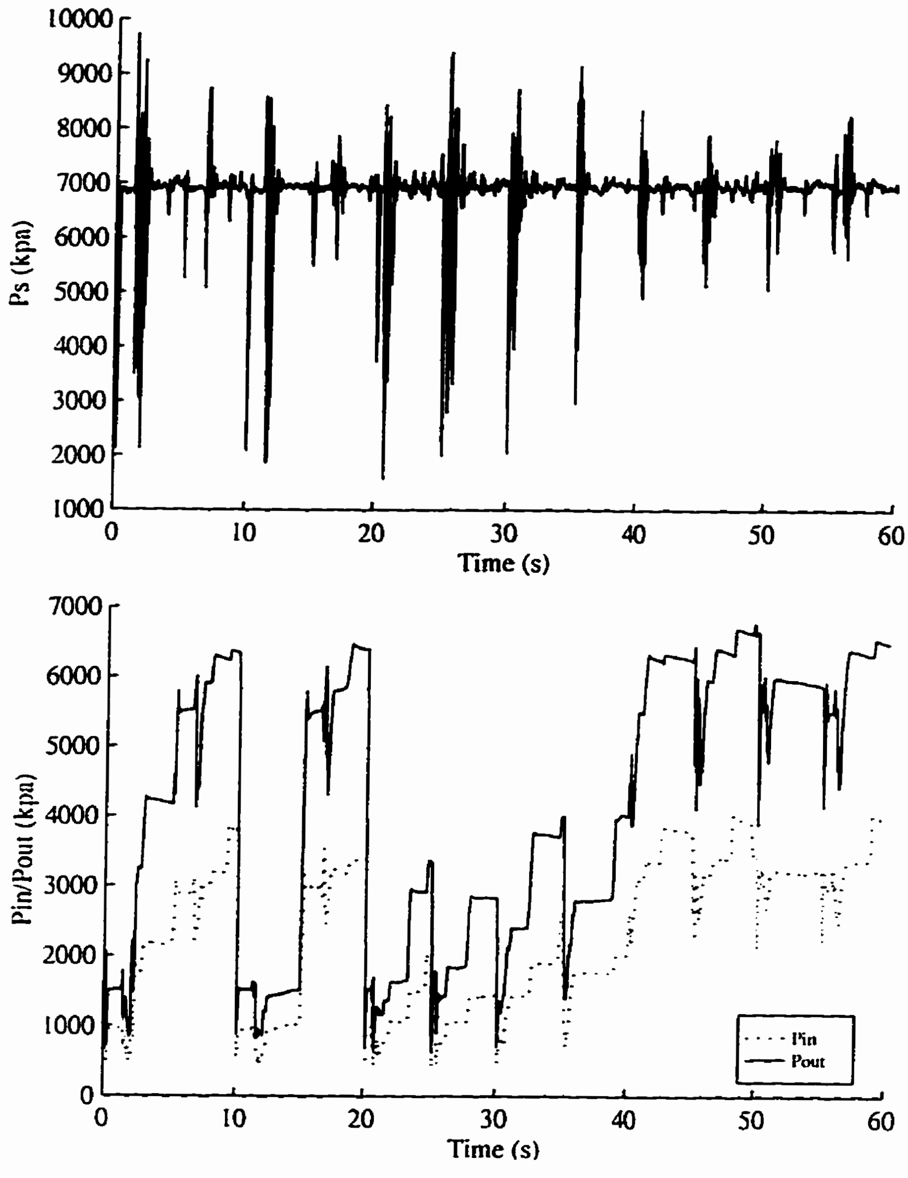

Fig. 6-8 Supply pump pressure, supply and return line pressures pertaining to Fig. 6-6.

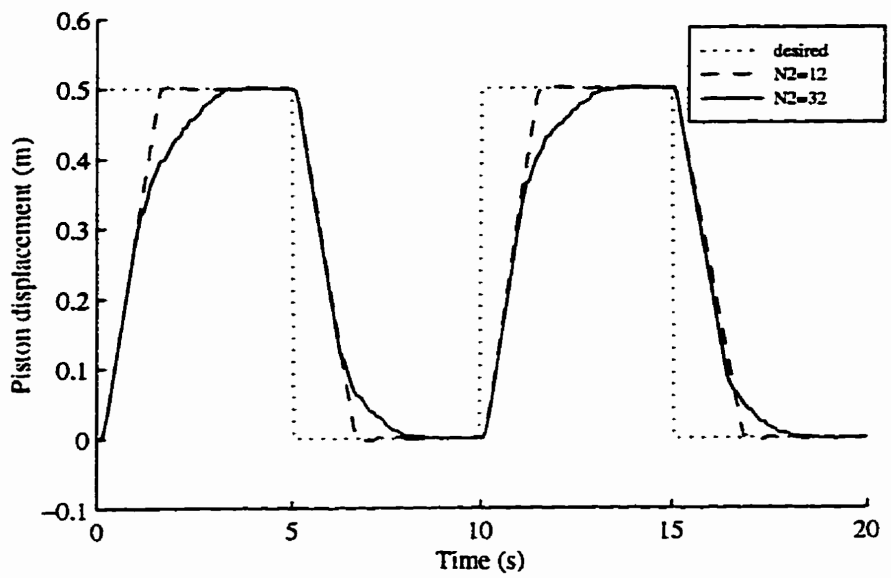

Fig. 6-9 Piston displacement response with $N_2 = 12$.

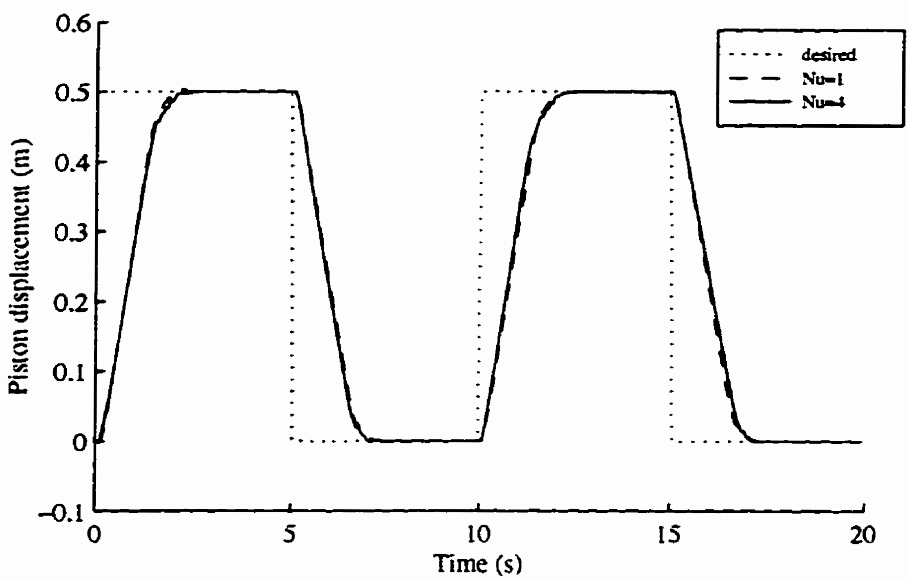

Fig. 6-10 Piston displacement response with $N_u = 4$.

Figure 6-10 shows the response when N_u was increased to 4. The response is almost identical to the result with $N_u = 1$, which suggested that the system is not sensitive to this parameter. $N_u = 1$ is preferred since larger N_u demands much more computational expense.

Figure 6-11 shows the result of increasing λ_c ten times to 0.05. It means that in the cost function more punishment was put on the control signal, which led to a less active control. In fact, Fig. 6-11 shows a faster response with small overshoot because there was no enough control to brake the movement of the piston.

Figure 6-12 shows the response of decreasing λ_r from 1.0 to 0.2, which means only one fifth of the computed control signal increment was actually applied to the valve. The result is similar to the one shown in Fig. 6-11. Figure 6-13 shows the result of changing λ_f to 0.95 which was not much different from the one when λ_f was set to 0.99.

With the parameter setting as (6-13), a load of 180 lb was imposed on the hydraulic actuator. In this experiment, when the piston was extending, the load helped making the response faster; when the piston was retracting, the load tried to oppose the motion. Figure 6-14 also shows the response of the first 20 seconds. Although there was a little overshoot, the controller was still performing very well-the response was fast and accurate with no steady-state error.

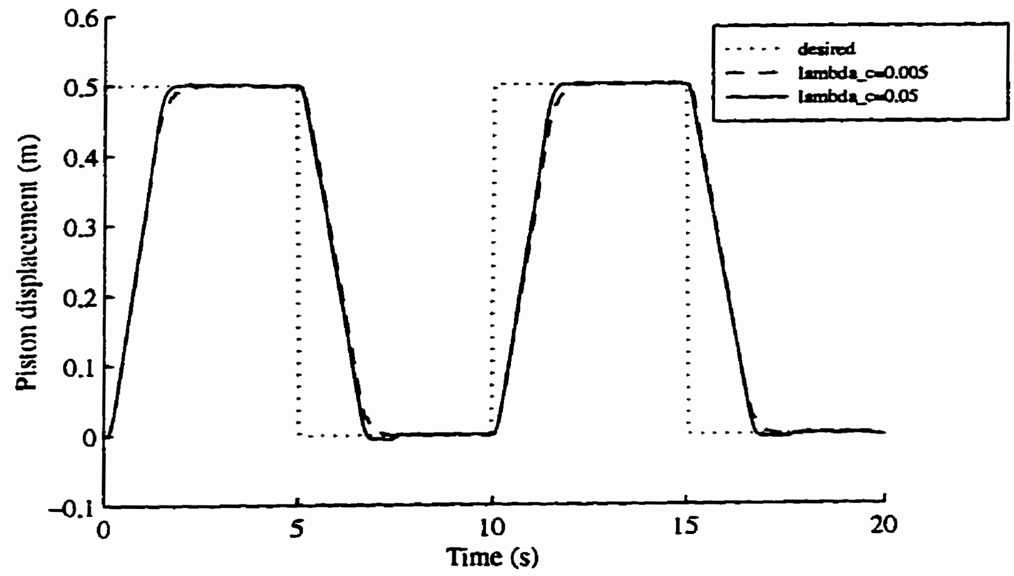

Fig. 6-11 Piston displacement response with $\lambda_c = 0.05$.

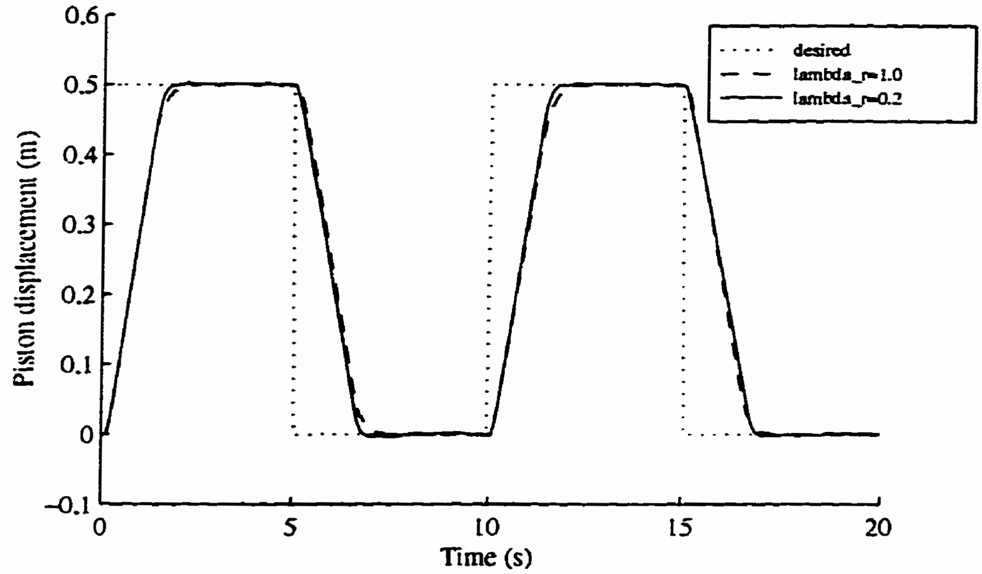

Fig. 6-12 Piston displacement response with $\lambda_r = 0.2$.

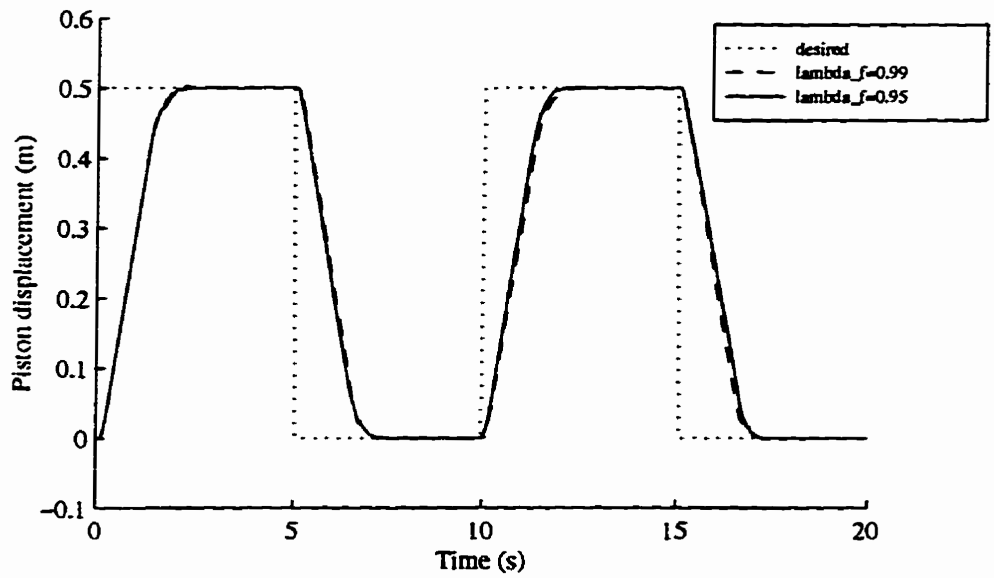

Fig. 6-13 Piston displacement response with $\lambda_f = 0.95$.

Further experiments were carried out for ramp and cosine tracking. The slopes for the ramp input were ± 0.05m/s during the first 40 seconds and ± 0.25m/s during the next 8 seconds. The frequency of the cosine wave was initially set to 0.05Hz, and then was changed to 0.25Hz. Figures 6-15 and 6-16 demonstrate the responses together with their respective tracking errors.

6.1.3.2 MVC Implementation

For minimum variance controller, the velocity of the piston was calculated by taking the derivative of the position signals. It was found that quite accurate velocity could be obtained by using only two consecutive position signals. According to equation (6-12),

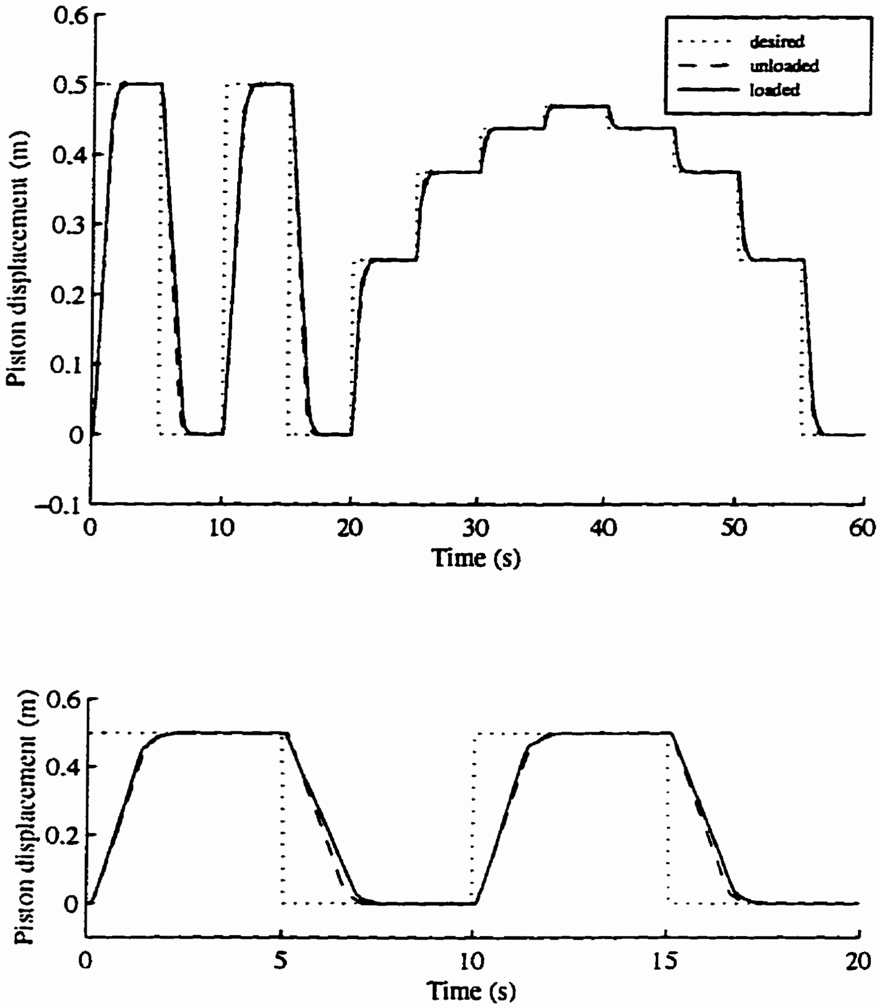

Fig. 6-14 Piston displacement response with load presented.

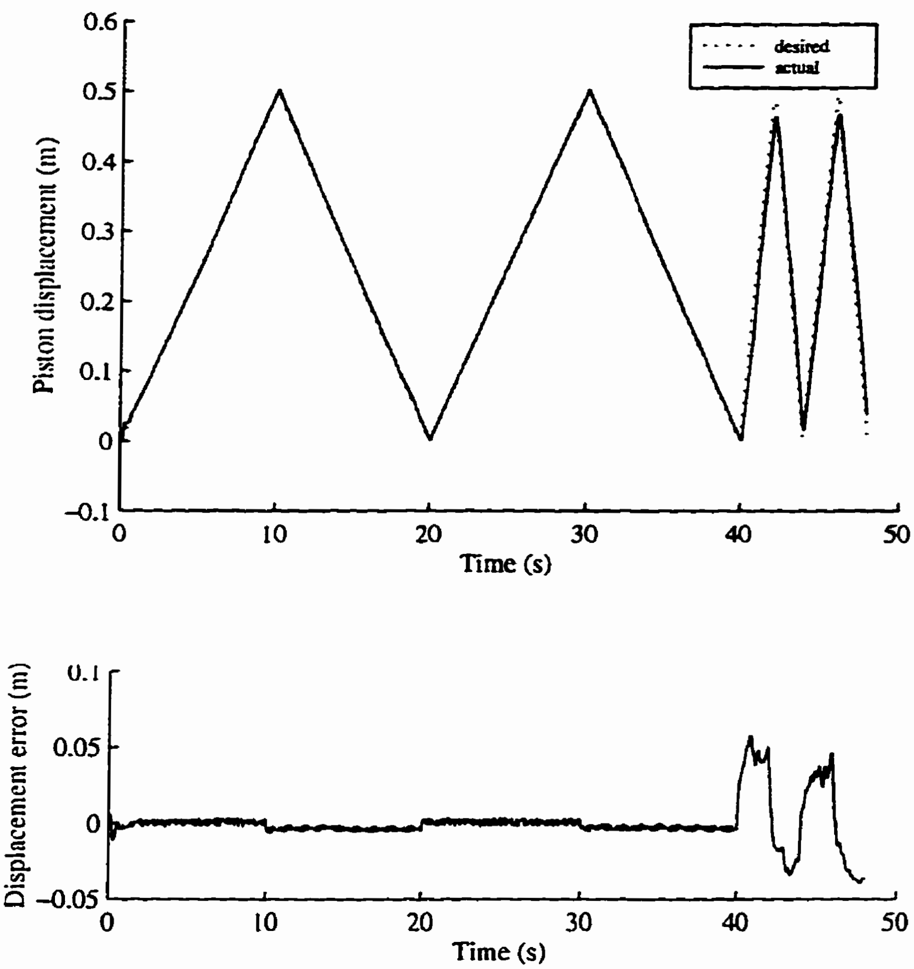

Fig. 6-15 Piston displacement and tracking error to a ramp input.

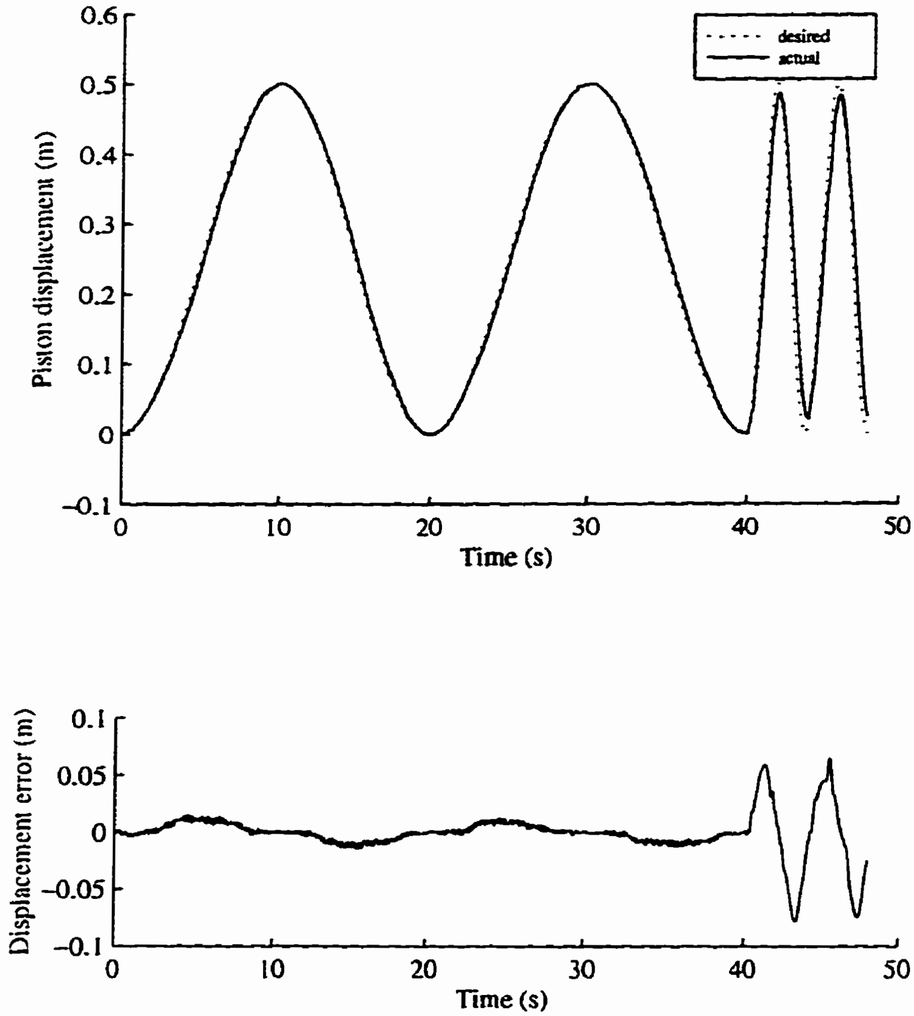

Fig. 6-16 Piston displacement and tracking error to a cosine input.

five parameters were to be estimated. First an off-line estimation was performed to find initial values. Fig. 6-17 shows the block diagram for the off-line parameter estimation in which u is the control signal and $\dot{x}$ the velocity of the hydraulic actuator. The control input used was the same as shown in Fig. 6-4. The following data were obtained:

$$a_1 = -1.167,\ a_2 = 0.264,\ b_0 = 0.00519,\ b_1 = 0.00703,\ h = 0.00237 \quad (6\text{-}14)$$

The boundary conditions set for the diagonal matrix **D** and the upper triangular matrix **U** were:

the sum of elements in **D** was bounded within [10, 18],

the sum of elements in **U** was bounded within [9, 100].

The best performing step input response was obtained with the following parameter setting:

$$c_1 = 0.5,\ \lambda_r = 0.02,\ \lambda_f = 0.99 \quad (6\text{-}15)$$

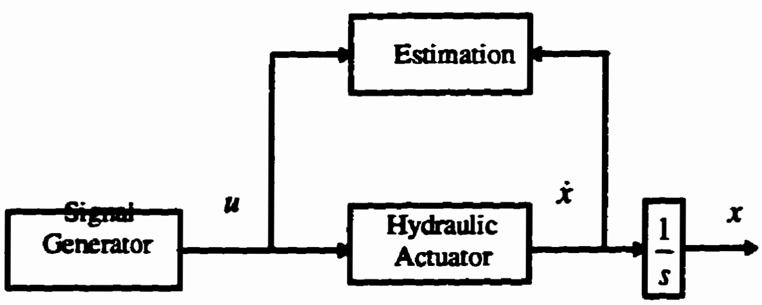

Fig. 6-17 Configuration of off-line estimation for the MVC system.

Figure 6-18 shows the piston displacement, which is actually a little faster then the one belonging to the generalized predictive controller (see Fig. 6-6). Due to presence of dead-band in the valve, there was a steady-state error in the response. The controller generated a non-zero signal during the steady-state, which was not enough to operate the servovalve. Figure 6-19 shows the parameter estimation. The supply pressure, P_s, input and output line pressures, P_I and P_O, are also shown in Fig. 6-20.

With the parameter setting as in (6-15), a load of 180 lb was applied to the hydraulic actuator. The result is shown in Fig. 6-21. With the load, the response exhibits slight oscillations which can also be observed from the control signal.

Additional experiments were carried out to test the system's tracking ability to ramp and cosine inputs. The set-points were exactly the same as the ones for GPC scheme.

Figures 6-22 and 6-23 show the responses with larger tracking errors as compared with Figs. 6-15 and 6-16.

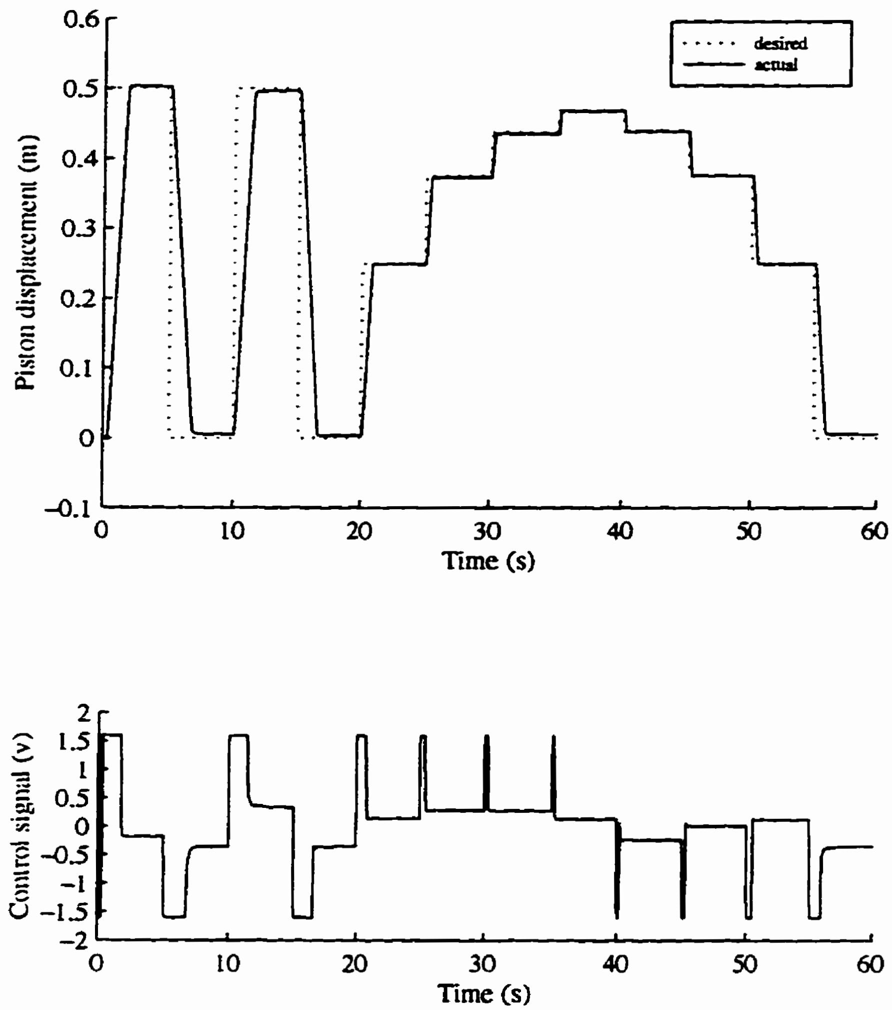

Fig. 6-18 Piston displacement and control input with c_1=0.5, λ_r=0.02, λ_f=0.99.

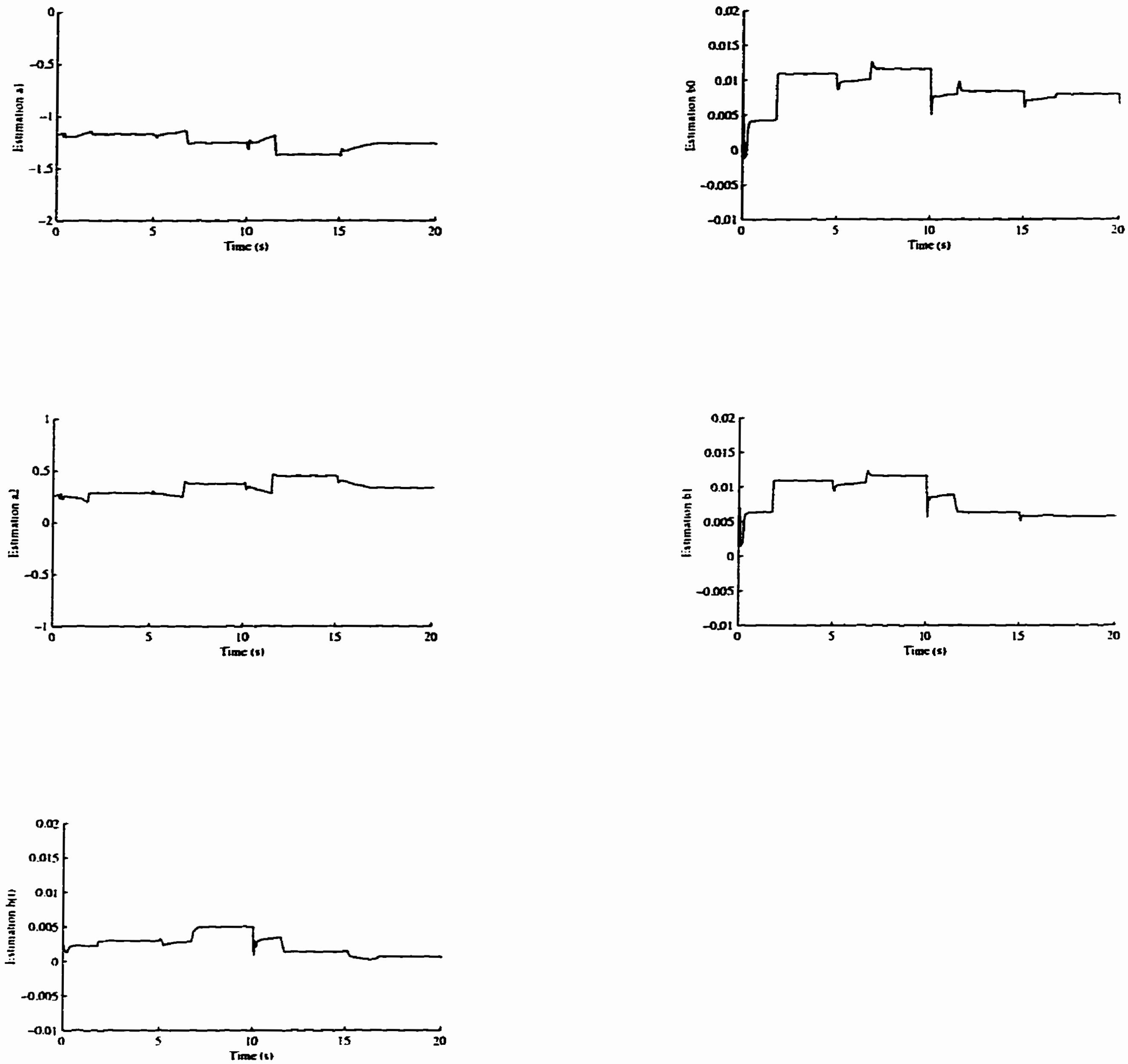

Fig. 6-19 Parameter estimation pertaining to Fig. 6-18.

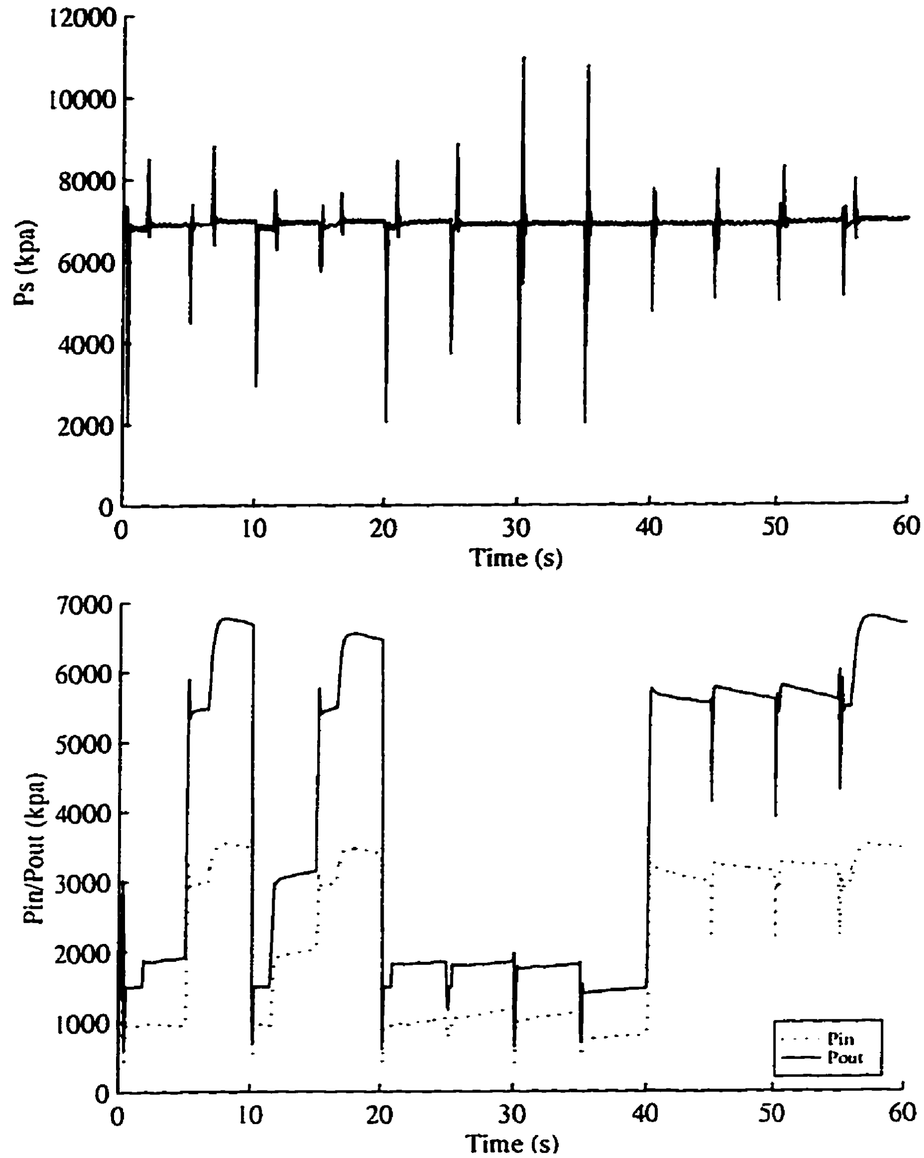

Fig. 6-20 Supply pump pressure, supply and return line pressures pertaining to Figure 6-18.

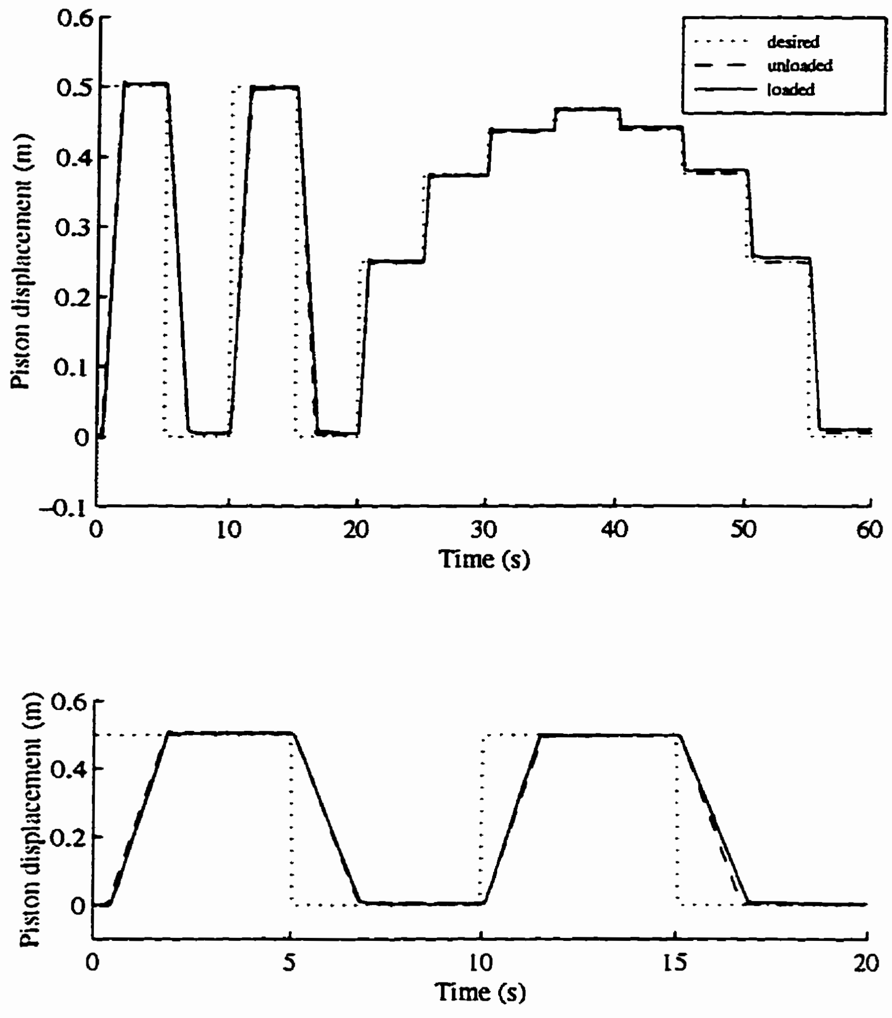

Fig. 6-21 Piston displacement response with load presented.

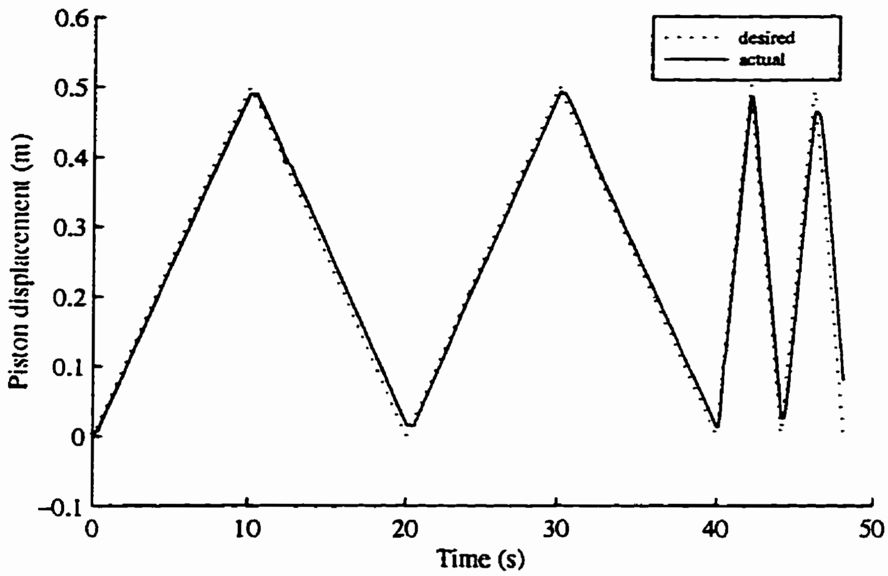

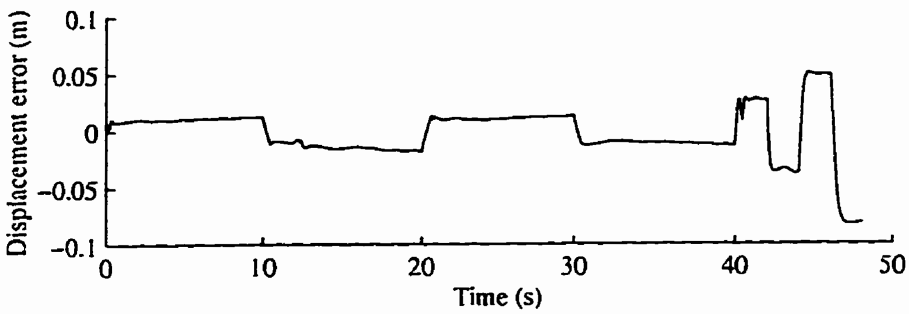

Fig. 6-22 Piston displacement and tracking error to a ramp input.

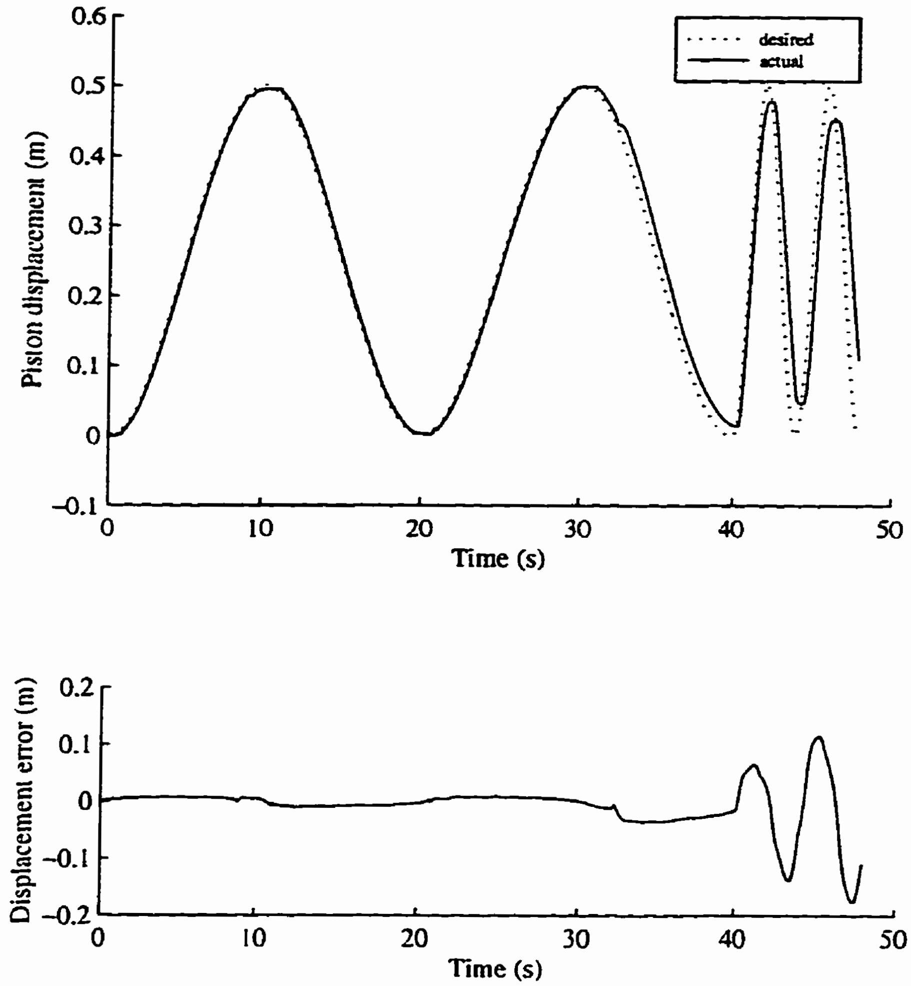

Fig. 6-23 Piston displacement and tracking error to a cosine input.

6.2 FORCE CONTROL

6.2.1 Experimental Setup

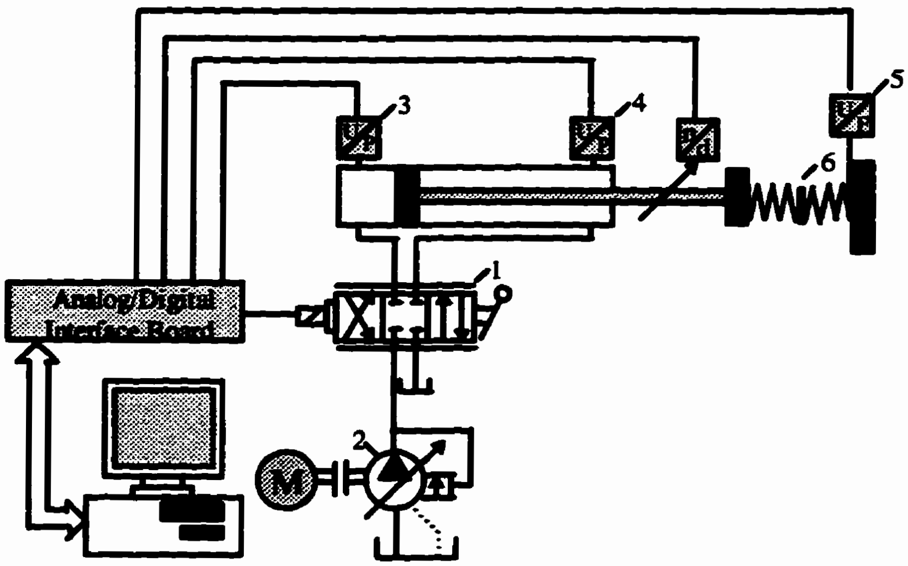

1- Servovalve 3- Supply Line Pressure Transducer 5- Force Encoder
2- Pump 4- Return Line Pressure Transducer 6- Springs

Fig. 6-24 Schematic of the experimental test station for force control.

The experimental setup for force control was the same as that of the position control, except that the load was replaced by a set of springs (see Fig. 6-24). The end of the piston was commanded to push the springs with a desired force. Most of the experiments were carried out with two springs used in tandem. The overall stiffness in this case was 3404 N/m. Several tests were also done with only one spring used, increasing the environment stiffness to 6940 N/m. Again, the servovalve had a dead-band of [-0.4volt, 0.4volt]. A sampling time of 0.01 second was chosen for the experiments.

6.2.2 System Analysis

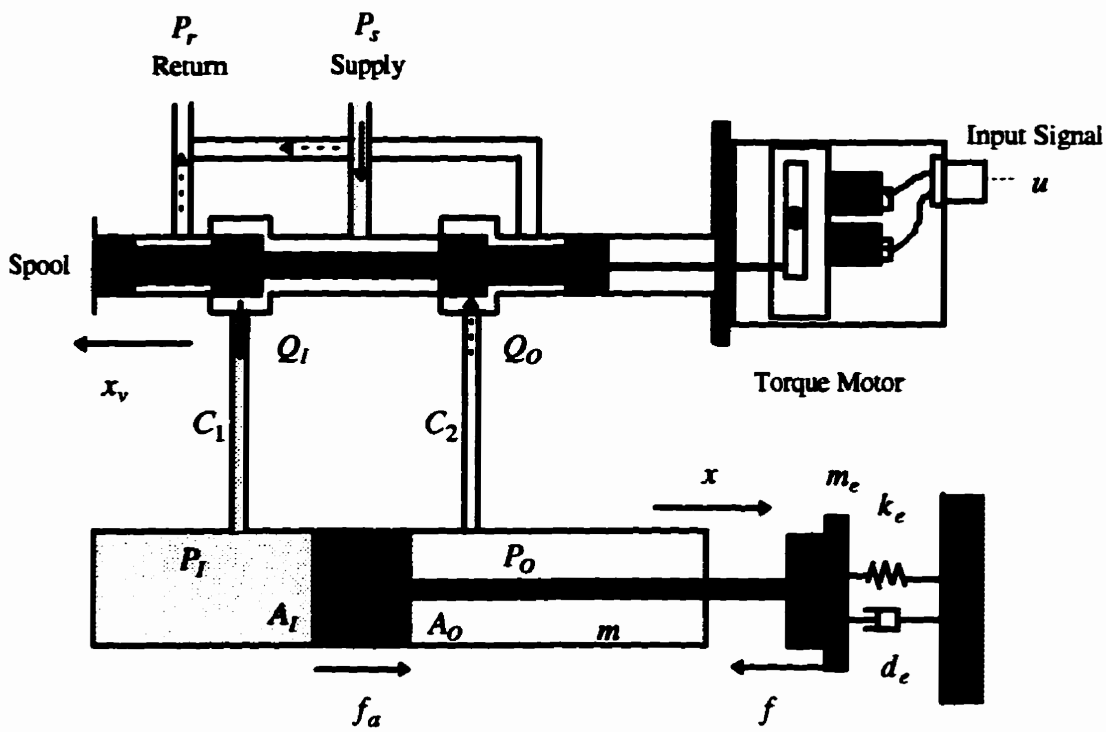

Fig. 6-25 Hydraulic actuator in contact with environment.

Figure 6-25 shows the hydraulic actuator interacting with environment which is modeled by a second order mass-damper-spring system.

For the open-loop analysis of force control, equations (6-1) through (6-4) still hold, but equation (6-5) should be modified since the actuator is no longer in free motion. Considering the contact force f, (6-5) is revised as:

$$f_a - f = m\ddot{x} + d\dot{x} \tag{6-16a}$$

where $$f = m_e\ddot{x} + d_e\dot{x} + k_e \tag{6-16b}$$

Writing equation (6-16) in s-domain yields:

$$F_a - F = (ms^2 + ds)X \tag{6-17a}$$

$$F = (m_e s^2 + d_e s + k_e)X \tag{6-17b}$$

Substituting (6-17b) into (6-17a) gives:

$$F_a = (m + m_e)Xs^2 + (d + d_e)Xs + k_e \tag{6-18}$$

Substituting (6-3) into (6-4) and comparing the result with (6-18) arrives at:

$$\frac{X(s)}{U(s)} = \frac{K_u(A_I + A_O)}{[(m_e + m)s^2 + (d_e + d)s + k_e](Cs + K_p) + (A_I^2 + A_O^2)s} \tag{6-19}$$

Substituting (6-17b) into (6-19) gives the transfer function from u to f:

$$\frac{F(s)}{U(s)} = \frac{K_u(A_I + A_O)(m_e s^2 + d_e s + k_e)}{[(m_e + m)s^2 + (d_e + d)s + k_e](Cs + K_p) + (A_I^2 + A_O^2)s} \tag{6-20}$$

Equation (6-20) is a third order system, and its z-transform including a zero order holder is in the form of:

$$\frac{F(z)}{U(z)} = \frac{b_0 z^{-1} + b_1 z^{-2} + b_2 z^{-3}}{1 + a_1 z^{-1} + a_2 z^{-2} + a_3 z^{-3}} \tag{6-21}$$

Therefore, the discrete form of the output $f(t)$ is:

$$\begin{aligned} f(t) &= -a_1 f(t-1) - a_2 f(t-2) - a_3 f(t-3) \\ &\quad + b_0 u(t-1) + b_1 u(t-2) + b_2 u(t-3) + h(t) \end{aligned} \tag{6-22}$$

Again $h(t)$ is added as a forcing term to look after the effects of other nonlinearities. Equation (6-22) is used for both the GPC and the MVC algorithms for force control.

For the position control, different transfer functions, (6-6) and (6-7), were used for the generalized predictive and the minimum variance controllers, respectively; for the force control, however, transfer function (6-20) was used for both controllers. One reason was that the signal of $\dot{f}$ could not be obtained directly and must be derived from the signal of f. f is usually very noisy, leading to inaccurate $\dot{f}$. Another reason was that using the transfer function from u to $\dot{f}$ does not reduce the order of the system. In fact, the transfer function from u to $\dot{f}$ can be easily written out from equation (6-20):

$$\frac{sF(s)}{u(s)} = \frac{K_u(A_I + A_O)(m_e s^2 + d_e s + k_e)s}{[(m_e + m)s^2 + (d_e + d)s + k_e](Cs + K_p) + (A_I^2 + A_O^2)s} \qquad (6\text{-}23)$$

which is still a third order system.

6.2.3 Results

6.2.3.1 GPC Implementation

Two springs were used in tandem as the environment. The overall stiffness was equal to 3404 N/m. It was assumed that the piston was always keeping in touch with the environment. To ensure this assumption, the rod end kept an initial force of 40 N against the environment.

In order to avoid possible large overshoots that could easily overload the force sensor, the initial values of the plant model parameters were needed to be assigned based on off-line estimation. Equation (6-22) reveals that 7 parameters had to be estimated. Figure 6-26 shows the block diagram for the off-line parameter estimation in which u is the control signal and f the contact force. The control input used for off-line estimation has already been shown in Fig. 6-4. The initial values obtained were:

$$a_1 = -1.350,\ a_2 = -0.0207,\ a_3 = 0.369,$$

$$b_0 = 0.380,\ b_1 = -0.635,\ b_2 = 1.874,\ h = -0.0517 \qquad (6\text{-}24)$$

The limit values for the diagonal matrix **D** and the upper triangular matrix **U** were set to:

the sum of elements in **D** was bounded within [0.04, 1],

the sum of elements in **U** was bounded within [-1, 2].

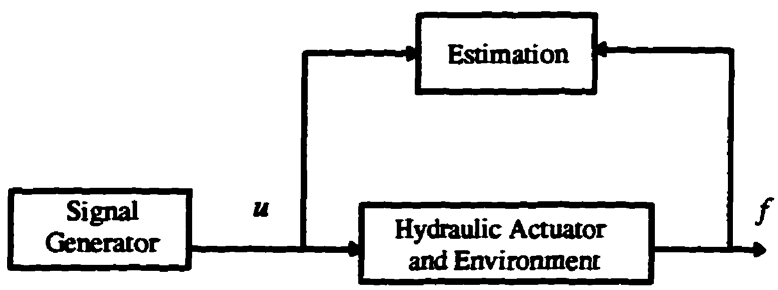

Fig. 6-26 Configuration of off-line estimation for force control.

The system was tested first for step inputs. The best response was found with the following parameter setting:

$$N_1 = 1,\ N_2 = 35,\ N_u = 1,\ \lambda_c = 0.1,\ \lambda_r = 0.2,\ \lambda_f = 0.99 \qquad (6\text{-}25)$$

Figure 6-27 shows the response of contact force f and the control signal. During the first 5 seconds the contact force was stabilized at 40 N; then the force set-point was changed to different levels. For this well-tuned result, there was no overshoot and no steady-state error, and the response was quite fast. Fig. 6-28 shows the piston displacement. The parameter estimation is shown in Fig. 6-29. The supply pressure and line pressures are plotted in Fig. 6-30.

Figure 6-31 shows the effect of varying N_2 on the response. When N_2 was reduced to 22, the response became slightly oscillatory. Figure 6-32 shows the response when N_u was increased to 2. The small piston oscillation was amplified by the high stiffness, resulting in large oscillation in the response of contact force. Figure 6-33 shows the result of decreasing λ_c to 0.001. The response became a little slower. Figure 6-34 shows the result of increasing λ_r to 1.0. The force response result became slightly oscillatory. Figure 6-35 shows the result of changing λ_f to 0.95 which is not much different from the one when λ_f was set to 0.99.

The stiffness of the environment was then increased to 6940 N/m by removing one spring from the system. The same step inputs as in Fig. 6-27 was used. The initial parameters and the design parameters were also the same as the ones shown by (6-24) and (6-25), respectively. Figure 6-36 shows the results. Despite the environmental stiffness change, the overall response was quite good. The piston displacement is shown in Fig. 6-37.

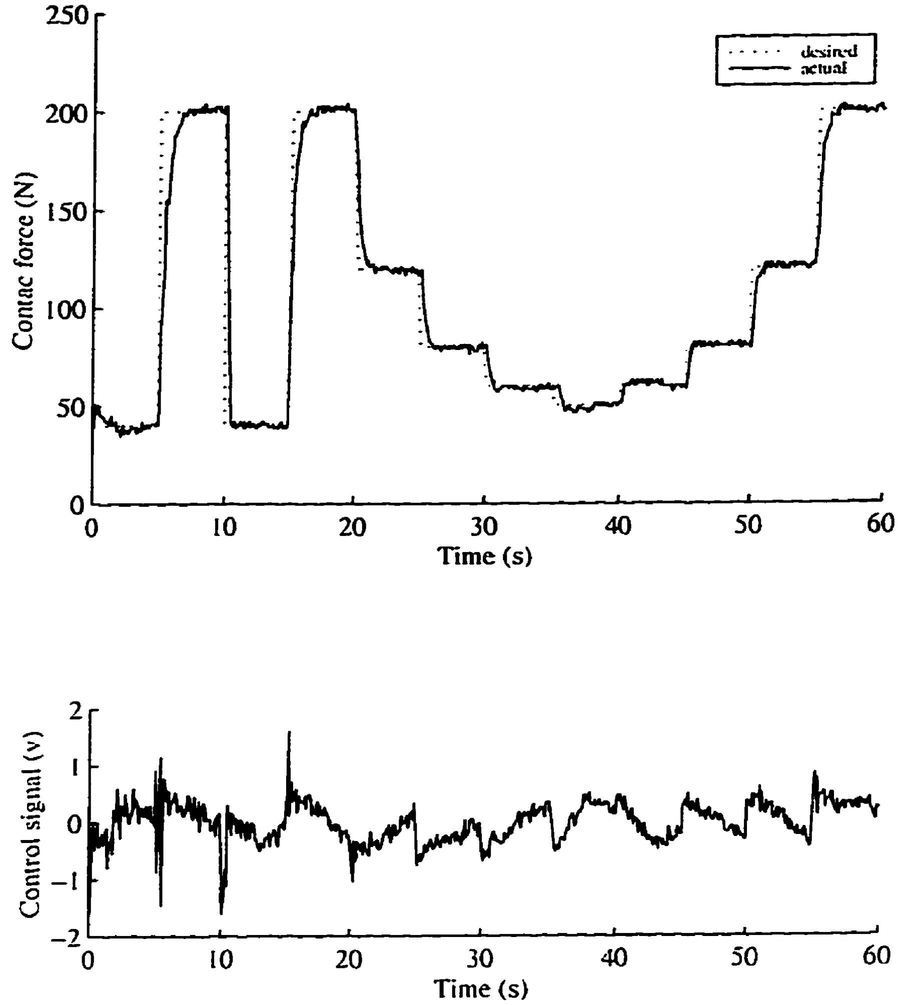

Fig. 6-27 Contact force and control input with

$N_1=1$, $N_2=35$, $N_u=1$, $\lambda_c=0.1$, $\lambda_r=0.2$, $\lambda_f=0.99$.

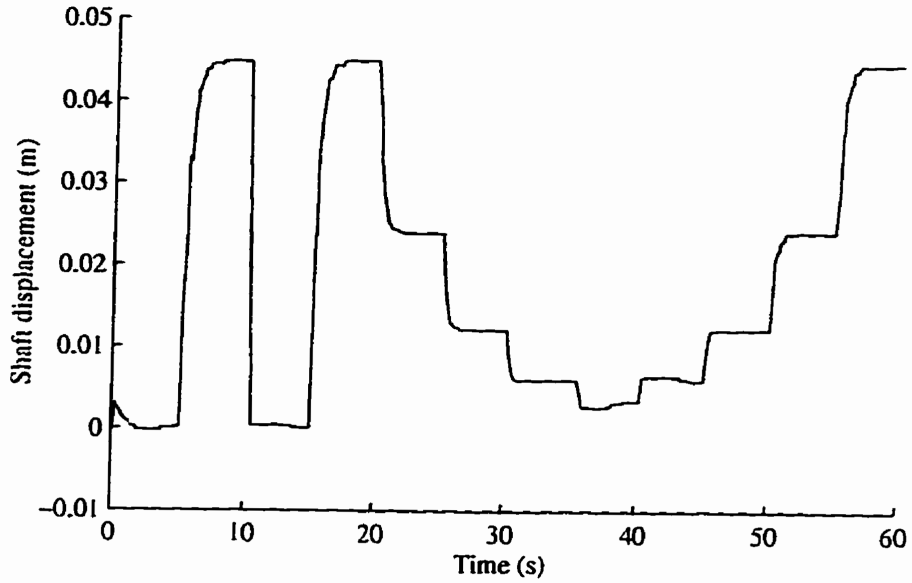

Fig. 6-28 Piston displacement pertaining to Figure 6-27.

Figures 6-38 and 6-39 show the system response to ramp and cosine inputs. The slopes for the ramp input were ± 16 N/s during the first 40 seconds and ± 80 m/s during the next 8 seconds. The frequency of the cosine wave was initially set to 0.05Hz and then was changed to 0.25Hz. The experiments was performed with two springs used in tandem, *i.e.*, the environment stiffness was 3404 N/m. Both figures show that in the beginning the response had large errors due to the inaccurate plant model parameters. The system quickly adapted by identifying more accurate parameters. The responses afterwards were getting better with much smaller tracking errors.

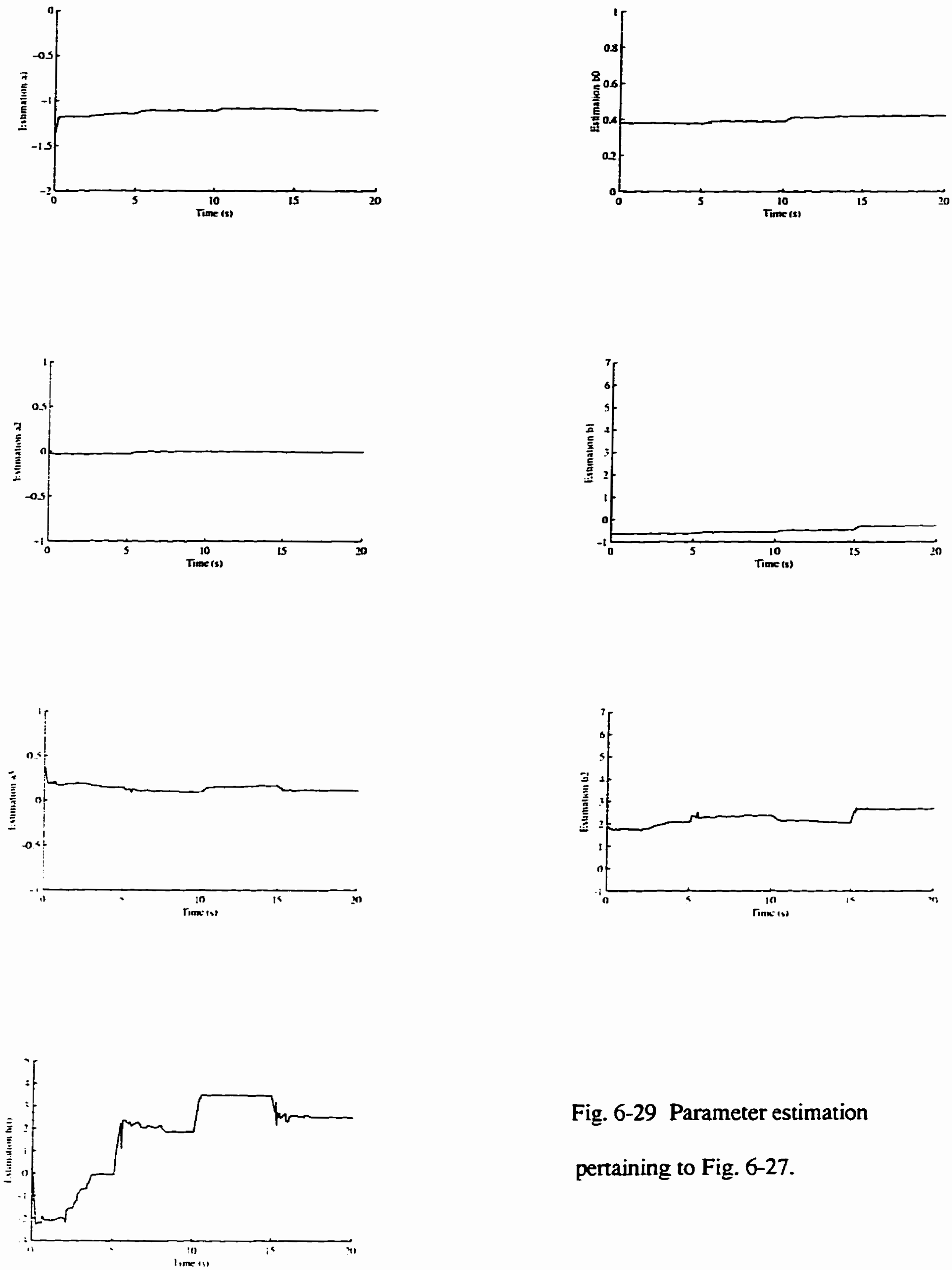

Fig. 6-29 Parameter estimation pertaining to Fig. 6-27.

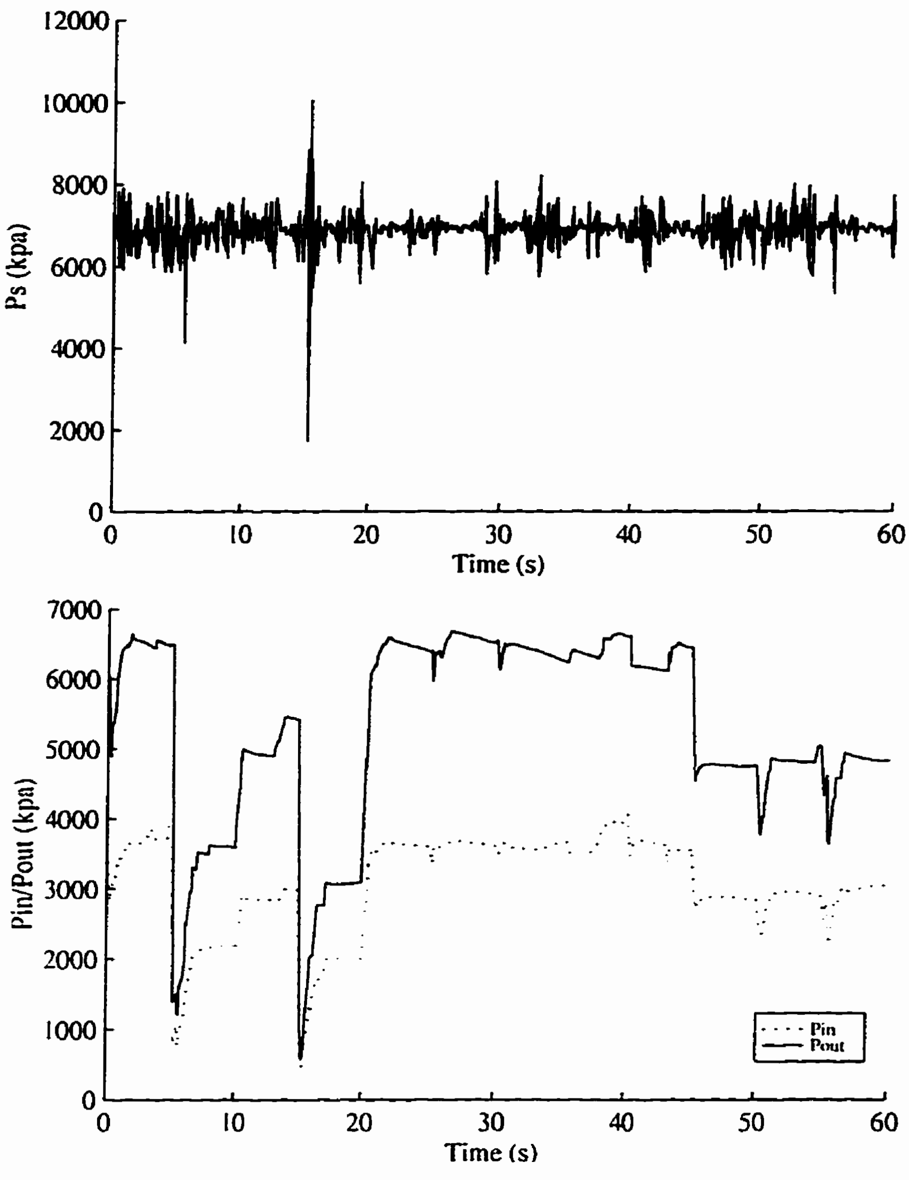

Fig. 6-30 Supply pump pressure, supply and return line pressures pertaining to Fig. 6-27.

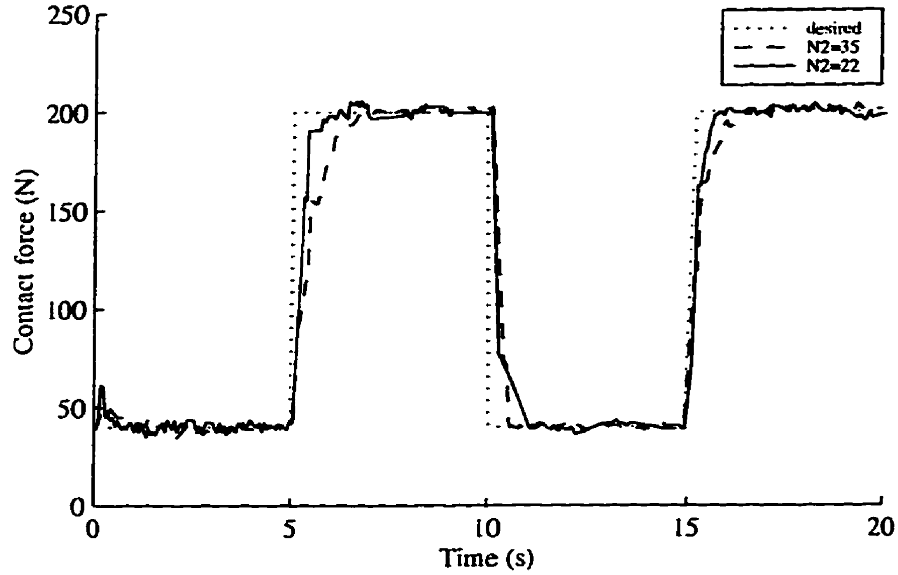

Fig. 6-31 Contact force response with $N_2 = 22$.

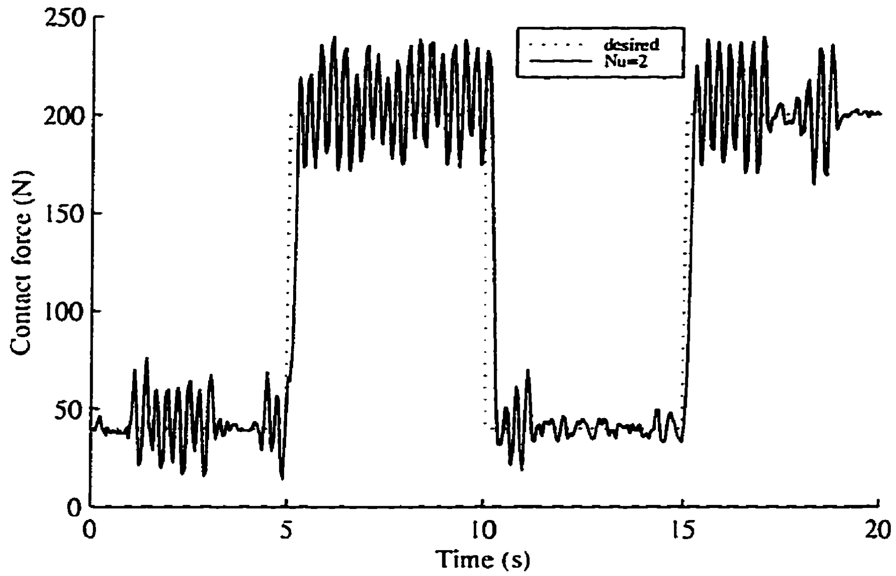

Fig. 6-32 Contact force response with $N_u = 2$.

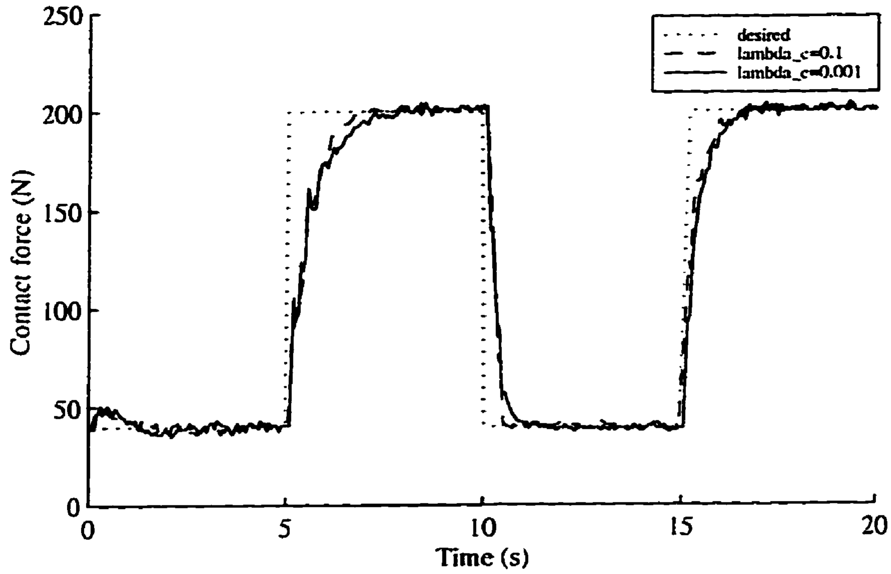

Fig. 6-33 Contact force response with $\lambda_c = 0.001$.

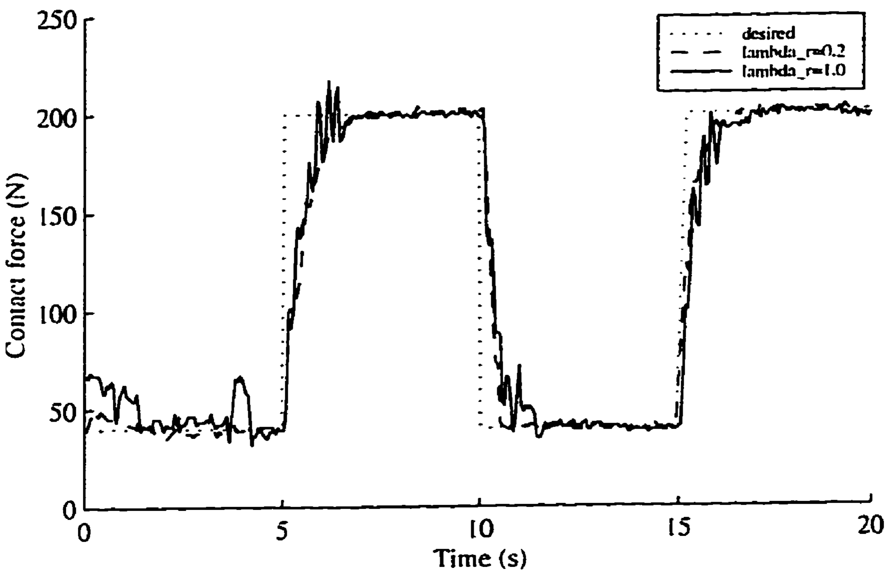

Fig. 6-34 Contact force response with $\lambda_r = 1.0$.

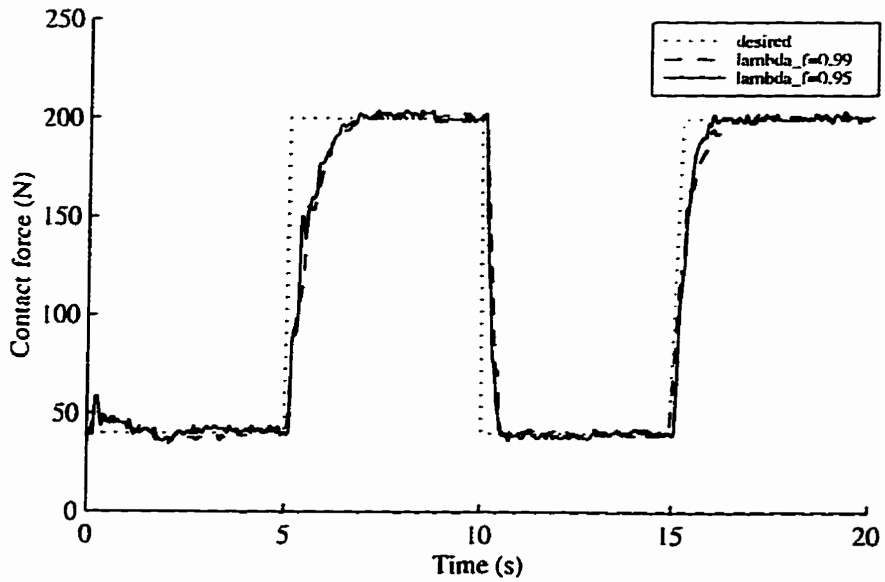

Fig. 6-35 Contact force response with $\lambda_f = 0.95$.

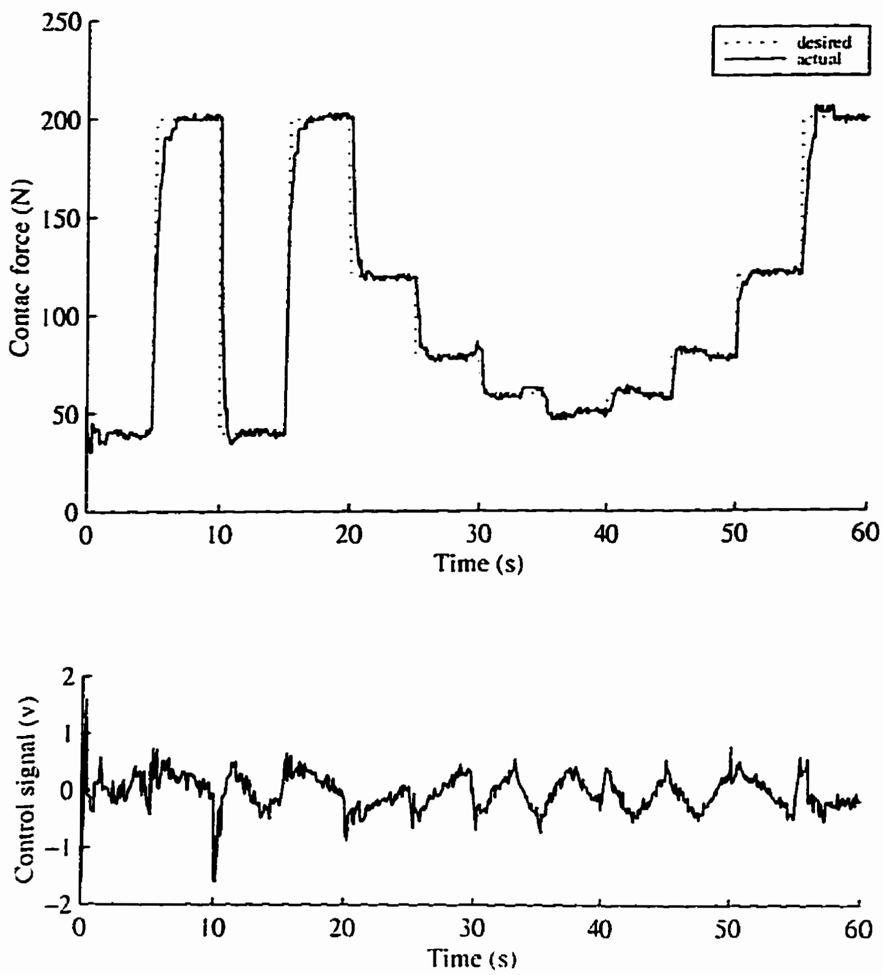

Fig. 6-36 Contact force and control input with increased environment stiffness.

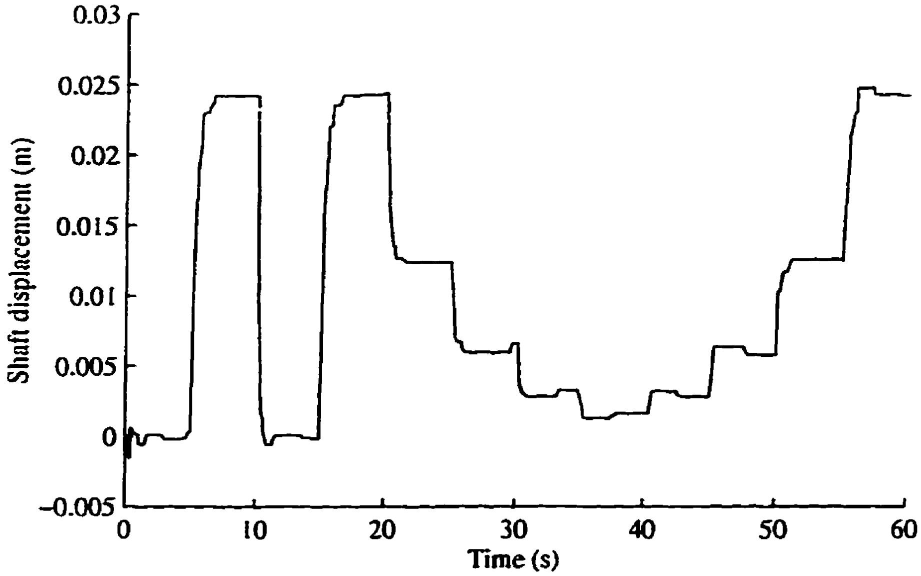

Fig. 6-37 Piston displacement pertaining to Fig. 6-36.

6.2.3.2 MVC Implementation

The discrete time output, equation (6-22), was used for minimum variance force controller. The initial parameter values shown in (6-24) were used, and so did the boundary conditions for matrices **U** and **D** listed in Section 6.2.3.1.

The best performing step response was obtained with the following parameter setting:

$$\lambda_r = 0.03,\ \lambda_f = 0.99 \tag{6-26}$$

Figure 6-40 shows the response of contact force. Due to the dead-band in the hydraulic valve, the response exhibits a steady-state error. The largest error was ≈ 11.5 N. Any set-point change below this value may not be sufficient to activate the system. With reference to Fig. 6-40 the system failed to respond to the set-point change of 10 N.

Figure 6-41 shows the piston displacement, and Fig. 6-42 shows the parameter estimation. The supply pressure and line pressures are shown in Fig. 6-43.

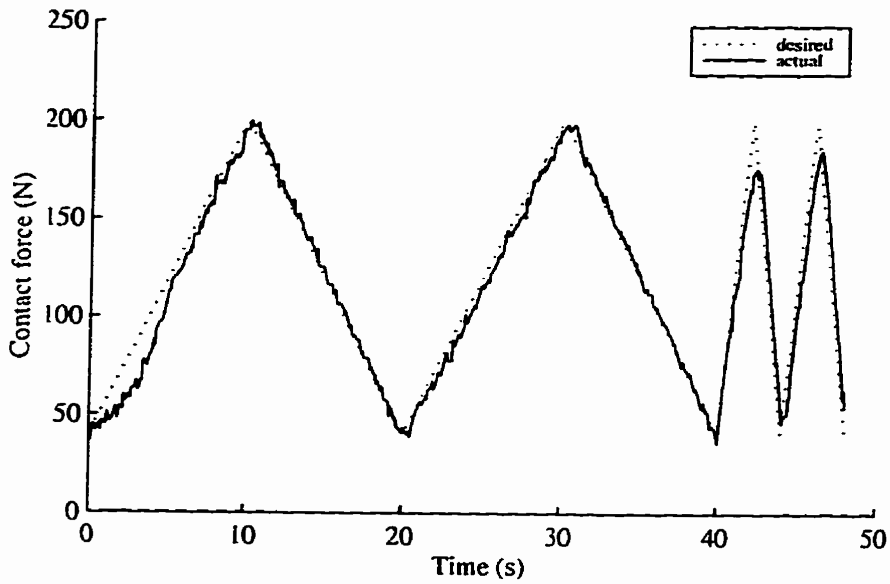

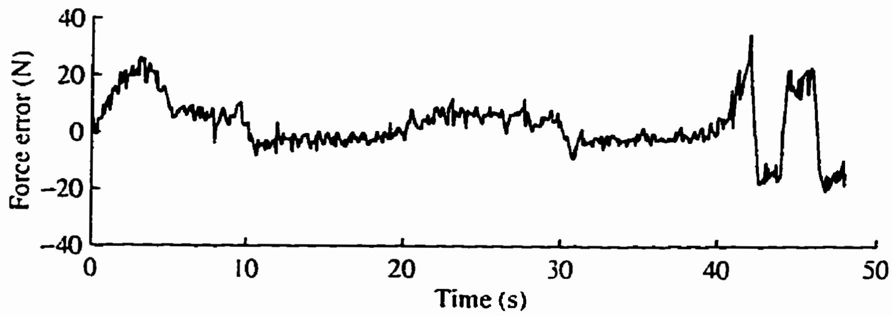

Fig. 6-38 Contact force and force tracking error to a ramp input.

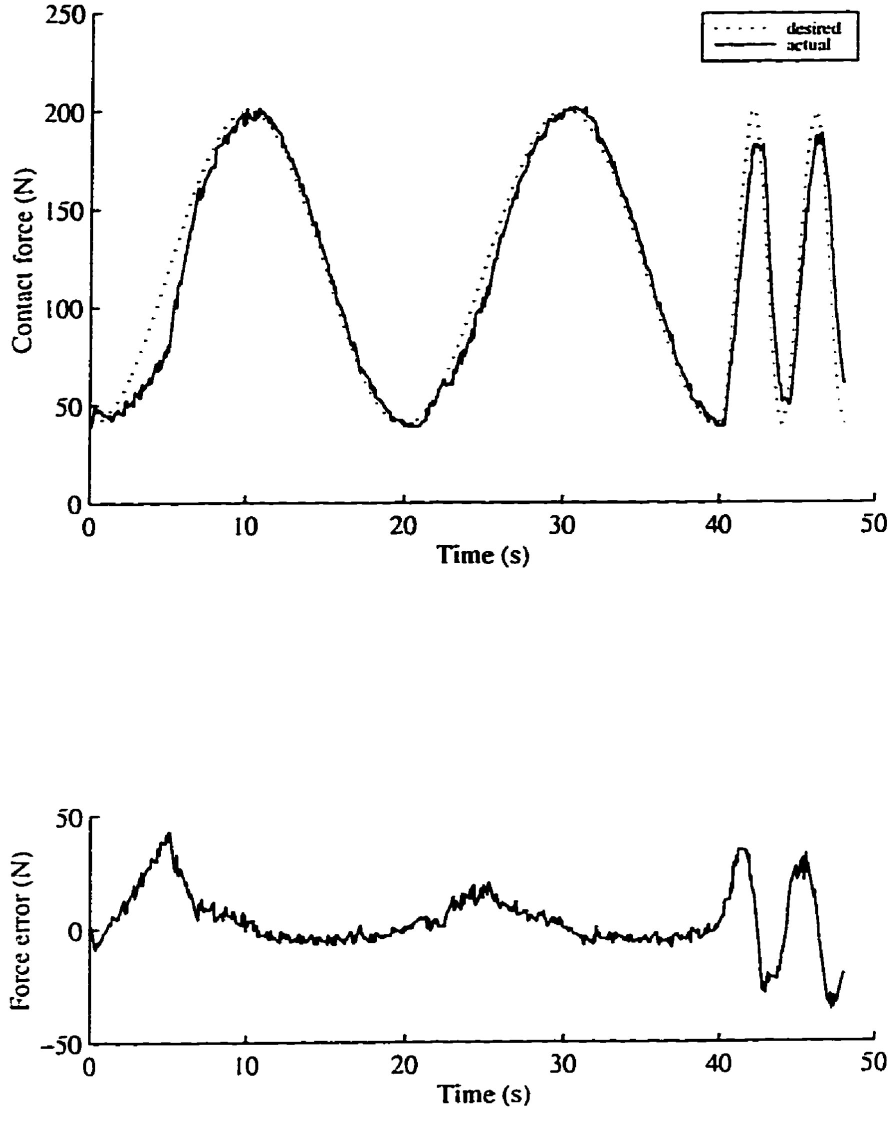

Fig. 6-39 Contact force and force tracking error to a cosine input.

In order to increase the stiffness of the environment, one spring was removed which left the environmental stiffness changed to 6940 N/m. The system was tested with the same step inputs as in Fig. 6-40, the same initial parameter setting shown in equation (6-25) and the same design parameter shown in equation (6-27). See Fig. 6-44 for the result.

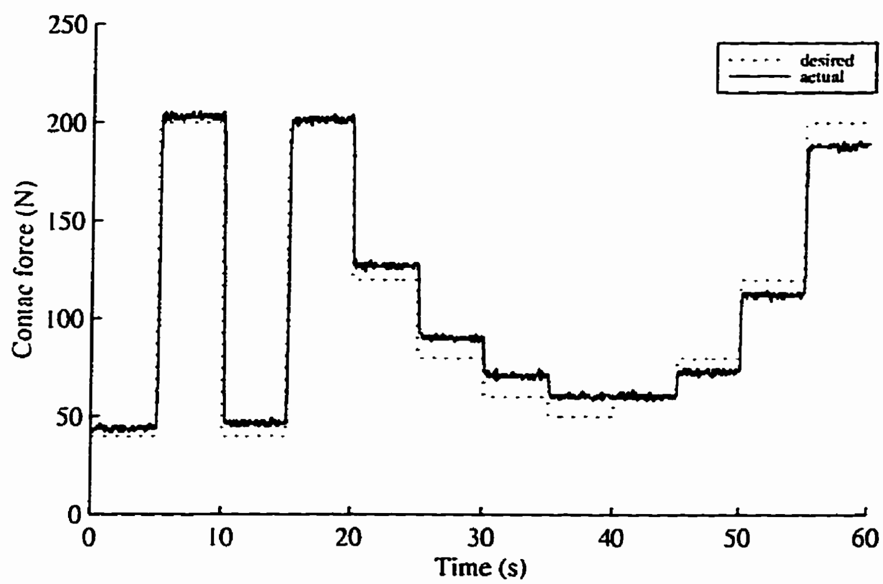

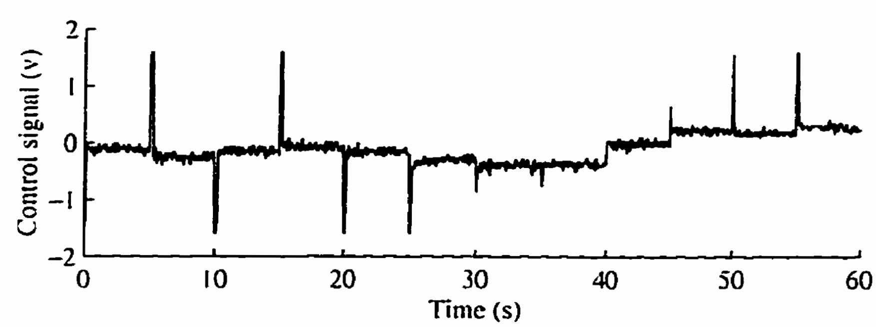

Fig. 6-40 Contact force and control input with λ_r=0.03, λ_f=0.99.

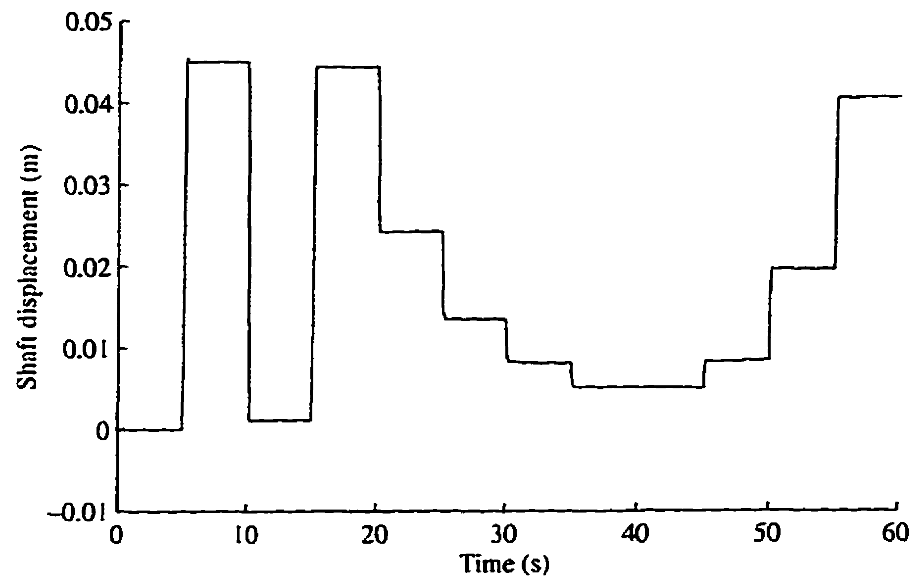

Fig. 6-41 Piston displacement pertaining to Fig. 6-40.

Obviously, the contact force exhibits large overshoots in responding to certain set-point changes, which can also be clearly seen from the piston displacement in Fig. 6-45.

Figures 6-46 and 6-47 show the system response to ramp and cosine tracking set-points. The experiments have been done with the environmental stiffness of 3404 N/m. As is seen, there were large tracking errors, reflecting the inferior force tracking ability of the MVC controller.

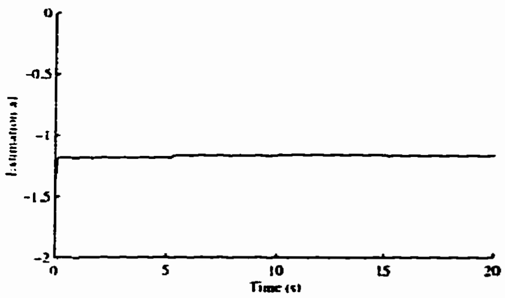

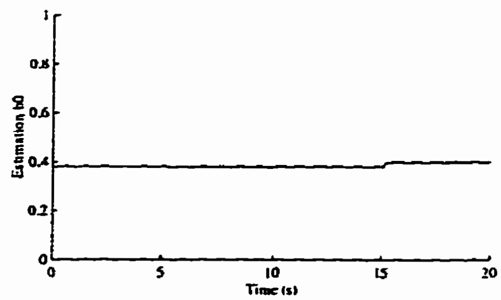

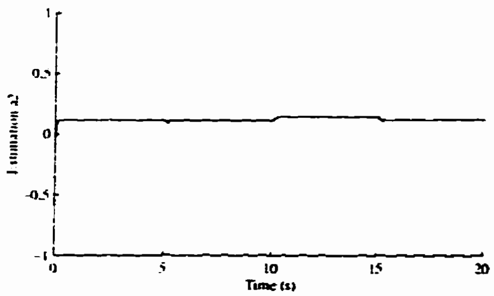

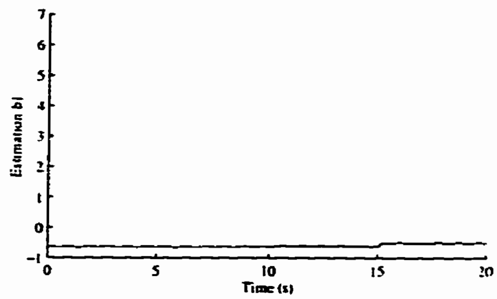

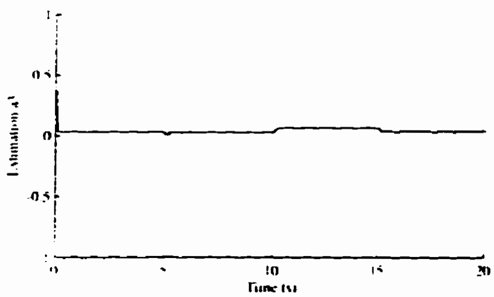

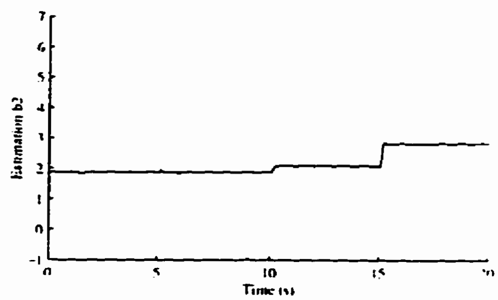

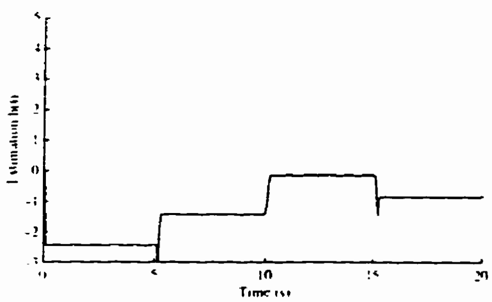

Fig. 6-42 Parameter estimation pertaining to Fig. 6-40.

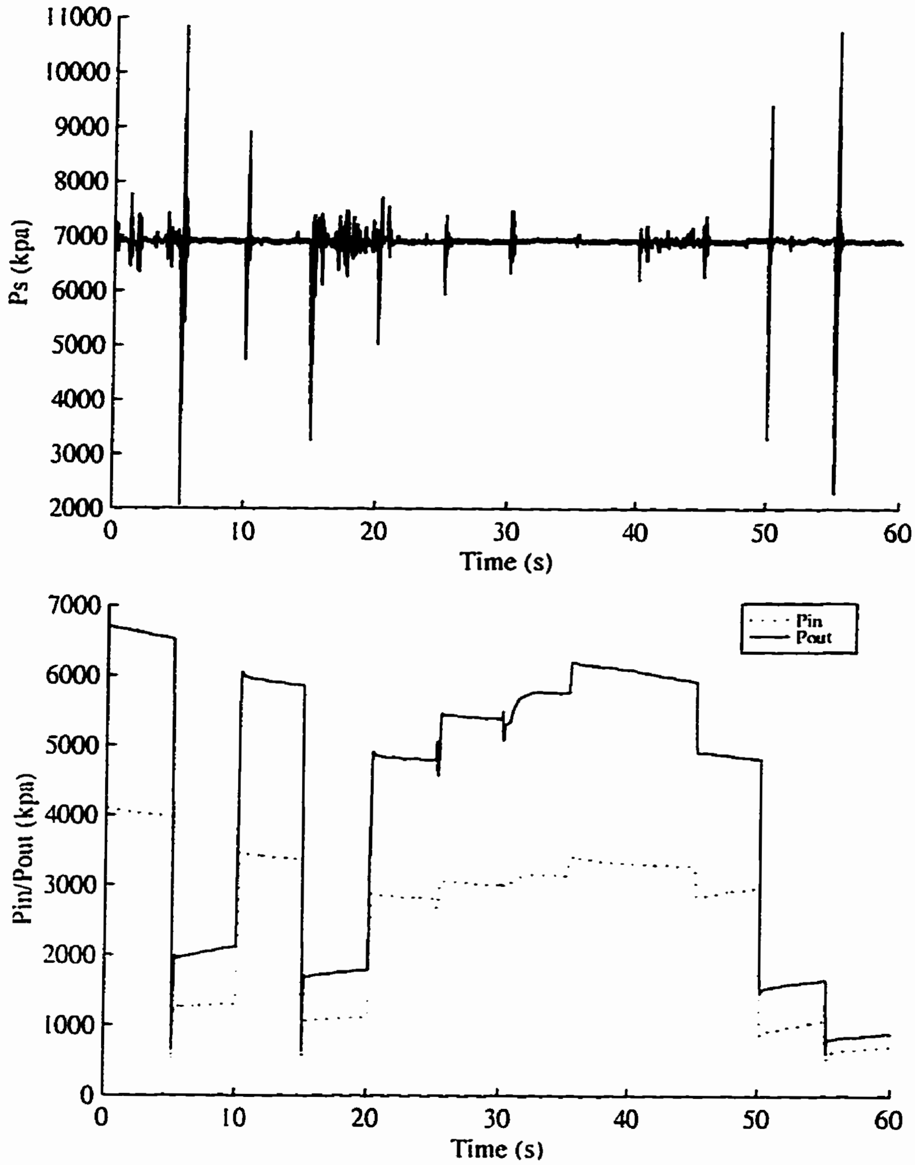

Fig. 6-43 Supply pump pressure, supply and return line pressures pertaining to Fig. 6-40.

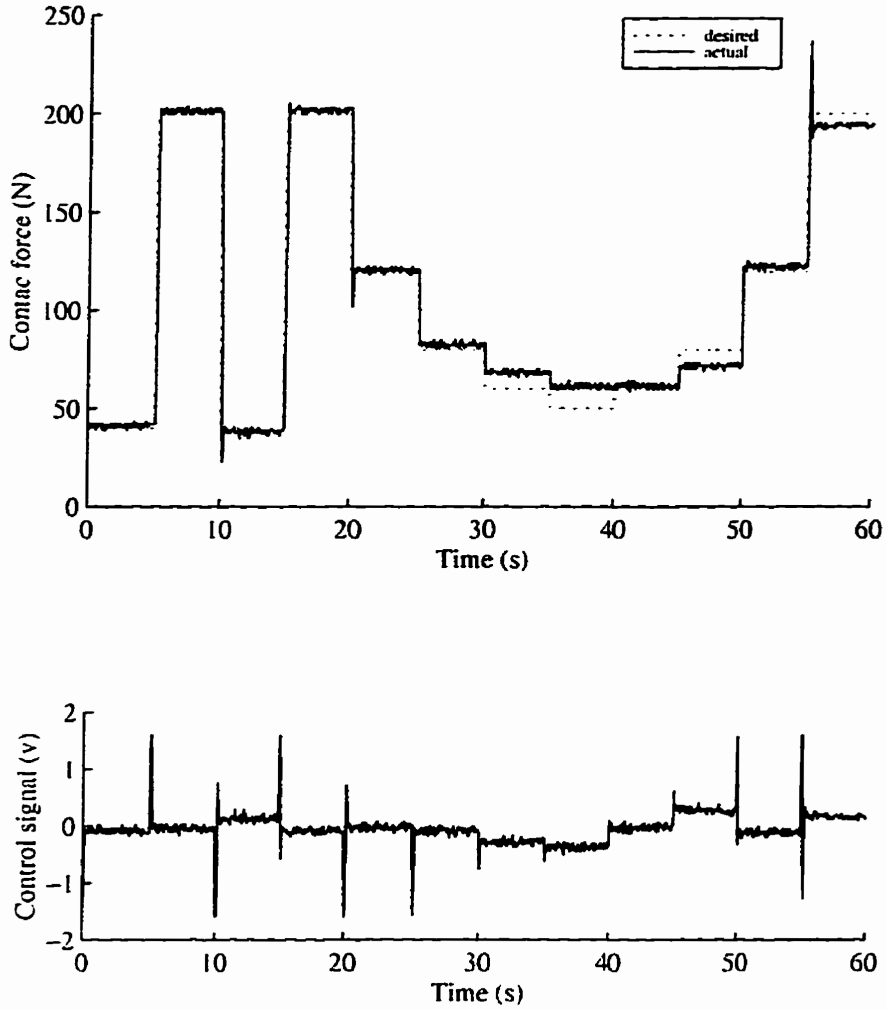

Fig. 6-44 Contact force and control input with increased environment stiffness.

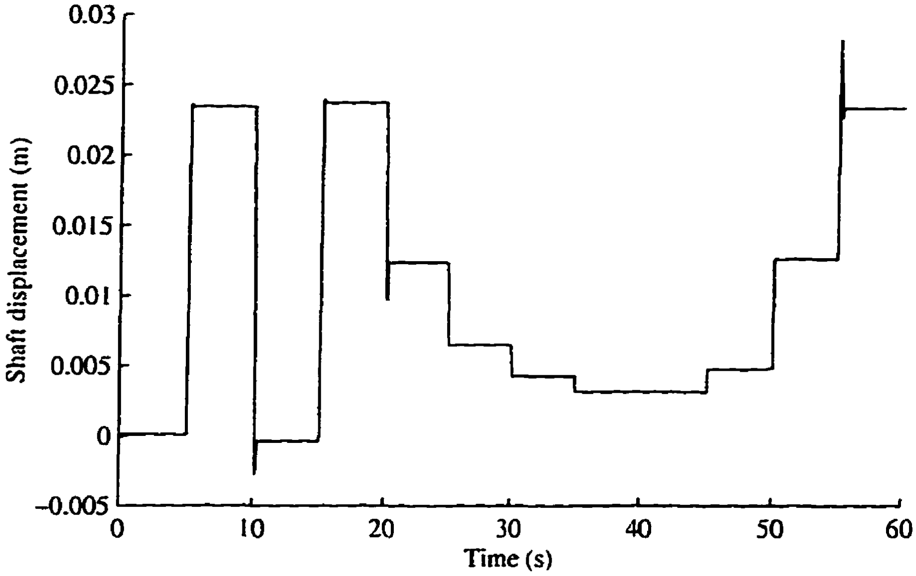

Fig. 6-45 Piston displacement pertaining to Fig. 6-44.

6.3 SUMMARY

The experiments in both position and force control of hydraulic actuator demonstrated the feasibility and potential of adaptive generalized predictive controller. The controller was capable of precise control and quick adaptation to plant changes. Minimum variance controller also achieved good control performance in both position and force control, but it was inferior in adaptability, the ability to overcome dead-band in the servovalve and tracking. During the course of the experiments, it was found that the on-line estimation required special attention in order to prevent possible parameter shifting and to ensure the numerical accuracy and stability.

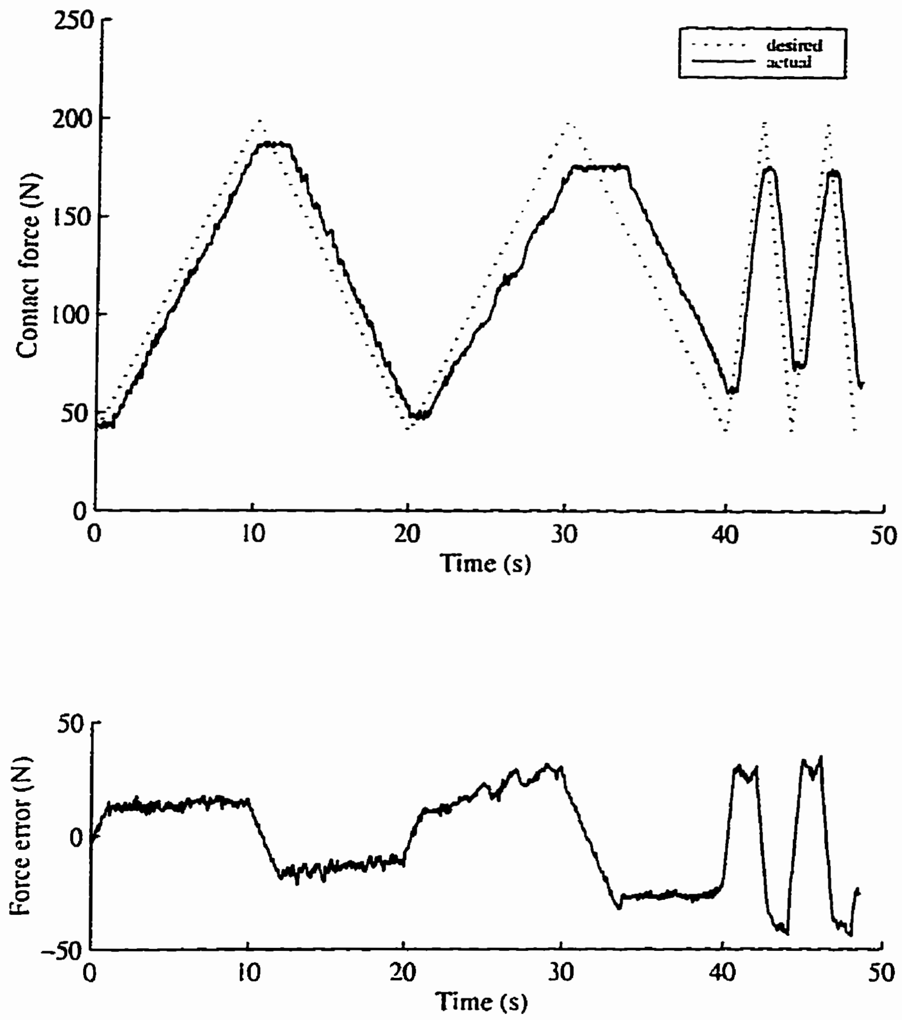

Fig. 6-46 Contact force and force tracking error to a ramp input.

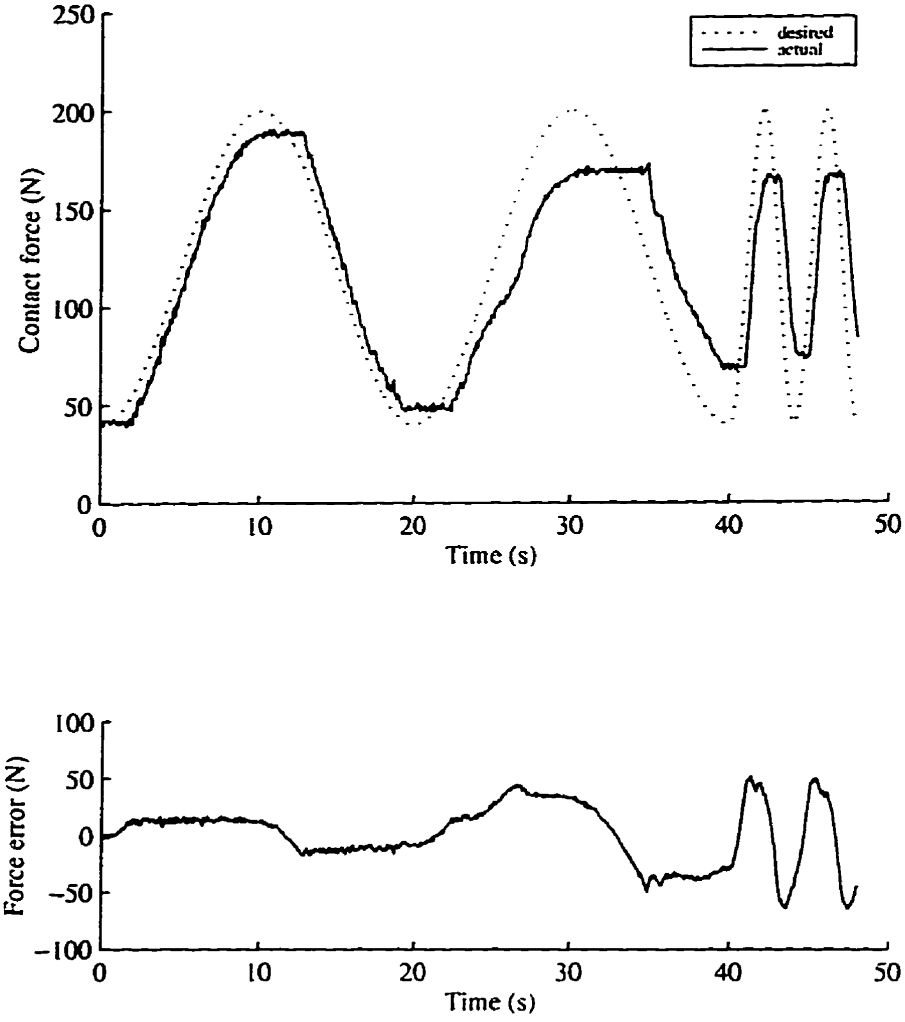

Fig. 6-47 Contact force and force tracking error to a cosine input.

CHAPTER SEVEN

CONCLUSIONS

7.1 CONTRIBUTIONS OF THIS WORK

In this thesis, adaptive control of hydraulic manipulators using a generalized predictive control (GPC) algorithm has been studied through computer simulation of a two-link hydraulic manipulator as well as experimentation with a single hydraulic actuator. Proper mathematical models were established for both single-input single-output (SISO) and multi-input multi-output (MIMO) force and/or position control. Detailed study of the effects of design parameters was carried out. In particular, the adaptability of the controllers were tested with varying load, hydraulic compliance and environment stiffness. The results were also compared with those corresponding to a minimum variance control (MVC) strategy.

The application of an adaptive GPC algorithm to the control of hydraulic manipulators was successful. Due to the nature of long range prediction of the plant output and the inherent integral action of the controller, GPC algorithm proved to be reliable at precise control of both position and contact force even in the presence of actuator dead-band due to joint friction and hydraulic flow dead-band. Moreover, GPC demonstrated an excellent ability to quickly adapt to changes in load, hydraulic compliance, and environmental characteristics.

During the course of this study, it was found that the well-known MVC algorithms could also achieve good performance. However, comparing with GPC algorithms, minimum variance controllers, (i) were less capable in adapting to dynamic changes in the plant, (ii) failed in overcoming the actuator dead-band, and, (iii) were inferior in tracking specified trajectories. On the other hand, the implementation of the generalized predictive controller was found to be more computationally demanding than that of the minimum variance controller.

Regarding the comparison between the application of SISO- and MIMO-GPC, the computer simulation performed on a two-link hydraulic manipulator model revealed that the MIMO-GPC algorithm significantly reduced the computational time while the system performance was enhanced by having the interaction between links taken care of. On the other hand, since the algorithm viewed the manipulator as a single system, the order of the plant to be identified was increased, thus, the number of the parameters to be estimated.

In practice, this may not be preferred because the estimation of a large number of parameters is time demanding and may lead to inaccurate results.

7.2 RECOMMENDATIONS FOR FUTURE WORK

It is recommended that the future development of adaptive control of hydraulic manipulator with emphasis on the GPC algorithm could be done along the following directions:

1. Quantify the data obtained in this thesis, especially those related to the comparison between GPC and MVC algorithms and those between SISO and MIMO GPC algorithms to offer more convincing and accurate information. For instance, the computational expense of each algorithm with similar performance specifications could be quantified by either the number of arithmetic operations in CPU or the amount of time consumed during each period of sampling period. Further, sensitivity analysis could be performed to understand the effect of parameters on the linearized plant model. Thus, the number of the parameters to be estimated may be reduced by removing some insignificant parameters from the plant model.

2. Generalize the application of GPC algorithm to an n-link hydraulic manipulator. Apparently, there would be no significant changes for SISO-GPC algorithm. However, for MIMO GPC algorithm, to treat the n-link manipulator similar to the treatment of a 2-link one, as was outlined in this thesis, is not the best choice. The

number of the parameters, to be estimated on-line, can become unmanageable. Alternative solutions need to be worked out.

3. The parallel algorithm of matrix manipulation could be incorporated to reduce the computational time required by the controller. Having developed an efficient method, there will be no major obstacle left for the GPC algorithm to fully enter the practice of real-time control of fast plants such as hydraulic manipulators.

REFERENCES

1. Al-Zaher, A., *Study of Position Control on Two Classes of Hydraulically Actuated Manipulators*, M. Sc. Thesis, Department of Mechanical and Industrial Engineering, University of Manitoba, 1994.
2. Whitney, D. E., "Historical Perspective and State of the Art in Robot Force Control", *Proceedings of the 1985 IEEE International Conference on Robotics and Automation*, pp. 262-268, St. Louis, Missouri, 1985.
3. Raibert, M. H. and Craig, J. J., "Hybrid Position/Force Control of Manipulators", *Journal of Dynamics Systems, Measurement and Control*, Vol. 102, pp. 126-133, 1981.
4. Craig, J. J., *Adaptive Control of Robotic Manipulators*, Addison-Wesley Publishing Company, Reading, Massachusetts, 1988.
5. Koivo, A. J., *Fundamentals for Control of Robotic Manipulators*, John Wiley & Sons, Inc., New York, 1989.
6. Narendra, K. S. and Annaswamy, A. M., *Stable Adaptive Systems*, Prentice Hall, Englewood Cliffs, New Jersey.
7. Sepehri, N., Dumont, G. A. M., Lawrence, P. D. and Sassani, F., "Cascade Control of Hydraulically Actuated Manipulators", *Robotica*, Vol. 8, pp. 207-216, 1990.
8. Kotzev, A., Cherchas, D. B., Lawrence, P. D. and Sepehri, N., "Generalized Predictive Control of A Robotic Manipulator with Hydraulic Actuators", *Robotica*, Vol. 10, pp. 447-459, 1992.

9. Plummer, A. R. and Vaughan, N. D., "Robust Adaptive Control for Hydraulic Servosystems", *Journal of Dynamic Systems, Measurement, and Control*, Vol. 118, pp. 237-244, 1996.

10. Clarke, D. W., Mohtadi, C., Tuffs, P.S., "Generalized Predictive Control - Part I. The Basic Algorithm", *Automatica*, Vol. 23, No. 2, pp. 137-148, 1987.

11. Clarke, D. W., Mohtadi, C., Tuffs, P.S., "Generalized Predictive Control - Part II. Extensions and Interpretations", *Automatica*, Vol. 23, No. 2, pp. 149-160, 1987.

12. Asada, H. and Slotine, J.-J. E., *Robot Analysis and Control*, John Wiley and Sons, Inc., New York, 1986.

13. Isermann, R., *Digital Control Systems*, Springer-Verlag, New York, 1981.

14. Goodwin, G. C., Sin, K. S., *Adaptive Filtering Prediction and Control*, Engleland Cliffs, New Jersey, Prentice-Hall, 1984.

15. Harris, C. J., *Self-tuning and Adaptive Control*, Peter Peregrinus Ltd. on behalf of the IEE, 1981.

16. Chow, C. M., Kuznetsov, A., Clarke, D., "Application of Multivariable Generalized Predictive Control to the Simulink Model of a Paper Machine", *Proceedings of the 1994 IEEE Conference on Control Applications*, Vol. 3, pp. 1675-1681, Glasgow, U.K., 1994.

17. Koivo, A. J., Guo, T.-H., "Adaptive Linear Controller for Robotic Manipulators", *IEEE Transactions on Automatic Control*, Vol. AC-28, No. 2, pp. 162-170, 1983.

18. Ljung, L., Soderstrom, T., *Theory and Practice of Recursive Identification*, The MIT Press, Cambridge, Massachusetts, 1983.

19. Bierman, G. J., *Factorization Methods for Discrete Sequential Estimation*, Academic Press, New York, 1977.

20. Astrome, K. J., Wittenmark, B., *Adaptive Control*, Addison-Wesley Publishing Company, Reading, Massachusetts, 1989.

21. Dugard, L., Dion, J. M., Nguyen, T., Thanh, T., " End Point Adaptive Control of A Two-link Flexible Arm", *Proceedings of the 4th IFAC Symposium*, pp. 329-334, Grenoble, France, 1992.